

AD 731841
AFML-TR-71-151

**MANUFACTURING METHODS
FOR
SAMARIUM COBALT MAGNETS**

Das, A. Gale, D. Joaquin, A. Kelley, L. Lesensky, A. Paladino,
W. Reid, P. Weihrauch, E. Wettstein

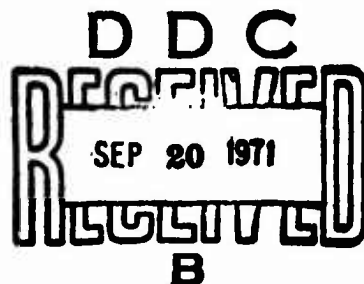
Raytheon Company

**TECHNICAL REPORT AFML-TR-71-151
August 1971**

Approved for Public Release - Distribution Unlimited

**Air Force Materials Laboratory
Air Force Systems Command
Wright-Patterson Air Force Base, Ohio 45433**

Reproduced by
**NATIONAL TECHNICAL
INFORMATION SERVICE**
Springfield, Va. 22151



NOTICES

When Government drawings, specifications, or other data are used for any purpose other than in connection with a definitely related Government procurement operation, the United States Government thereby incurs no responsibility nor any obligation whatsoever; and the fact that the Government may have formulated, furnished, or in any way supplied the said drawings, specifications, or other data, is not to be regarded by implication or otherwise as in any manner licensing the holder or any other person or corporation, or conveying any rights or permission to manufacture, use, or sell any patented invention that may in any way be related thereto.

Copies of this report should not be returned to the Research and Technology Division unless return is required by security considerations, contractual obligations, or notice on a specific document.

SECTION NO.	
CPSTI	WHITE SECTION <input checked="" type="checkbox"/>
ONS	TECH SECTION <input type="checkbox"/>
UNANNOUNCED	<input type="checkbox"/>
JUSTIFICATION	
BY	
DISTRIBUTION/AVAILABILITY CODE	
DECL.	AVAIL. and/or SPECIAL
A	

Unclassified

Security Classification

DOCUMENT CONTROL DATA - R & D		
Security classification of title, body of abstract and indexing annotation must be entered when the overall report is classified		
1. ORIGINATING ACTIVITY (Corporate author) RAYTHEON COMPANY Microwave and Power Tube Division Waltham, Mass. 02154		2a. REPORT SECURITY CLASSIFICATION Unclassified
		2b. GROUP
3. REPORT TITLE Manufacturing Methods for Samarium-Cobalt Magnets		
4. DESCRIPTIVE NOTES (Type of report and inclusive dates) Final Report IR-612-9B (F)		
5. AUTHOR(S) (First name, middle initial, last name) D. Das, A. Gale, D. Joaquin, A. Kelley, L. Lesensky, A. Paladino, W. Reid, P. Weihrauch, E. Wettstein		
6. REPORT DATE June 1971	7a. TOTAL NO. OF PAGES 148	7b. NO. OF REFS 9
8a. CONTRACT OR GRANT NO. F33615-70-C-1097	9a. ORIGINATOR'S REPORT NUMBER(S) PT-3051	
9. PROJECT NO. TE-9M-257/612-9	9b. OTHER REPORT NO(S) (Any other numbers that may be assigned this report) IR-612-9B (F)	
10. DISTRIBUTION STATEMENT Approved for Public Release - Distribution Unlimited		
11. SUPPLEMENTARY NOTES	12. SPONSORING MILITARY ACTIVITY Air Force Materials Laboratory Air Force System Command Wright-Patterson AFB, Ohio	
13. ABSTRACT Processes and techniques have been established for the pilot line manufacturing of samarium-cobalt permanent magnets for use in high performance periodic permanent magnet focused traveling-wave tube amplifiers. The objective of achieving a capacity for 1000 magnets per month was exceeded. Typical properties of magnets produced in quantity are: energy product $(BH)_{\max}$ of $13 - 15 \times 10^6$ GOe, B_r of 7800 ± 200 gauss, and H_c of 6800 ± 300 Oe. Extensive measurements were made to establish temperature characteristics of second quadrant properties, long term stability, and maximum temperature use in an operating device. Irreversible temperature coefficients for magnetic properties up to 255°C were found to depend linearly on demagnetizing field, whereas reversible temperature coefficients varied only slightly. Magnet rings assembled in a PPM stack (high demagnetizing factor) exhibited $< 4\%$ measurable change in peak axial field at 225°C for over 900 hours. Device evaluation of magnets clearly established the superior performance possible with samarium-cobalt. Higher power and the attendant higher temperature are now achievable with TWT's.		

DD FORM 1473
1 NOV 65

Unclassified

Security Classification

Unclassified

Security Classification

14	KEY WORDS	LINK A		LINK B		LINK C	
		ROLE	WT	ROLE	WT	ROLE	WT
	Samarium-Cobalt Magnets High Energy Product Melting Grinding Alloy Drying Pressing Permanent Magnets Traveling-Wave Tube						

Unclassified

Security Classification

AFML-TR-71-151

MANUFACTURING METHODS
FOR
SAMARIUM COBALT MAGNETS

D. Das, A. Gale, D. Joaquin, A. Kelley, L. Lesensky, A. Paladino,
W. Reid, P. Weihrauch, E. Wettstein

Raytheon Company

TECHNICAL REPORT AFML-TR-71-151
August 1971

Approved for Public Release - Distribution Unlimited

Air Force Materials Laboratory
Air Force Systems Command
Wright-Patterson Air Force Base, Ohio 45433

FOREWORD

The Samarium-Cobalt Manufacturing Methods Program was carried out by the Microwave Tube Operation, Microwave and Power Tube Division of Raytheon Company, Waltham, Massachusetts. This work was sponsored by the Air Force Materials Laboratory, Air Force Systems Command, United States Air Force, Wright-Patterson Air Force Base, Ohio, under Contract No. F33615-70-C-1097, Project No. 612-9B. The Air Force Project Engineer was Mr. H. K. Trinkle.

At Raytheon, the work was under the general supervision of Dr. Albert E. Paladino, Manager of the Materials, Processes and Techniques Laboratory. The Project Engineer, Dr. Dilip K. Das, was assisted by Mr. William Reid, Mr. Ernst Wettstein, Dr. Paul Weihrauch, Dr. Leonard Lesensky, Mr. Albert Gale, Mr. D. Joaquin, and Mr. A. Kelley. The period covered by this report is 1 December 1969 to 31 May 1971. The Raytheon internal report number is PT-3051.

This technical report has been reviewed and is approved.



JAMES I. WITTEBORT
Chief, Electronics Branch
Manufacturing Technology Division

ABSTRACT

Processes and techniques have been established for the pilot line manufacturing of samarium-cobalt permanent magnets for use in high performance periodic permanent magnet focused traveling-wave tube amplifiers. The objective of achieving a capacity for 1000 magnets per month was exceeded. Typical properties of magnets produced in quantity are: energy product $(BH)_{\max}$ of $13 - 15 \times 10^6$ GOe, B_r of 7800 ± 200 gauss, and H_c of 6800 ± 300 Oe. Extensive measurements were made to establish temperature characteristics of second quadrant properties, long term stability, and maximum temperature use in an operating device. Irreversible temperature coefficients for magnetic properties up to 255°C were found to depend linearly on demagnetizing field, whereas reversible temperature coefficients varied only slightly. Magnet rings assembled in a PPM stack (high demagnetizing factor) exhibited $< 4\%$ measurable change in peak axial field at 225°C for over 900 hours. Device evaluation of magnets clearly established the superior performance possible with samarium-cobalt. Higher power and the attendant higher temperature are now achievable with TWT's.

TABLE OF CONTENTS

I	INTRODUCTION	1
II	FINE PARTICLE RARE-EARTH MAGNETS	3
III	UNIT PROCESSES FOR SAMARIUM-COBALT MAGNETS	6
	1. Melting	6
	2. Alloy Crushing and Grinding	12
	3. Drying Techniques	19
	4. Storing	20
	5. Pressing	20
	6. Sintering	26
	7. Finishing and Splitting	27
	8. Magnet Evaluation, Processing and Stability	27
	9. Packaging and Shipping	75
IV	MEASUREMENTS OF PPM STACKS AND COMPARISON WITH THEORY	77
V	MICROWAVE DEVICE APPLICATION OF SAMARIUM-COBALT MAGNETS	79
	1. Objective	
	2. Environmental Testing of the QR1642 Traveling-Wave Amplifier Tube	79
IV	SUMMARY	112

LIST OF ILLUSTRATIONS

1	Hysteresis Loops Illustrating Factors Effecting Maximum Energy Product	4
2	The Sm-Co Phase Diagram	7
3	Pilot Line Melting Furnace	8
4	Vertical Sections of Sm-Co Alloy Melts	10
5	Views from Vertical Sections Sm-Co	11
6	Comparison of Grinding Efficiency of a 1 lb Charge in a 1.5 gallon attritor mill and in an 0.75 gallon vibratory mill	13
7	Comparison of Particle Size Distribution Obtained in Roll Mill and Disc Mill Intermediate Grinding	15
8	Particle Size Distribution for Standard 20-Minute Attritor Grinding Compared to 18-Minute Grinding	17
9	Axial Peak Field in a PPM Stack vs Particle Size for Attritor Grinding	18
10	Automatic Powder Compacting Press and Electromagnet Power Supply	22
11	Die Set in Place for Pressing Traveling-Wave Tube Magnets	23
12	Effect of Press Loading on As-Pressed and Sintered Density	25
13	Schematic of Hysteresis Tracer	29
14	Hysteresis Tracer	31
15	Magnetization vs Applied Field of a Sm-Co TWT Magnet Using Vibrating Sample Magnetometer	34
16	Magnetization vs Applied Field of a Sm-Co TWT Magnet Using Integrating Fluxmeter Hysteresis Tracer	34
17	Pulse and DC Magnetization of Sm-Co TWT Magnets	36
18	Pulse Magnetizing Coil	37
19	Typical Current and Field Pulses in 0.6 in. ID High Field Coil	38
20	Raytheon 8100 A Pulser, 15 kJ	39
21	Peak Axial Field in PPM Stack vs Magnetizing Field	43
22	Remanence, Coercive Force and B_{recoil} vs Magnetizing Field	44
23	Testing and Adjusting Fixture	48
24	Tester-Adjuster with Coil and Measuring Head	49
25	Stabilizing Coil and Measuring Head	49
26	Calibration of Magnet Adjuster	50

LIST OF ILLUSTRATIONS (Cont.)

27	Reading on Test Head Outside and Inside Adjusting Coil	51
28	Sm-Co Magnets with Irreversible Thermal Loss	55
29	Magnetic Characteristics of Sm-Co Magnets with Low Irreversible Loss	55
30	Thermal Stability of Sm-Co TWT Magnets	56
31	Thermal Processing	59
32	Magnetization vs Field Measured at Room Temperature	60
33	Magnetization vs Field Measured at Room Temperature	60
34	Thermal Loss of Flux in TWT Magnets vs Demagnetizing Field	62
35	Irreversible Loss of Flux in TWT Magnets vs Demagnetizing Field (set 2)	63
36	Reversible Loss of Flux in TWT Magnets vs Demagnetizing Field (set 2)	63
37	Irreversible Loss of Flux vs Temperature (set 2)	64
38	Reversible Loss of Flux vs Temperature for Various Demagnetizing Fields (set 2)	64
39	Flux Loss vs Temperature (set 4)	65
40	Reversible Loss of Flux vs Temperature (set 4)	66
41	Irreversible Loss of Flux vs Temperature (set 4)	66
42	Reversible Thermal Losses of Peak Axial Field in a PPM Stack after Heating to 255° C for 1 hour	67
43	Long Term Baking at 230° C, Set 2	70
44	Reversible Flux Change at Low Temperature	72
45	Powder Characteristics for Oxidation Test	74
46	Weight Gain for Powder at 250° C in Air	76
47	Pole Design for Periodic Permanent Magnet Circuit for the QR1642 TWT	80
48	Photograph of QR1642	81
49	Environmental Test Station	81
50	QR1642 No. 1 Peak Power vs Frequency Before and After Environmental Testing	101
51	QR1642 No. 1 Peak Power vs Frequency Before and After Environmental Testing	101

LIST OF ILLUSTRATIONS (Cont.)

52	QR1642 No. 2 Peak Power vs Frequency Before and After Environmental Testing	102
53	QR1642 No. 2 Peak Power vs Frequency Before and After Environmental Testing	102
54	QR1642 No. 3 Peak Power vs Frequency Before and After Environmental Testing	103
55	QR1642 No. 3 Peak Power vs Frequency Before and After Environmental Testing	103
56	QR1642 No. 4 Peak Power vs Frequency Before and After Environmental Testing	104
57	QR1642 No. 4 Peak Power vs Frequency Before and After Environmental Testing	104
58	QR1642 No. 5 Peak Power vs Frequency Before Environmental Testing	105
59	QR1642 No. 5 Peak Power vs Frequency Before Environmental Testing	105
60	QR1642 No. 1 Maximum Temperature on OD of Magnets vs Duty Cycle	106
61	QR1642 No. 1 Maximum Temperature on OD of Magnets vs Duty Cycle	106
62	QR1642 No. 2 Maximum Temperature on OD of Magnets vs Duty Cycle	107
63	QR1642 No. 2 Maximum Temperature on OD of Magnets vs Duty Cycle	107
64	QR1642 No. 3 Maximum Temperature on OD of Magnets vs Duty Cycle	108
65	QR1642 No. 3 Maximum Temperature on OD of Magnets vs Duty Cycle	108
66	QR1642 No. 4 Maximum Temperature on OD of Magnets vs Duty Cycle	109
67	QR1642 No. 4 Maximum Temperature on OD of Magnets vs Duty Cycle	109
68	QR1642 No. 5 Maximum Temperature on OD of Magnets vs Duty Cycle	110
69	QR1642 Temperature vs Duty Cycle	111
70	Flow Chart for Manufacture of Sm-Co Magnets	113

LIST OF TABLES

I	Magnet Characteristics (Target Specifications)	2
II	Summary of Results Obtained in Attritor Grinding a 2500 Gram Charge	18
III	Intrinsic Magnetic Properties vs Grinding Time in Large Attritors	19
IV	Second Quadrant Properties of Sintered Magnets Fabricated in the Automatic Press	24
V	Comparison of Functional Measurements in a PPM Stack	26
VI	Calibration of Magnetization for Hysteresis Tracer	32
VII	Hysteresis Tracer Measurements of Alnico and Pt-Co	33
VIII	Properties of Magnets Fabricated in Automatic Press (Set 2)	41
IX	Peak Axial Field in PPM Stacked TWT Magnets	42
X	Irreversible Temperature Coefficients vs Magnetizing Field	45
XI	Low Irreversible Thermal Loss in a PPM Stack	54
XII	Survey of Magnet Characteristics	68
XIII	QR1642 Axial Field in 230° C	69
XIV	Long Term Humidity Test	69
XV	Axial Peak Field after Low Temperature	71
XVI	Temperature Coefficient at Low Temperature	73
XVII	Comparisons of Calculated and Measured PPM Characteristics	78
XVIII	QR1642 No. 1 Step 4.1	83
XIX	QR1642 No. 1 Step 4.3	84
XX	QR1642 No. 1 Step 4.6	85
XXI	QR1642 No. 1 Step 4.9	86
XXII	QR1642 No. 2 Step 4.1	87
XXIII	QR1642 No. 2 Step 4.3	88
XXIV	QR1642 No. 2 Step 4.6	89
XXV	QR1642 No. 2 Step 4.9	90

LIST OF TABLES (Cont.)

XXVI	QR1642 No. 3 Step 4. 1	91
XXVII	QR1642 No. 3 Step 4. 3	92
XXVIII	QR1642 No. 3 Step 4. 6	93
XXIX	QR1642 No. 3 Step 4. 9	94
XXX	QR1642 No. 4 Step 4. 1	95
XXXI	QR1642 No. 4 Step 4. 3	96
XXXII	QR1642 No. 4 Step 4. 6	97
XXXIII	QR1642 No. 4 Step 4. 9	98
XXXIV	QR1642 No. 5 Step 4. 1	99
XXXV	QR1642 No. 5 Step 4. 3	100
XXXVI	Properties of Sintered Sm-Co Magnets	116

SECTION I

INTRODUCTION

There has been a continuing search for permanent-magnet materials with improved magnetic properties for use in high performance devices such as traveling-wave tubes. High energy product, a figure of merit for permanent-magnet materials taking into account both remanent magnetization and coercive force, has been the principal property of interest. High Curie temperature and temperature stability of magnetic properties were also prime concerns.

Extensive investigation of intermetallic compounds between rare-earth and 3d-transition series metals conducted in the Air Force Materials Laboratory led to the discovery of a whole family of permanent-magnet materials of the type RCO_5 , theoretically possessing high energy products.¹ These compounds possess a single easy axis of magnetization together with extremely high uni-axial anisotropy, making them promising candidates for fine-particle permanent magnets.

Technological development of these magnets proceeded along several routes, all with the common objective of producing a mechanically rugged compact of oriented single or nearly single domain particles. Approaches that were taken by various investigators included simple cold press compaction, potting in various epoxies, high pressure isostatic pressing, and sintering of cold-pressed compacts. The latter method, involving powder metallurgical sintering techniques, was the method developed at Raytheon for the rare-earth cobalt material, Sm-Co.²

The objective of the program was extension of laboratory techniques to establish a pilot line for manufacture of samarium-cobalt magnets for permanent-magnet focused, high performance, traveling-wave tube amplifiers. Specifically, manufacturing methods, processes, techniques, and special equipment were to be established for the economical fabrication of samarium-cobalt magnets in production quantities, with characteristics listed in Table I. The superior functional characteristics of magnets manufactured in a pilot line production facility were to be demonstrated in a typical, high performance traveling-wave tube (TWT). The project was divided into four phases, briefly outlined below.

Phase I - Analysis

During this phase, various methods for manufacturing samarium-cobalt magnets were investigated. Each unit step used in a powder metallurgical process was studied with the objective of selecting techniques that were economical and capable of producing high quality magnets.

-
- 1 K. Strnat, G. Hoffer, J. Olson, and W. Ostertag, "A Family of New Cobalt-Base Permanent Magnet Materials", J. Appl. Phys. 38 1001 (1967).
 - 2 D. Das, "Twenty Million Energy Product Samarium-Cobalt Magnet", IEEE Transactions on Magnetism, Vol. Mag. 5. No. 3, Sept. 1969, p. 214-216.

Phase II - Determination of Manufacturing Process

The objective of this phase was to make final selections of processes and techniques that comprise the most economical and reliable manufacturing operation. This determination was based on information obtained in Phase I.

Phase III - Preproduction Pilot Line

The establishment of a pilot line capable of producing traveling-wave tube magnets at a rate of 1000 per month was the objective of this phase.

Phase IV - Microwave Device Application of Samarium-Cobalt Magnets

The objective of this phase was to demonstrate the superior functional characteristics of a Raytheon traveling-wave tube with PPM stack of samarium-cobalt magnets.

Table I. Magnet Characteristics (Target Specifications)

Residual Induction (B_r)	> 7500 gauss
Coercive Force (H_c)	> 7500 Oe
Intrinsic Coercive Force (H_{ci})	> 12000 Oe
Energy Product (BH_{max})	15×10^6 gauss-oersted
Temperature Stability	0.05% per °C
Magnet Life	Flux variation of < 5% over 1000 hours at 150°C for a magnet with load line of minus 1.
Curie Point	> 700°C
Mechanical Properties	
Integrity	< 3% weight loss during normal handling (during shipping and assembly of TWT's)
Hardness	$R_c \cong 50$
Impact Strength	Capable of withstanding normal handling, assembly, and operation of TWT consistent with MIL-5400 Class II environmental requirements.
Flexural Strength	> 5000 psi
MIL-E-5400 Tests	
Corrosion	None
Temperature Extremes	Within 95% of original (-55°C to 250°C) room temperature properties.

SECTION II

FINE PARTICLE RARE-EARTH MAGNETS

The approach to making fine particle magnets was based on the model of single domain particles. In theory, magnetic particles can be reduced to a size where it is energetically unfavorable to form domain walls which cause demagnetization by motion in reverse magnetic fields. In a single domain particle, magnetization reversal occurs by a rotation process requiring applied fields which are a substantial fraction of the magnetocrystalline anisotropy field. In compounds of the form RCO_5 , anisotropy fields in excess of 100 kOe were measured and, on this basis, coercive forces far larger than those of any known materials were predicted for fine particle magnets consisting of these compounds. In addition, some of the compounds had high Curie temperatures, offering the possibility of stability at high temperatures. Finally, measured values of the saturation magnetization indicated that magnets of both high flux density and high energy product might be fabricated from these materials.

The anticipated high energy products were based on certain relationships between the intrinsic magnetic properties. These are illustrated in Figure 1 where the solid lines are the induction (B vs H) and intrinsic ($4\pi M$ vs H) second quadrant hysteresis curves for an ideal fine particle magnet in which the demagnetization process is controlled by the crystal anisotropy. Optimum properties are obtained when several conditions are satisfied. With perfect crystallographic alignment, the remanent magnetization, $4\pi M_r$, is equal to the saturation magnetization, $4\pi M_s$. In material of large magnetocrystalline anisotropy in which the individual magnet particles have an intrinsic coercive force, mH_c , ** greater than $4\pi M_s$, the induction curve is a straight line with an induction coercive force, bH_c , *** equal to $4\pi M_r$. When both conditions are fulfilled and the powder compact is fully dense, the result, as indicated in Figure 1, is the largest theoretical maximum energy product, $(BH)_{max}$, equal to $(2\pi M_s)^2$.

For the specific compound $SmCo_5$, $4\pi M_s$ is 9600 gauss and the anisotropy field, H_a , is ≈ 290 kOe. A value of H_a of this magnitude made an mH_c sufficient to approach the theoretical maximum $(BH)_{max}$ of 23×10^6 GOe seem feasible. On the other hand, low mH_c (especially when it is of the same order or less than $4\pi M_s$), imperfect alignment and the inability to achieve theoretical density result in hysteresis curves of the type illustrated by the broken lines in Figure 1. Insufficiently aligned powders and low density result in a remanent magnetization, $4\pi M_r$, less than the maximum possible $4\pi M_s$. In this situation, the energy product will always be less than the theoretical maximum, as the comparison of the $(BH)_{max}$ areas in Figure 1 illustrates.

* B_r is also used for remanent magnetization.

** H_{ci} is also used for intrinsic coercive force.

*** H_c is also used for induction coercive force.

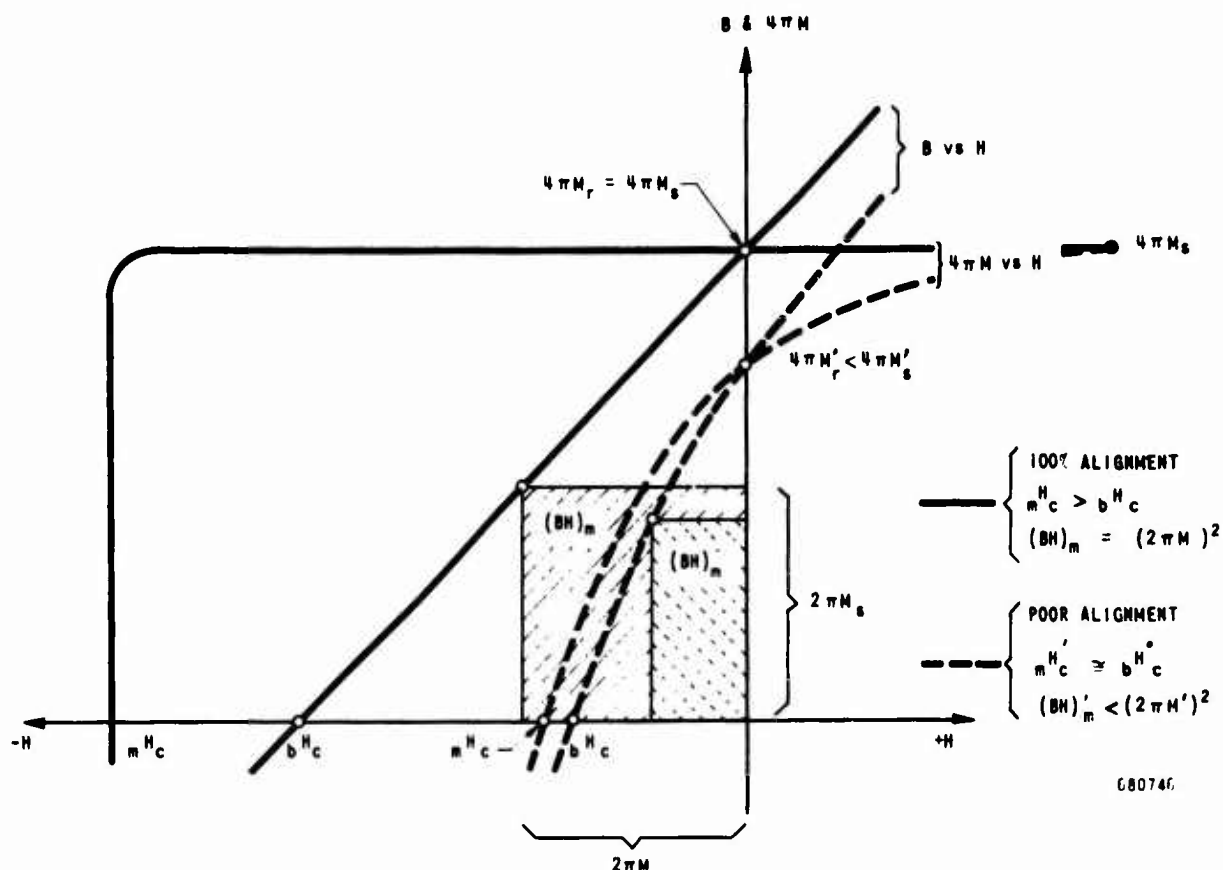


Figure 1 . Hysteresis Loops Illustrating Factors Effecting Maximum Energy Product

The initial efforts to develop fine particle magnets based on rare-earth cobalt compounds with high crystal anisotropy were disappointing. Crystal anisotropy controlled magnets require micron size particles, a size range readily achieved by any one of several comminution techniques. However, for the RCO_5 compounds investigated, values of mH_c were strongly dependent on processing parameters, particularly the method of grinding. It was found that size reduction was accompanied by a gradual increase in mH_c which, after reaching a peak of several thousand Oe, abruptly dropped with further grinding. With particle sizes below the peak in mH_c , it became progressively more difficult to align the powders. This behavior was common to most of the rare-earth magnet materials of interest. The one exception was SmCo_5 in which values of mH_c exceeding 15,000 Oe were obtained, despite a similar dependence on grinding.

The dependence of coercivity on grinding has been explained by distinguishing the role of lattice defects and surface defects introduced in grinding; the latter act as nucleation sites for domain formation and lower the coercive force, whereas lattice defects and their associated stress fields impede domain wall motion and increase the coercivity. The strong dependence of second quadrant properties, particularly coercive force, is attributed to domain walls being driven into distinct pinning states related to the value of the magnetizing field.

The defects introduced by the grinding deformation may also reduce the uniaxial anisotropy, and thus lower the local magnetocrystalline anisotropy field. In this case not only would the coercive force be reduced but, due to the increased difficulty of magnetically aligning the particles, the remanent magnetization and energy product would be lowered as well.

Although the specific nature of the defects is not clear, there is a body of experimental evidence to support their existence and importance. For instance, particles whose surfaces have been chemically polished show a marked improvement in coercivity, presumably due to removal of domain nucleation sites. Thus the concept of domain wall vs rotation controlled magnetization reversal appears to have a reasonable experimental basis.

Although various rare-earth cobalt alloy systems were studied at Raytheon, the unique behavior of Sm-Co led to an emphasis on this material, which culminated in a laboratory process for making high coercivity and high energy product magnets. The laboratory process developed at Raytheon consisted of melting a Sm-Co alloy and reducing it to powder by a short, high impact grinding procedure. Magnetically-aligned cold pressed samples were sintered in a carefully controlled manner to produce dense compacts of high energy product magnets. In addition to producing the densification necessary for achieving a high induction, the sintering procedure appeared to remove those surface imperfections responsible for domain nucleation and low coercive force. Furthermore, during sintering, preferential grain growth occurred, resulting in a larger percentage of favorably aligned particles than were found prior to sintering. The excessive grain growth that accompanies the sintering of single phase SmCo_5 was kept at a minimum by deliberately adjusting the alloy composition in melting to incorporate Sm_2Co_7 as a grain growth inhibitor.

From this laboratory experience, the following general process for fabricating Sm-Co permanent magnets was established:

- a. A two-phase alloy is formed by melting the components, Sm and Co, in a suitable crucible surrounded by a non-oxidizing atmosphere.
- b. The melted ingot is crushed to a size suitable for further grinding (average particle size of approximately $10\ \mu$). Wet grinding requires a drying process that does not oxidize the powder.
- c. After drying, the powder is pressed in an aligning magnetic field to a size close to the dimensions required in final application. Pressed compacts are approximately 65% of theoretical density and require further densification to greater than 90% by sintering in a non-oxidizing atmosphere.
- d. For traveling-wave tube applications, sintered ring magnets are machined to final dimensions, magnetized, measured, thermally cycled above the operation temperature to stabilize magnetic properties, measured once again, and then split.

From this laboratory process, the aim of this program was to determine specific methods and equipment for economical quantity production of high performance magnets.

SECTION III

UNIT PROCESSES FOR SAMARIUM-COBALT MAGNETS

1. MELTING

The first unit process in manufacturing Sm-Co magnets is the alloying of the component metals. Throughout the program, sample lots of samarium were purchased from several sources. Evaluation indicated that some samples contained second-phase impurity exceeding 10 volume-percent, although less than 5 volume-percent was necessary for a good magnet alloy. This requirement was met by a domestic source and a foreign source; the greater part of the metal used in this program was supplied by the former. The material was specified to be 99.9 weight-percent pure according to spectrographic analysis. Cobalt was supplied in the form of shot of 99.9 weight-percent purity. The as-received material is fired at 1140°C for 2 hours in dry hydrogen prior to use.

Cost for samarium metal ranges between \$90 and \$150 per pound, depending upon quantity purchased and purity. Cobalt costs between \$3 and \$6 per pound.

Consideration of the Sm-Co phase diagram (Figure 2) suggests some of the problems to be expected in achieving uniform, reproducible alloys. Due to the peritectic melting of samarium compounds in this system, the relative amounts of the various phases will depend on the starting composition, cooling rate, and temperature uniformity during solidification; in short, the details of the melting practice will affect phase composition.

Another difficulty arises from the high vapor pressure of samarium. Vacuum melting is not appropriate and even in an inert atmosphere the alloy composition must be adjusted to compensate for the anticipated loss of samarium by evaporation. Finally, the choice of a crucible material is critical because of the prohibitive cost of high quality crucibles, as well as the dangers of impurity contamination and crucible failure arising from the high chemical reactivity of samarium.

Despite these difficulties, a laboratory scale melting procedure was developed, and at the start of the program melting was done in an rf (350 kHz) furnace of 50 g capacity with high purity helium at atmospheric pressure providing a protective atmosphere. The degree of alloy contamination from reaction with the crucible was kept at an acceptable level by rapid melting in recrystallized alumina. To further minimize impurity pick-up and to guard against premature crucible failure, a technique was developed for coating the crucible with a non-reactive layer. A slurry consisting of yttria powder in nitro-cellulose was painted on the crucible interior, dried and air fired at 1700°C prior to use.

In the 50 g size, the charge was cooled in the crucible after melting, and the alloy had to be broken from the crucible. Under these conditions it was found that a charge composition of 39 weight-percent samarium gave the best magnetic properties. However, because of the limited capacity, an immediate requirement was to evaluate and purchase melting equipment of production capacity.

Experimental melts were made by arc melting and low frequency induction melting. The absence of a crucible made arc melting attractive, but the need to remelt several times to achieve metallurgical homogeneity and the expected difficulty in scaling-up the process to make large melts led to its elimination.

Results of low frequency induction melting were encouraging. After successful fabrication of high quality magnets from several experimental alloys,

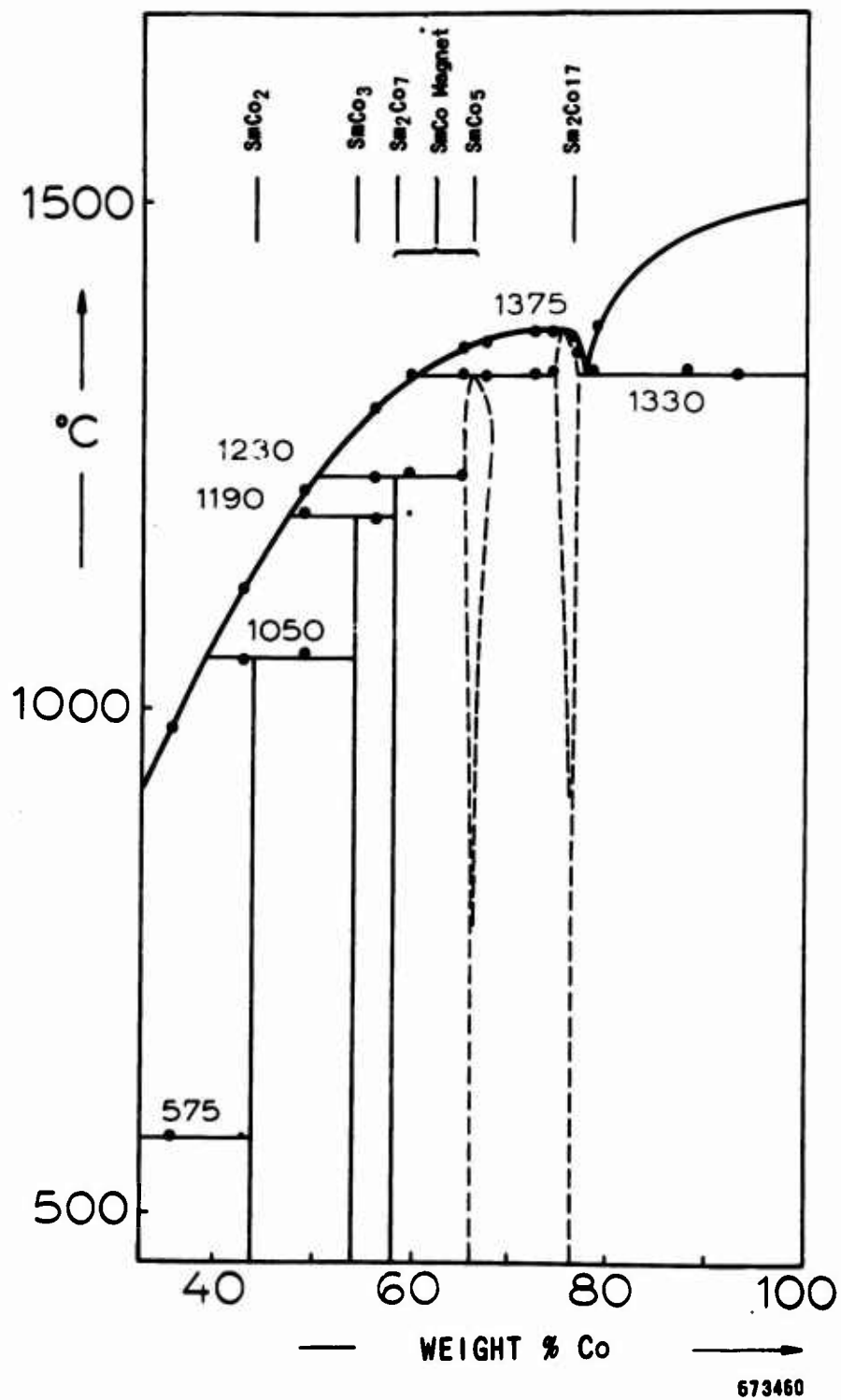


Figure 2. The Sm-Co Phase Diagram

a complete system was acquired and installed in the pilot line as shown in Figure 3. This equipment is capable of melting charges of up to 300 lb in 10^{-5} torr or in a purged, controlled atmosphere. There are provisions for alloy additions during melting, temperature measurement, and casting of the alloys in either chilled or heated molds. The motor generator supplies power at 9600 Hz. Built-in variable capacitors in the circuit allow for matching with the load, and there is an additional feature that provides continuous maintenance of a pre-set power input during the melting operation.

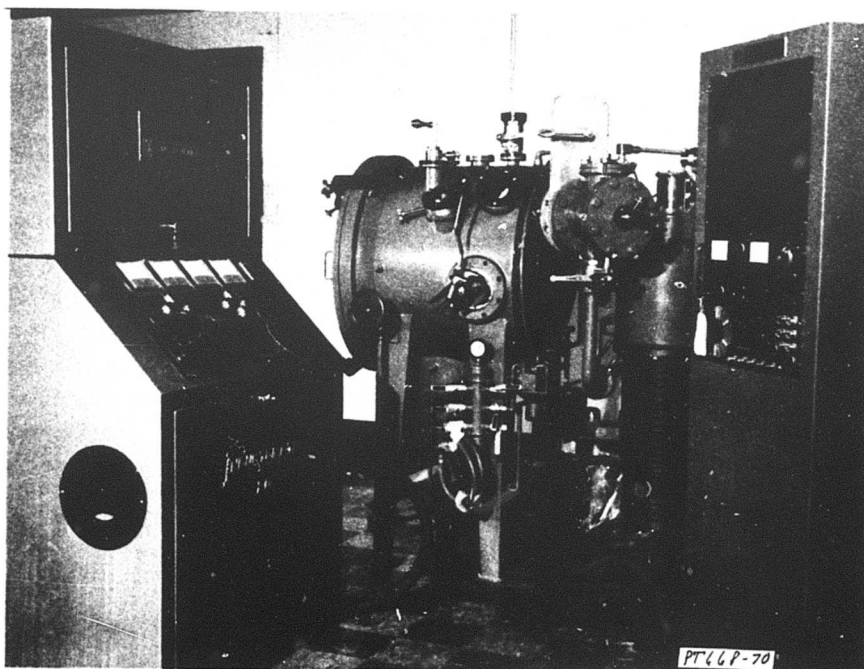


Figure 3. Pilot Line Melting Furnace

Prior to alloy melting the system is pumped to below 5×10^{-4} torr. A partial pressure of helium is introduced to purge any residual air in the gas lines, followed by a final pump down to below 5×10^{-4} torr. The chamber is back-filled with helium to a slight positive pressure (~ 1 psi).

Melting schedules were developed for 600, 1500 and 2500 gram charges, with a primary concern of avoiding thermal shock failure of the recrystallized alumina crucible. In this procedure the power is increased slowly and melting requires extended times. When melting appears to be complete, the alloy is held for 10 additional minutes at 1500°C , and then the power is turned off. The charge is allowed to solidify and cool in the crucible (requiring 1 - 2 hours prior to removal), and the crucible is broken to remove the alloy.

At each increase in the melt size, a complete metallographic survey was made of a representative ingot, including views of vertical and horizontal sections. Typical views, presented in Figure 4 show a structure of two major phases. Both X-ray and electron probe measurements indicate that the light phase is SmCo_5 . The dark areas are primarily Sm_2Co_7 with small amounts of the other phases not yet identified, but most likely SmCo_3 and possibly SmCo_2 . The phase distribution is comparable in the various ingot sizes, although, as a rule, alloy uniformity was observed to suffer in larger melts due to a reduction in cooling rate.

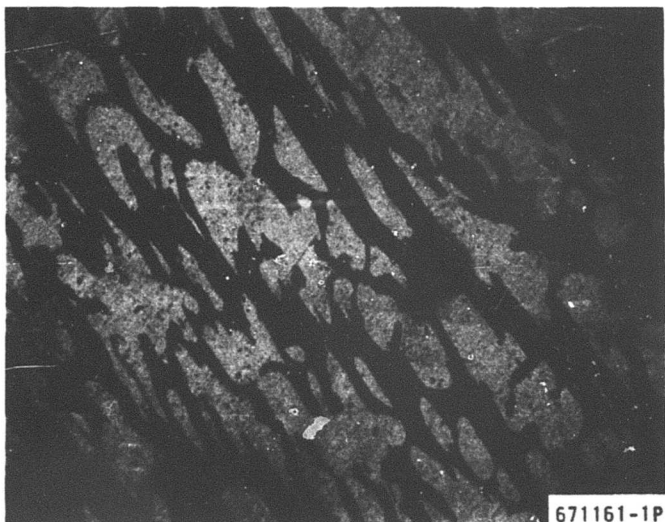
The absence of large scale segregation in the magnet alloy was confirmed in part by magnetic measurements of TWT magnets in the PPM format. The peak field values, as well as their uniformity, were not significantly altered when comparing differences in melt size, samarium of variable purity obtained from several manufacturers, and holding times at the melting temperature varying from 10 to 40 minutes.

Despite the success achieved with the melting procedure, the method was considered a temporary expedient from the start. The cost of a single-use alumina crucible contributes about \$8 to the cost of a pound of the finished alloy. It was also felt that, by solidifying in the crucible, alloy quality might not be as high as possible. Finally, in spite of the precautions taken, premature crucible failures remained a persistent problem, representing a significant economic loss. The ultimate aim was to develop a melting and pouring technique using a rugged, low cost and preferably re-usable crucible.

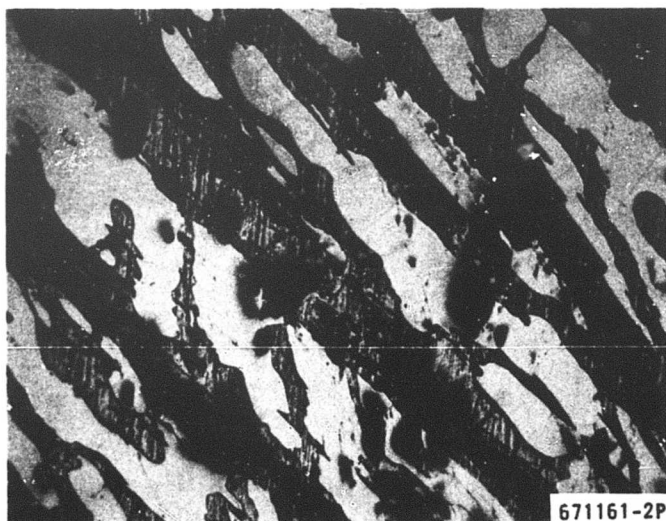
A series of melts of 600 gram size was made in an alundum crucible. All procedures were similar to standard practice except that the molten alloy was cast into a water-cooled copper mold. A protective layer of material formed on the crucible which prevented corrosion and degradation. As a result the crucible was used for several melts before being discarded.

Alloy charges of 2500-gram, 6000-gram and most recently 7500-gram size have been successfully melted in alundum crucibles and chill cast in a large copper mold. In the largest size, the average cooling rate measured on the top surface of the cast alloy is about $100^\circ\text{C}/\text{min}$ as compared to a measured rate of $30^\circ\text{C}/\text{min}$ for a 2500-gram melt solidified and cooled in the crucible. Metallographic sections of cast alloy are shown in Figure 5. The phase composition appears to be comparable to Figure 4, but, because of more rapid cooling, the as-cast material has a finer phase distribution. The quality of finished magnets has remained high and this procedure has become standard practice. Reuse of the larger alundum crucibles has been limited by cracking during crucible cooling. Nevertheless, the procedure has already resulted in more convenience as well as reduced costs.

(a)



(b)



(c)

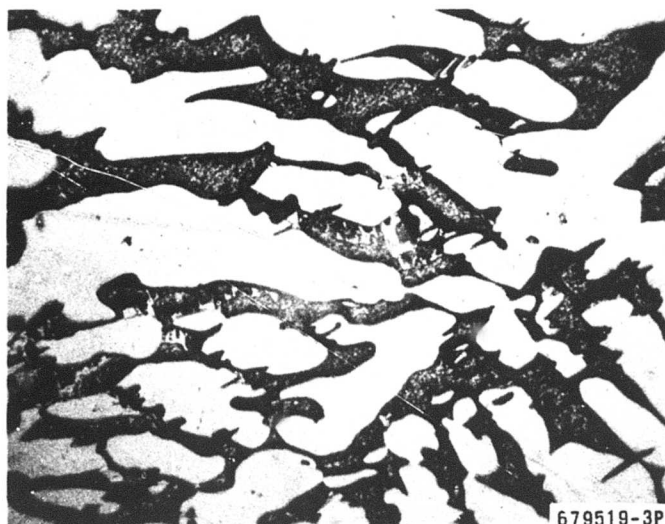
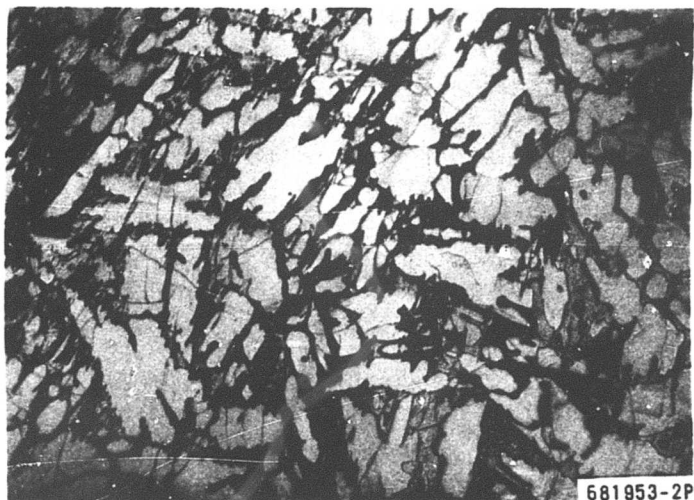


Figure 4. Views from vertical sections of Sm-Co alloy melts of (a) 50 gram, (b) 600 gram, (c) 2500 gram size solidified in the crucible, showing the distribution of the light SmCo_5 and dark Sm_2Co_7 phases. (Magnification 100X)

(a)



(b)



(c)



Figure 5. Views from vertical sections of (a) a 600 gram Sm-Co alloy casting, and (b) and (c) a 3500 gram Sm-Co alloy casting, showing the distribution of the light SmCo_5 and dark Sm_2Co_7 phases. View (c) is taken from near the chill interface where cooling is most rapid. (Magnification 100 X).

2. ALLOY CRUSHING AND GRINDING

Reducing the alloy to powder prior to pressing is one of the most critical steps in the manufacturing process. The grinding procedure must produce an unoxidized, uncontaminated powder having the following characteristics for optimum magnetic properties:

- A fairly narrow particle size distribution
- Particles with a minimum of both internal strain and surface damage.

The latter requirements are best achieved when size reduction occurs by high energy impact shattering of the particles rather than by abrasive wear. The grinding process itself must be economical and adaptable to a range of charge sizes to allow for variations in manufacturing demands.

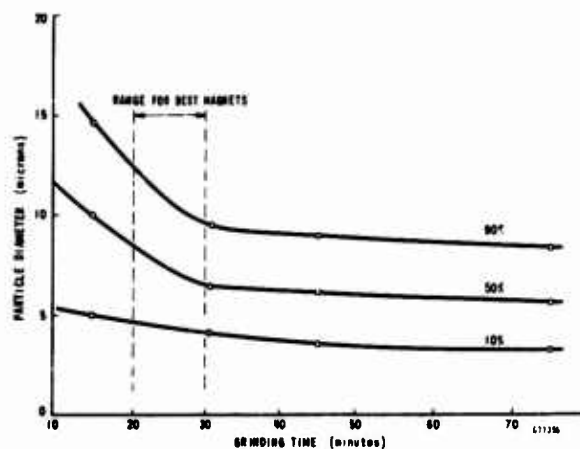
In laboratory scale grinding, alloy was first crushed in a jaw crusher and then ground in a shatter box. A motor-driven jaw crusher with adjustable output spacers was installed for the pilot line. The spacing was set to give a product which passes through 5 mesh with 90% remaining on 50 mesh.

From the start, a replacement for the laboratory grinding method was sought. Shatter box grinding is not amenable to large charges, and repeatable results were difficult to obtain. Vibratory, attritor and ball mills were considered more appropriate and were evaluated. Results of ball milling were not encouraging due to powder agglomerating and adhering to the corners of the grinding chamber.

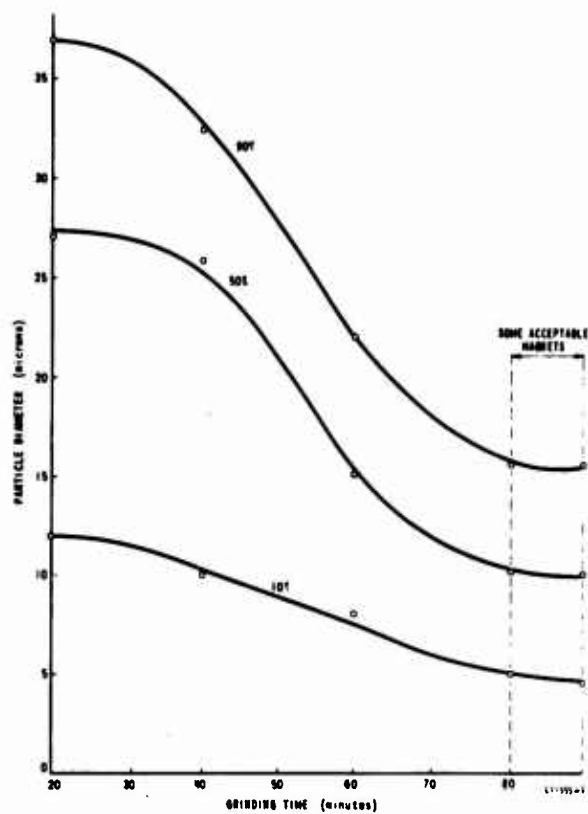
Systematic experiments were undertaken at vendor facilities under our supervision to evaluate both attritor and vibratory milling. One pound charges were ground while varying the milling parameters to determine a procedure for reproducing the best results obtained in the shatter box. Methods of evaluation consisted of:

- Particle size distributions measured directly from high magnification photomicrographs using a Leitz optical particle size analyzer.
- Measurements of peak axial field before and after temperature stabilization of TWT magnets stacked in the PPM format.
- Measurements of second quadrant properties.

To protect the powder from oxidation, grinding by both methods was done in alcohol and toluene while vibration milling was attempted in argon as well. Acceptable powder was obtained only when toluene was the grinding fluid. Figure 6 shows the grinding efficiencies of the two methods. The data



(a)



(b)

Figure 6. Comparison of grinding efficiency of a 1 lb charge in (a) a 1.5 gallon attritor mill and (b) in an 0.75 gallon vibratory mill.

are plotted as the percentage of particles below a given size vs grinding time. Also indicated is the range over which acceptable magnets were prepared. It is evident that longer times are required in the vibratory mill to achieve a similar size reduction. In addition, the product has a broader distribution as evidenced by the spread between the 90% and 10% fractions. Finally, the quality of magnets made from vibratory ground powders was inferior to that of magnets made with attritor ground powder.

Examination of the particles with high resolution scanning electron microscopy indicated the reason for the superiority of attritor ground powder. The particles have faceted surfaces typical of cleaved particles and are similar in appearance to those produced in the shatter box, whereas rounded particles produced by abrasion appear in the sample from the vibratory mill. Adjusting such grinding parameters as fill factor and ball size might make the product of vibratory milling comparable to attritor ground powder. However, in view of the encouraging attritor results, a laboratory attritor of 250-gram capacity was obtained along with a production attritor with a range of capacities from 500 to 2500 grams. The variety of charges is accommodated by substituting milling chambers from 2 pints to 1.5 gallons in size. At this point work with other grinding techniques was halted and experiments continued exclusively in the attritor mills.

For best results in the attritor, it was determined that an intermediate grinding step was needed after crushing, and roll milling proved adequate. The jaw crushed product is cycled through the roll mill several times, as the roll separation is reduced, until all material is ground to -50 mesh (less than 300 microns). This procedure, involving repeated processing and intermediate sieving to separate the oversize particles after each cycle, proved time consuming. Moreover, the powder would occasionally spark and in some instances would completely ignite due to the high impact of the rollers. Providing an inert atmosphere was not convenient, so other intermediate grinding approaches were considered. A disc grinding mill appeared suitable for the pilot line and was installed. Modifications to the equipment were made so that grinding is done in an inert gas atmosphere, thus eliminating any fire hazard.

Experiments were carried out to establish the conditions for producing powder comparable to the satisfactory product of roll milling. Figure 7 shows similar particle size distributions produced by roll milling and after pulverizing in a single pass with the disc spacing set at 0.005 in. Particles greater than 60 microns, while accounting for only 2% of the particles, occupy about 50% of the volume.

To determine the dependence of particle size on grinding time and to test the effect of a more uniform attritor charge, a disc pulverized sample was sieved through a -200 mesh screen to separate the larger particles. Both the as-pulverized powder and the sieved powder underwent attritor grinding for various lengths of time in the smaller attritor. Despite the larger particles in

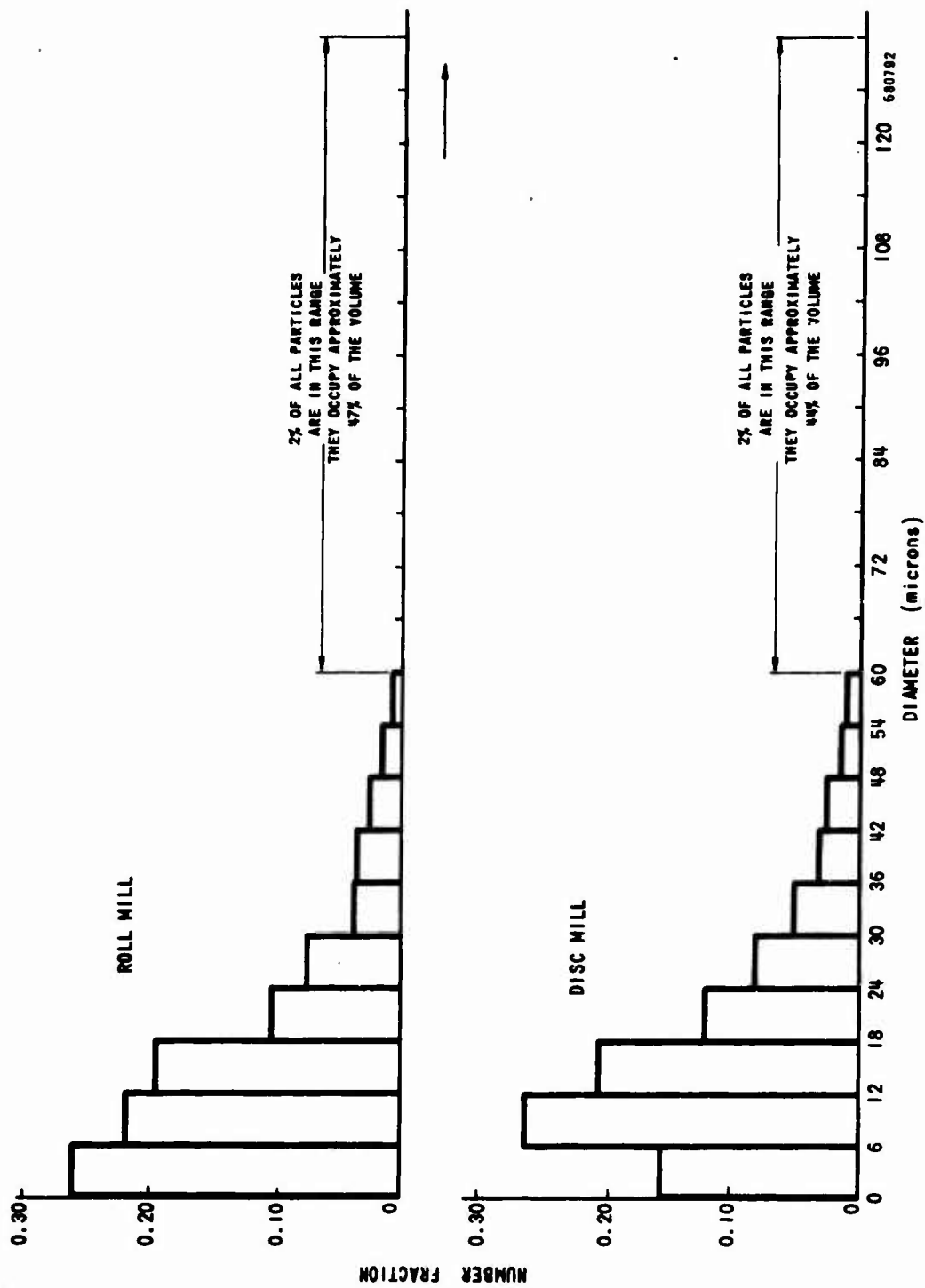


Figure 7. Comparison of particle size distribution obtained in roll mill and disc mill intermediate grinding.

the initial unsieved material, after grinding for 20 minutes the powders were indistinguishable and both made acceptable TWT magnets.

When another alloy was pulverized with a disc spacing of about 0.008 inch, the powder and magnet properties were similar after 20 minute attritor grinding. These results indicate that in attritor grinding, the large particles have a high probability of encountering a grinding collision and are quickly reduced in size. Thus the final particle size of attritor grinding is relatively insensitive to small differences in the pulverized charge.

These results led to the adoption of a standard grinding procedure in which the attritor charge consists of pulverized powder produced in a single pass with the 0.008 in. disc spacing. This is followed by attritor grinding for 20 - 22 minutes, depending on which time gives the better magnets when fabricated from sample lots of powder.

Figure 8 compares particle size distributions for several alloys after standard 20 minute attritor grinding and one powder sample after 18 minutes in the attritor. The results are plotted on probability paper as the volume percent greater than a stated particle size vs size. With the exception of the 18 minute ground material, all gave acceptable magnets and all have an average particle size in a range between 15 and 21 microns. However, the unacceptable powder has only a slightly higher average, with the major differences in the less than 10 micron particle size range. This magnetic property dependence on grinding is no doubt related to factors other than particle size (such as particle surface characteristics and lattice perfection), but size distribution is still the only means of characterizing good vs poor material short of testing finished magnets.

With the increase in alloy melting capacity, efforts to increase the grinding batch size continued. An experimental charge was ground in the large attritor and samples were removed at 2 minute intervals up to 14 minutes and at 1 minute intervals thereafter. A complete particle size analysis was made and TWT ring magnets fabricated from this sample.

The results are summarized in Table II with values of the volume weighted mean particle diameter, D_v , and the sintered density included. As indicated, magnets of acceptable quality for TWT* application are produced with powders ground for between 14 and 18 minutes. A comparison with earlier results is presented in Figure 9, where the axial peak field measured in the PPM stack after a 1-hour cycle at 225°C is plotted against the maximum sieve aperture through which 90% of the particles pass. The particle size for acceptable magnets is somewhat larger when produced in the large attritor than in the 250 gram size. Intrinsic magnetic properties are included in Table III and the range over which magnets are acceptable for TWT applications is indicated. The intrinsic energy product $(4\pi MH)_{\max}$ gives the best correlation with PPM stack measurements.

* For complete details on TWT acceptability, see Sections III-8 and IV.

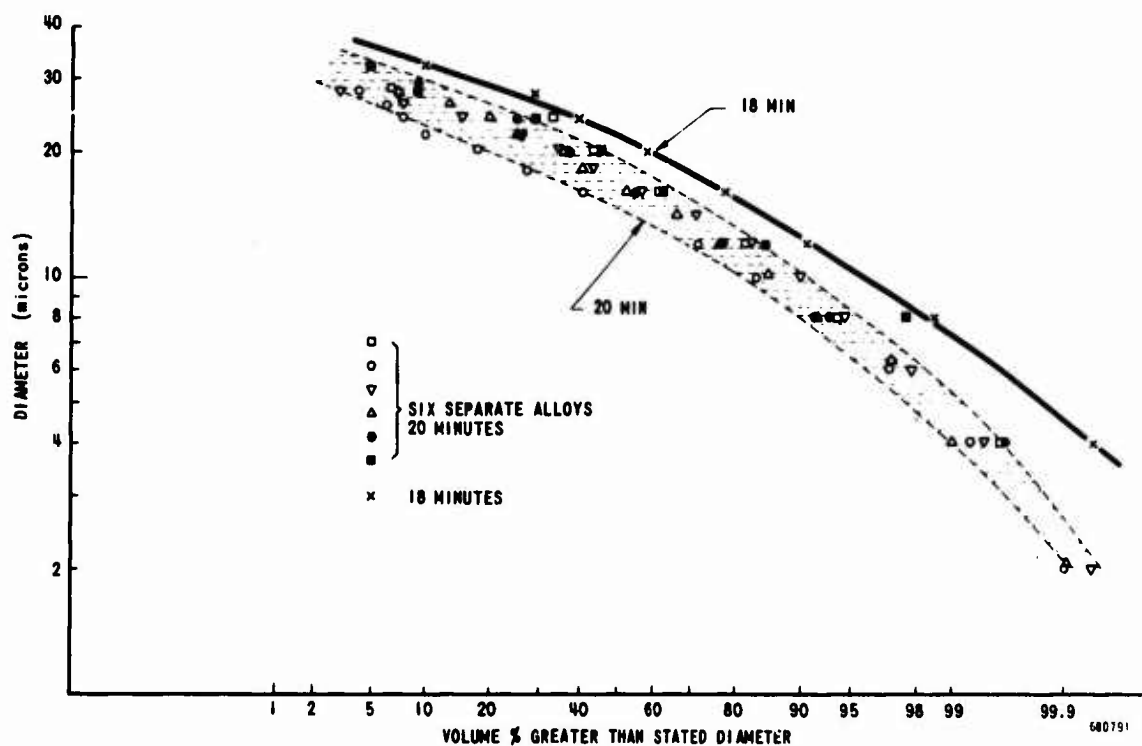


Figure 8. Particle size distribution for standard 20-minute attritor grinding compared to 18-minute grinding.

Table II
Summary of Results Obtained in
Attritor Grinding a 2500-gram Charge

Total Grinding Time (min)	\bar{D}_v (microns)	Percent of Theoretical Density (%)	Peak Axial Field in PPM Stack (Oe)	
			Before Heating	After Cycling 1 Hour at 225°C
6	--	90.8	2850	575
12	32	86.5	3375	1625
14	31	94.1	3850	3500
15	29	93.4	3850	3525
16	28	93.4	3850	3525
17	26	92.5	3675	3300
18	25	92.5	3850	3475
19	24	94.5	3425	2825
20	23	94.4	3025	2225
21	--	93.1	2700	1175
22	--	93.1	2325	1150
23	--	90.0	575	200
24	18	89.7	475	225

Acceptable for TWT Application

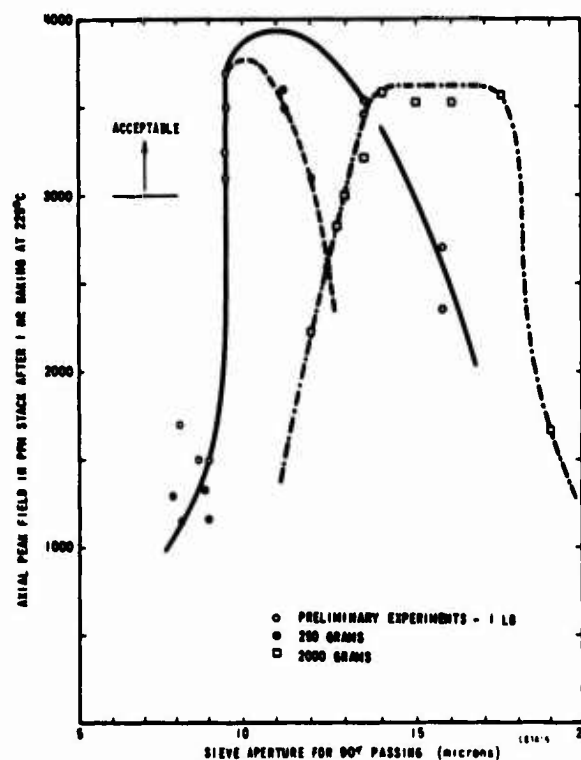


Figure 9. Axial Peak Field in a PPM Stack vs Particle Size for Attritor Grinding

Table III

Intrinsic Magnetic Properties vs
Grinding Time in Large Attritor

Grinding Time (min)	B _r (G)	H _c (Oe)	H _{ci} (Oe)	(4πMH) _{max} (10 ⁶ GOe)	(BH) _{max} (10 ⁶ GOe)
6	5,760	5,100	20,000	36.4	10.8
12	7,130	6,350	28,500	71.8	12.1
14	8,050	6,800	24,500	80.5	14.1
15	8,100	6,950	22,500	76.3	14.7
16	8,150	7,000	21,500	78.0	15.3
17	8,170	6,450	18,500	53.2	14.9
18	7,880	7,200	20,500	78.0	14.7
19	8,270	6,650	15,500	49.8	15.1
20	7,810	6,200	12,000	40.6	13.7
21	7,630	4,250	5,000	24.2	12.9
22	7,830	4,400	5,100	27.6	9.6
23	7,280	2,000	2,000	12.8	9.0
24	7,270	2,000	2,000	13.7	7.5

Acceptable for
TWT application

3. DRYING TECHNIQUES

The laboratory method used for drying the ground powder consisted of bell-jar vacuum evaporation of the toluene vehicle. To avoid the reduced drying rates due to freezing of the toluene, the powder slurry is heated to 30°C while in the bell jar. The original laboratory system was capable of drying 50-gram lots with a cycle time of 40 minutes per lot.

In anticipation of increasing powder requirements, manufacturers of commercial vacuum drying equipment were contacted. Of the available types, roll dryers are designed for softer materials; problems of clogging and degradation of the vacuum valves were anticipated with tumble dryers.

Several commercial shelf dryers were appropriate for the pilot line but none had all the features considered necessary for rapid, economical drying of samarium-cobalt powder. Therefore, a vacuum shelf dryer was designed and built. Similar in principle to the laboratory system, its special features include:

1. 5 electrically heated aluminum trays, each with a capacity for holding at least 2 lb of dry powder.
2. A specially designed cold trap with dry ice-alcohol coolant and a pumping rate of 2 quarts of toluene per hour (the amount of toluene in 10 lb of powder is about 0.9 quart).
3. A vacuum pump and associated plumbing compatible with this rate.

The procedure evolved consists of decanting the toluene after grinding and placing the alloy in the trays. Additional toluene is removed by pressing the wet powder with absorbent paper towels. After the trays are loaded in the dryer, the system is purged with nitrogen gas for several minutes, heater power applied, and the main vacuum valve opened. Toluene evaporation is initially very rapid as evidenced by the fact that the temperature measured in the powder slurry falls to -25°C within 5 minutes. Thereafter, the temperature slowly rises.

Temperature measurements of the powder slurry serve as an adequate process control, since drying is complete when the temperature approaches 30°C . The corresponding drying time for a 10-lb load is about 30 minutes. At this time, the heaters are turned off, the main vacuum valve closed, and the powder is exposed to air after back-filling the bell jar with nitrogen gas. Powder processed in this manner has been used in magnet fabrication without any change in magnet quality when compared with results from powder processed in the laboratory dryer.

With the available pumping capacity and drying rate, up to 15 lb of powder can be dried in a one-hour cycle with no increase in the size of the components. In a longer processing cycle, somewhat larger quantities of powder could be dried in this system with the addition of a slightly larger bell jar and trays with greater capacity. This is due to the fact that the trap can be kept in almost continuous use by periodically closing the vacuum valve and draining the toluene condensate, an operation requiring about 5 minutes.

4. STORING

Oxidation of Sm-Co alloy occurs at room temperature and it was anticipated that this might become a significant problem after long storage periods. Although dried powder exposed to air for periods in excess of one week has been used to produce acceptable magnets, other powder ground only slightly finer discolored and yielded magnets of inferior quality. Therefore, after grinding and prior to drying, powder is stored in toluene in sealed vessels. No deterioration has been detected after several weeks of storage. With only limited powder requirements, the powder can be dried in small quantities as the need arises. However, with the large quantities required, an inventory of ready-to-press dry powder must be kept on hand. To minimize the hazards and to protect the powder from oxidation, this material is stored in a nitrogen dry box without noticeable deterioration.

5. PRESSING

Samarium-cobalt magnets made in the laboratory were dry pressed in an aligning field produced with an electromagnet. The entire cycle of die filling, field application, pressing, part ejection, etc. was performed manually. The basic consideration in selection of a commercial automatic powder compacting press was the adaptability of the press cycling to the magnetic field application.

The aligning magnetic field must couple synchronously with the press during the entire pressing cycle, and press programming must be sufficiently flexible to allow for adjustments in the cycle for maximizing powder alignment. Loading capacity, variability in rate, accessibility of vendor service, and generally, judgment of overall quality were also considered.

A 100-ton automatic powder compacting press manufactured by Mannesmann Meer Co. fulfilled these requirements. It has daylight clearances of 27 in. horizontal and 37 in. vertical with a 4 in. ram stroke, and is fully automatic. The press can be operated at up to 12 strokes per minute and can be independently sequenced by pressure, distance and time. The feeder system attached to the back of the press consists of an explosion-proof hopper feeding the shuttle. Dies for the press are designed taking into consideration a 15% shrinkage after sintering. Die and punch clearances are maintained at 0.002 to 0.005 in.

The electromagnet for powder aligning was built by Raytheon's Microwave and Power Tube Division. Major characteristics of the electromagnet are listed below.

1. 550 turns of 0.005 copper foil with Mylar insulation between each turn.
2. 1/2 in. cold-rolled steel encasement with stainless hub. Dimensions: 24 in. overall OD x 8 in. ID x 8 in. high.
3. Weight: 600 lb
4. Field: 5700 gauss at 50 A open bore
5. Location in press: riding on lower ram.
6. Sorensen Nobatron DCR 150-70 A power supply, rated for 150 V, 70 A containing silicon rectifiers.
7. Magnet supply control unit made by Raytheon (keyed to the press relay deck and triggered by ram location). Polarity reversals are accomplished with mercury switches.

A photograph of the automatic powder compacting press and electromagnet power supply is shown in Figure 10 and the die set for traveling-wave tube magnets is shown in place in Figure 11.

Once the press is aligned and ready for operation, the hopper is filled with pretested powder. The die cavity is gravity fed and the amount of powder loaded is of constant volume, determined by the position of the lower punch. When the press cycle starts, the upper punch, with repelling remanence, enters the top lip of the die, pauses, and the dc power supply is triggered by a relay; the aligning field of 8 - 10 kOe is switched on, allowing the loose powder to align.

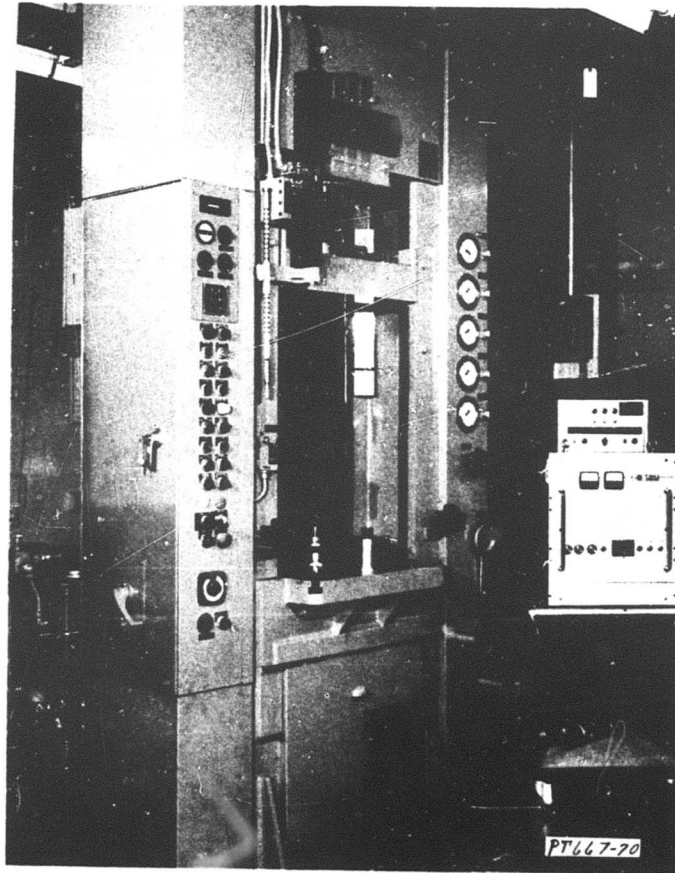


Figure 10. Automatic Powder Compacting Press and Electromagnet Power Supply



NOT REPRODUCIBLE

Figure 11. Die Set in place for Pressing Traveling-Wave Tube Magnets

At completion of the down stroke there is a dwell with the field on, followed by field reversal to demagnetize the compact. The electromagnet turns off as the upper punch leaves the die. The die strips downward bringing the mandrel with it and the part comes flush to the top of the die table and is pushed off by the shuttle on the next filling.

Samples were prepared as a function of applied load and aligning field, and green density, sintered density, second quadrant properties, and alignment factor $4\pi M_g/4\pi M_r$ were determined. Alignment of green pressed samples was found to be approximately 85% and 94% after sintering in most cases, and depended only slightly on aligning field. Fields between 8 - 10 kOe appeared adequate.

Green and sintered density as a function of loading is illustrated in Figure 12, and although there is a dependence of the former, there is little for sintered density achieved at 1130°C for one hour. Second quadrant properties are included in Table IV and little variation in properties was found with loading, as might be expected in view of the relative independence of density on loading. The intrinsic coercive force was also found to be constant at about 23,000 Oe. The inductive coercive force, H_c , is somewhat lower than the target of 7500 Oe, but as pointed out in earlier reports, performance in a PPM stack is more closely related to intrinsic than induction properties.

Table IV
Second Quadrant Properties of Sintered
Magnets Fabricated in the Automatic Press

Loading, k _{psi}	B_r , Gauss	H_c , Oe	$(B \times H)_{max}$, GOe $\times 10^6$
58.8	7990	6000	13.6
84.0	6470	5700	9.8
92.4	7960	6750	14.6
100.8	7850	6600	14.1
126.0	7870	7000	14.7
142.8	7870	7100	14.6

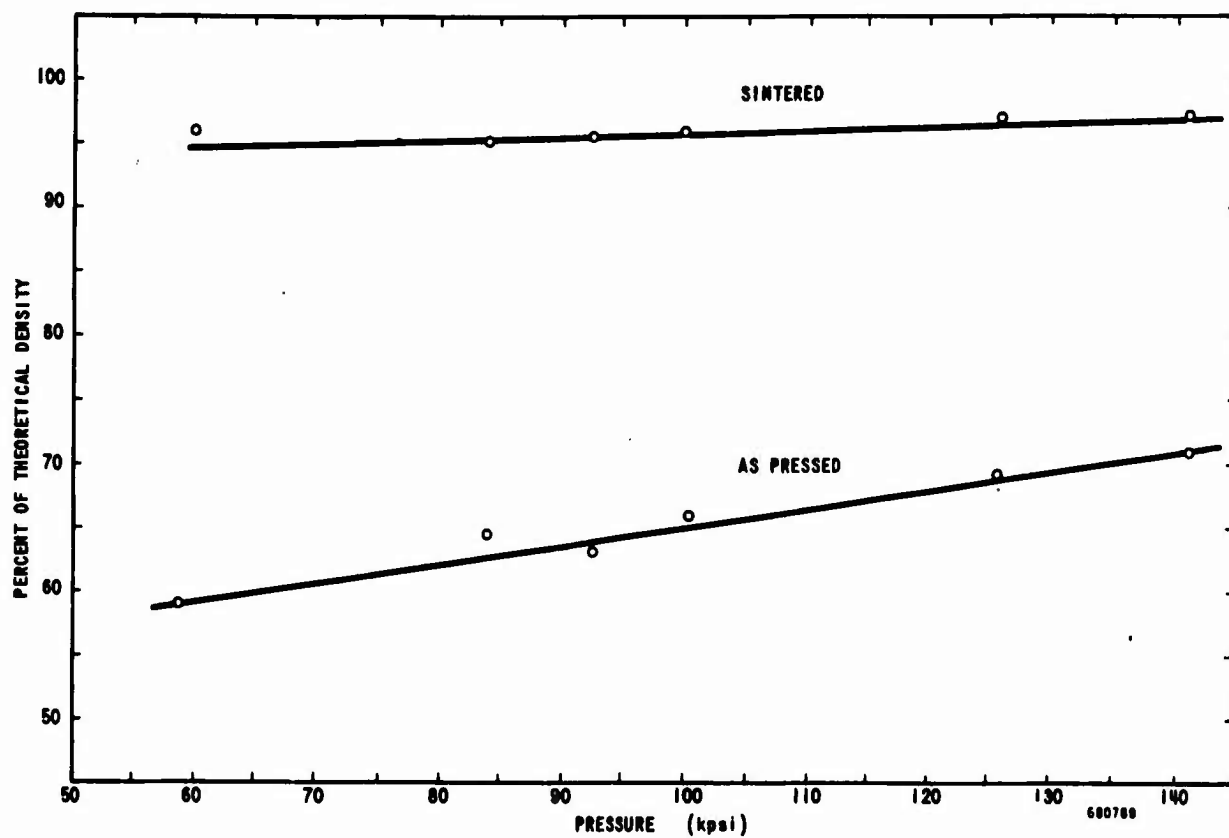


Figure 12. The Effect of Press Loading on As-Pressed and Sintered Density

6. SINTERING

Prior to the start of this program, a sintering furnace with pilot line capacity was acquired. It was chosen on the basis of design features that experience with laboratory facilities had indicated were necessary. The furnace consists of three 6-inch diameter tube elements separately controlled to maintain a set temperature within $\pm 0.5^\circ\text{C}$ along a 22-inch hot zone. Sintering is done in an atmosphere of pre-purified helium. Magnetic properties similar to those obtained under laboratory conditions were reproduced in this equipment by maintaining a constant temperature of 1130°C for 1 hour.

A change in the sintering temperature or the time at temperature has a strong effect on magnet properties. Magnets, fabricated from a typical alloy and processed into powder as part of a standard run, were sintered for one hour at 1120°C , 1130°C , and 1140°C . A second set of magnets was sintered for 2 hours at 1110°C , 1120°C , and 1130°C . Results comparing functional measurements (in a PPM stack) with intrinsic properties are presented in Table V. Acceptable magnets are obtained in one hour when the sintering temperature is kept within $\pm 10^\circ\text{C}$ of the standard. At the lowest sintering temperature, 1120°C , the final density is $\sim 90\%$ of the theoretical value and increases as the sintering temperature is raised. Peak field values in the PPM stack as well as values of B_r reflect the density and increase with sintering temperature. In general, intrinsic properties tend to increase and then decrease as the sintering temperature is raised.

Similar magnetic properties are obtained at a lower temperature if sintering is prolonged. The results indicate that a reduction in temperature of 10°C can be compensated by doubling the sintering time. The data serves to illustrate the allowable tolerance in the sintering process to produce acceptable magnets.

Table V

Comparison of Functional Measurements in a PPM Stack with Intrinsic Magnetic Properties and their Dependence on Sintering Time and Sintering Temperature.

Sintering Time (hr)	Sintering Temp. ($^\circ\text{C}$)	Percent of Theoretical Density	Peak Axial Field in PPM Stack, Oe		B_r (G)	H_c (Oe)	H_{ci} (Oe)	$(4\pi M H)_{\max}$ (10^6 GOe)	$(BH)_{\max}$ (10^6 GOe)
			Before Heating	After Heating 1 hr at 225°C					
1	1120	90.1	3275	3225	6900	6750	27500	97.0	11.0
1	1130	96.0	3500	3300	7670	7050	29900	98.0	14.0
1	1140	97.5	3525	3300	7500	6550	28500	80.3	12.7
2	1110	90.4	3325	2900	6920	6620	24000	82.3	11.0
2	1120	92.1	3500	3150	6900	6730	25500	104.0	11.0
2	1130	96.9	3625	3450	7730	7220	28000	84.0	14.6

7. FINISHING AND SPLITTING

The OD and ID tolerances of pressed, sintered magnets can be held to ± 0.005 in. and ± 0.003 in. respectively, and no additional finishing of these surfaces is required.

Surface grinding and lapping were investigated as methods to finish the magnet thickness to within the ± 0.001 in. tolerance required. Both were satisfactory in achieving this with little or no loss due to cracking; however, surface grinding is more rapid and economical, and was the method used in the pilot line. Facilities exist within several Raytheon production shops conveniently located in the proximity of the samarium-cobalt magnet pilot line.

Both diamond wheel cutting and pressure splitting scored magnets were investigated as methods of producing half-rings from complete torroids. Both approaches were satisfactory, provided sufficient coolant was used in diamond wheel cutting. The method used is determined by the user, and experience has indicated each has his own preference. For the device used on this program, magnets were scored, pressure split, and delivered in matched pairs. Facilities for either method exist for handling pilot line quantities of magnets.

A suitable jiggling procedure has been devised for slotting input-output magnets with a diamond wheel to the tolerances required, ± 0.005 in. Facilities exist for pilot line quantities.

8. MAGNET EVALUATION, PROCESSING, AND STABILITY

The objectives of this portion of the program were:

- Development of magnetic measurement techniques for quality control of production TWT magnets. Both functional measurements of peak axial fields and complete second quadrant measurements for correlation purposes were required for complete quality control.
- Evaluation of pulsed and dc magnetization methods to determine an economical procedure for the production of TWT magnets.
- Evaluation of TWT magnet stabilization and adjustment methods suitable for production purposes. This included investigation of thermal stability of magnets.

a. Magnetic Evaluation

(1) Measurement Techniques

Sm-Co permanent magnets for focusing electron beams in TWT's are used in the PPM stack configuration. After thermal stabilization in a stack, it is necessary to select those magnets whose peak axial field will fall in a specified range. For the QR1642 TWT, the test vehicle of this program,

the acceptable range of axial field is 3000 to 3400 Oe. In addition to measuring the field of each magnet, it has been necessary to eliminate low magnets and select highs and adjust them (by demagnetization) into the acceptable range. The methods of measurement considered for the various requirements of magnetic evaluation for manufacturing purposes and quality control included:

- Hysteresis tracer using integrating fluxmeter for evaluation of second quadrant properties of remanence, inductive coercive force and intrinsic coercive force.
- Recoil tester.
- Axial field measurement of PPM stacks.
- Classifiers in conjunction with the recoil tester and axial field measurement of PPM stacks.

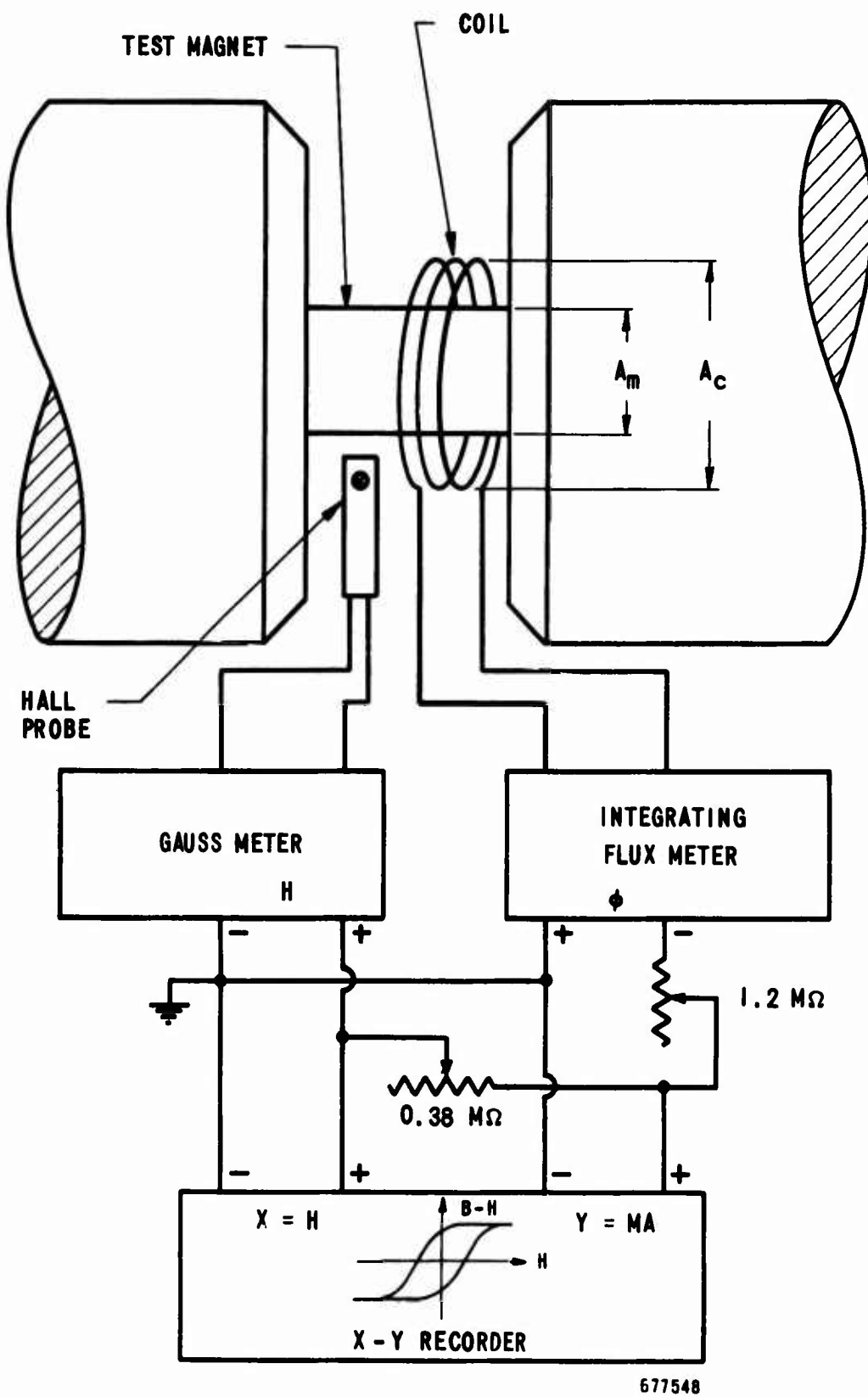
Axial field measurement is still a basic method for evaluating TWT magnets. However improvements in technique can reduce handling time. One of the time consuming aspects of magnet evaluation is the adjustment required to demagnetize magnets which are above a predetermined acceptable value. Significant improvement has been achieved through the efficient use of the probe-stabilizer head described on page 47. The hysteresis tracer evaluated under this program is now used for basic properties measurements for manufacturing quality control. A detailed description of this unit is given below, including various tests to evaluate the method. Measurements agree with those made on Raytheon's vibrating sample magnetometer.

(2) Integrating Fluxmeter - Hysteresis Tracer

A method for measuring second quadrant properties of pre-magnetized samples using an integrating fluxmeter hysteresis tracer was developed prior to the present contract, but improvement in integrator stability and sample geometry versatility were required. A simplified sketch and schematic of the method are shown in Figure 13 and a photograph of the equipment is shown in Figure 14. A magnetized sample is mounted between the poles of an electromagnet with no air gap between adjacent faces of the test sample and the electromagnet (thus excluding radial components of H). A Hall probe is used to measure H and a coil-integrating fluxmeter combination is used to derive a measurement of the magnetization of the test sample, as explained below.

The fluxmeter and Hall probe signals are combined linearly, using a resistor network, to yield the magnetization of the test sample. The flux Φ_c within the coil with no magnet present is given by:

$$\Phi_c = A_c B_{air} , \quad (1)$$



677548

Figure 13. Schematic of Hysteresis Tracer

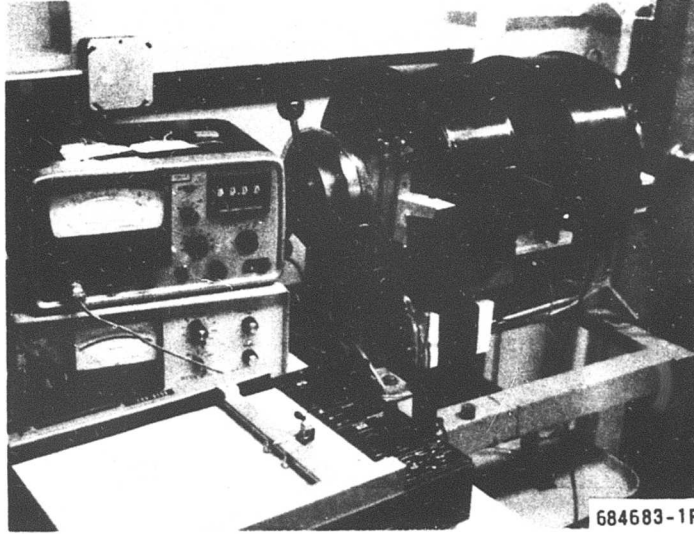


Figure 14. Hysteresis Tracer

while with a magnet present

$$\Phi'_c = \Phi_m + \Phi_{air} = A_m B_m + (A_c - A_m) B_{air} \quad (2)$$

where

A_c	=	effective cross section of coil
A_m	=	effective cross section of magnet
B_m	=	magnetic induction in magnet
B_{air}	=	magnetic induction in air
Φ_m	=	flux through magnet
Φ_{air}	=	flux in annular air space between sample and coil

By combining the Hall probe and the fluxmeter signals using a resistor network, as shown in Figure 13, one can derive a voltage V_a (with no magnet within coil) given by:

$$V_a = C_1 \Phi_c - C_2 H_{air} = (C_1 A_c - C_2) H_{air} = 0 \quad (3)$$

For all applied fields, the voltage V_a (with no magnet within coil) will remain at zero provided the constants C_1 and C_2 of the resistor network have been adjusted so that $C_2 = A_c C_1$.

With the test magnet present and $C_2 = C_1 A_c$

$$V_m = C_1 \left[A_m B_m + (A_c - A_m) H_{air} \right] - C_1 A_c H_{air} \quad (4)$$

Since $H_m = H_{air}$, then

$$V_m = C_1 A_m (B_m - H_m) = C_1 A_m (4\pi M) \quad (5)$$

where $4\pi M$ = magnetization of sample.

The voltage V_m is thus seen to be proportional to both the area and magnetization of the test magnet, provided that the adjustment of the constants $C_2 = A_c C_1$ has been made as described. The signal corresponding to V_m is presented on the Y-axis of the recorder and requires calibration with a material of known magnetization. The applied field, H , is presented on the X-axis of the recorder as the output of the Hall probe. The Hall probe is calibrated using standard magnets.

Six grade A nickel samples were fabricated for the purpose of calibrating the magnetization measurement and to verify the expected dependence on geometry. Table VI shows the results of the Ni measurements including a variety of lengths, cross-sectional areas, and sample shapes. Column 5 is a direct chart reading in mm and is proportional to MA_m . Numbers in column 6, derived from columns 4 and 5, are proportional to the sample magnetization, M . Quite good agreement was obtained for magnetization for sample lengths from 0.135 to 2.19 in. and for various sample shapes including slugs, rings and cubes. Sample No. 4 showed a relatively large deviation from the average value of M , and was probably due to the air gap at the rounded edges of the sample. The value of M for sample No. 4 is thus omitted in the calculation of the average deviation.

By assuming a standard value of 6080 gauss for the saturation magnetization of grade A Ni (high purity, electronic grade Ni) one can determine a calibration for the Y-axis in the hysteresis tracer presentation.

Further evaluation of the measurement method was made by measuring Alnico VIII, Pt-Co samples and two measurements on Sm-Co for comparison. The results are shown in Table VII and are compared with catalog values for these materials. The measurements are lower than catalog values, which was not unexpected.

Table VI
Calibration of Magnetization for Hysteresis Tracer

Grade A Nickel Sample	Shape	Dimensions			Cross-Section Am	MAm or Distance on Y-axis	M	Devia-tion
		O.D	I.D.	L				
		in.	in.	in.				
1	Slug	0.253		0.250	0.0503	42.5	845	6
2	Slug	0.375		0.175	0.1103	94.0	852	1
3	Slug	0.375		2.19	0.1103	94.0	852	1
4	Ring (Rd. Edges)	0.550	0.250	0.135	0.1890	156.5	(829)	(18)
5	Ring (Sharp Edges)	0.555	0.250	0.135	0.1934	164.7	852	1
6	Cube	0.256W	0.227H	0.255	0.0658	56.2	855	4

Average = 851 3

The hysteresis tracer presents MA (the product of sample magnetization and cross-sectional area) on the Y-axis. The Y-axis will be made direct reading in B by the use of a coil inside the iron pole piece with an iron flux path leading from the sample through the B coil, and thus direct plots of B vs H will be obtained.

The precision of this technique was then established, and comparison was made with a vibrating sample magnetometer (VSM) capable of complete hysteresis loop traces up to 100 kOe dc fields. A total of ten separate measurements on two samples measured in the integrating fluxmeter hysteresis tracer (IFHT) resulted in essentially the same average deviation for the two, B_r (7800 ± 60 gauss) and H_c (7000 ± 50 Oe). B-H curves were measured on another TWT sample by both techniques and are shown in Figures 15 and 16. The B_r values are 8180 and 8240 gauss for the VSM and hysteresis tracer respectively, while the H_c values were 7900 and 8000 Oe. The agreement is considered to be quite good and within the measurement precision. Complete hysteresis loops, including H_{ci} , which for most magnets is in excess of 20,000 - 25,000 Oe, can be obtained with the VSM. The integrating fluxmeter hysteresis tracer conveniently measures second quadrant properties of B_r , H_c and H_{ci} in an electromagnet with a 4 in. diameter pole face which provides fields up to 30,000 Oe. The measurements of Figure 16 were performed in a smaller electro-magnet.

Table VII Hysteresis Tracer Measurements of Alnico VIII and Pt-Co

No.	Material	Shape	Dimensions			Cross- Section A _m	M _r A _m /m	4 π M _r = B _r		H _{ci}		H _c	
			O.D.	I.D.	L			Mea- sure- ment	Cat. Value	Mea- sure- ment	Cat. Value	Mea- sure- ment	Cat. Value
in.	in.	in.	mm/in ²	Gauss	Oersted	Oersted							
1	Nickel	Ring	0.555	0.250	0.135	0.1934	171	Ref. =6080 *	---	---	---	---	
2	Alnico VIII	Ring	0.540	0.255	0.165	0.1780	177	6300 7300	2100	---	1900	1900	
3	Alnico VIII	Ring	0.285	0.130	0.250	0.0505	166	5910 7300	2100	---	1900	1900	
4	Pt-Co	Slug	0.250	-----	0.250	0.0490	168	5970 6400	6290	7090	5200	5480	
5	Pt-Co	Slug	0.225	-----	0.240	0.0397	148	5260 6400	5870	7090	5100	5480	
6	Pt-Co	Ring	0.550	0.248	0.135	0.1880	172	6120 6400	7100	7090	5400	5480	
7	SmCo	Ring	0.538	0.240	0.140	0.1820	219	7800 -----	18000	-----	6500	-----	
8	SrCo	Disc	0.556	-----	0.140	0.242	211	7500 -----	>15000	-----	7300	-----	

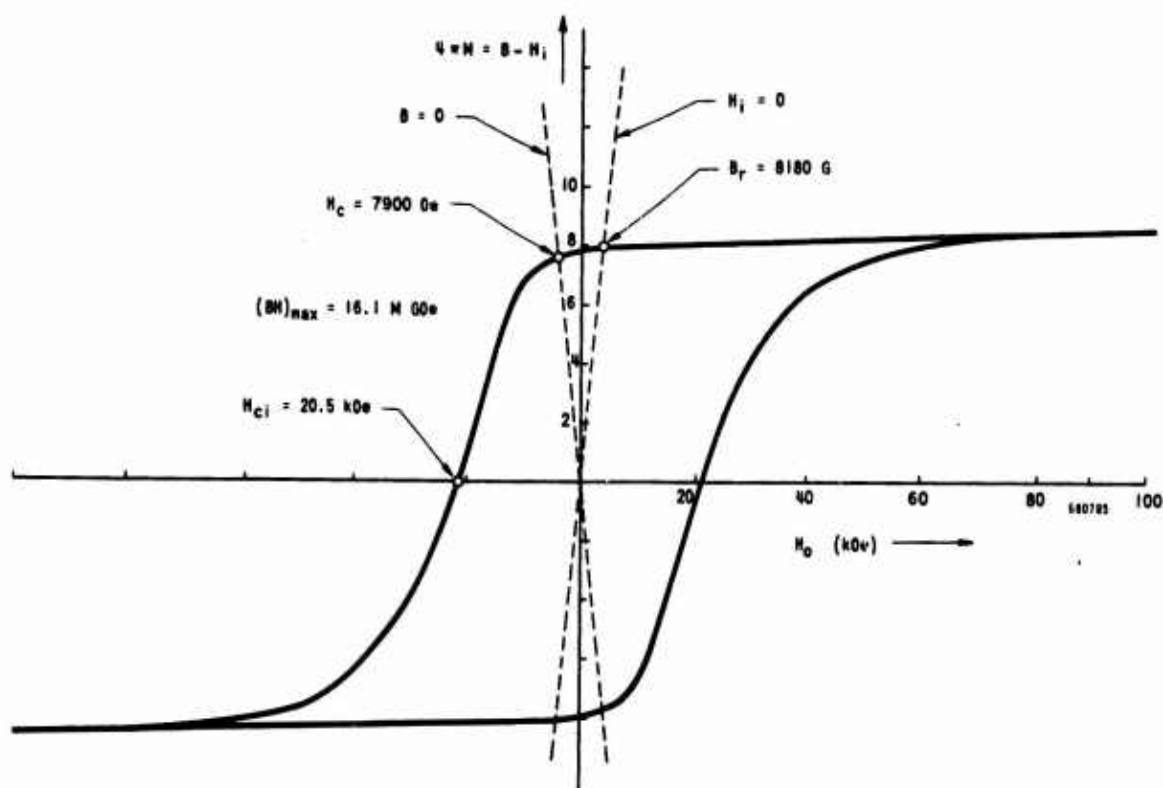


Figure 15. Magnetization $4\pi M$ vs Applied Field, H_0 , of a Sm-Co TWT Magnet using Vibrating Sample Magnetometer (VSM)

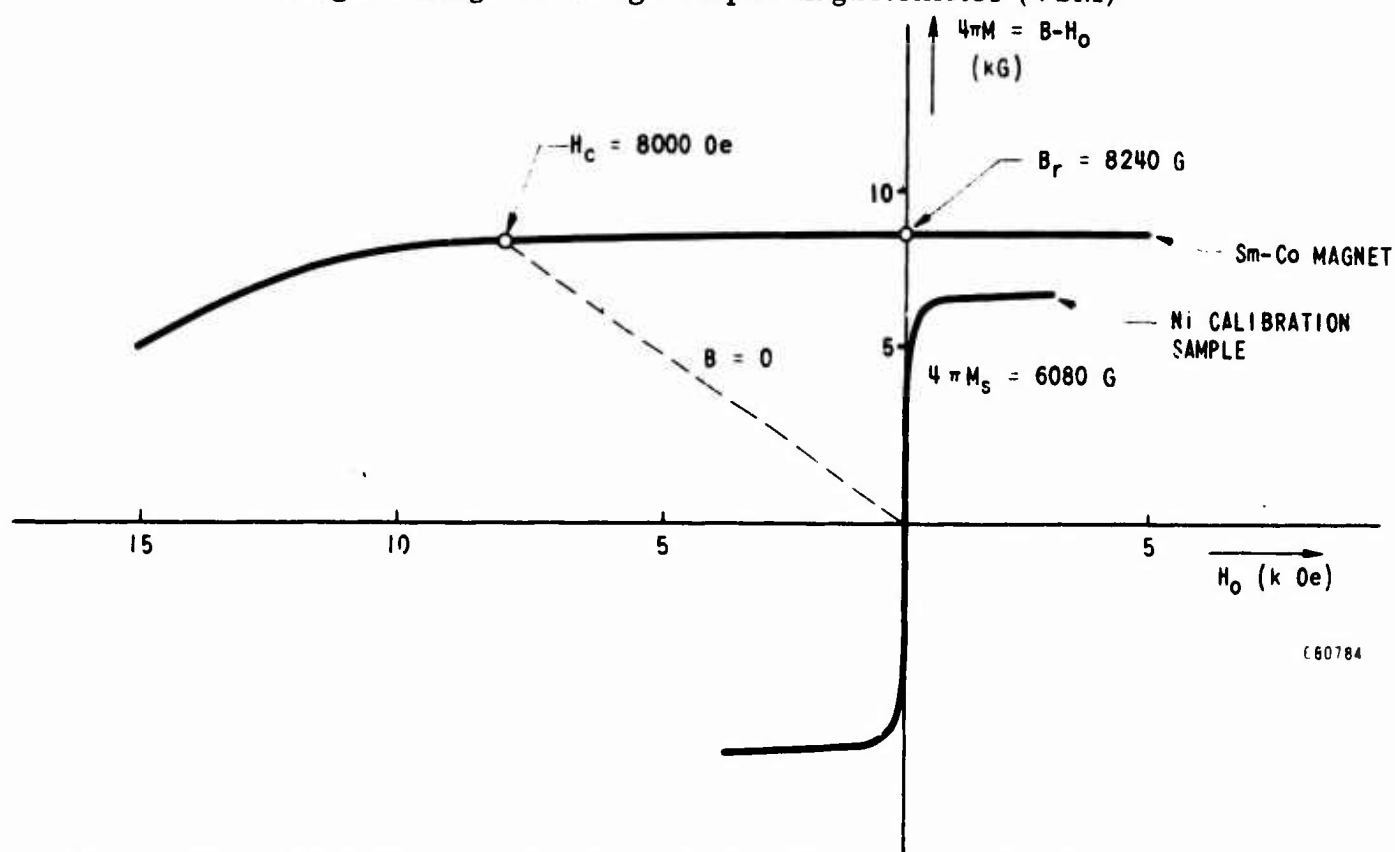


Figure 16. Magnetization, $4\pi M$, vs Applied Field, H_0 , of a Sm-Co TWT Magnet using Integrating Fluxmeter Hysteresis Tracer (IFHT)

The integrating fluxmeter hysteresis tracer uses a closed iron circuit to apply the magnetic field. Therefore, there is no demagnetizing field, H_d and the external field, H_o , is equal to the internal field, H_i , of the sample. Thus the remanence, B_r , and the coercive force, H_c , are given by the intersections of the hysteresis curve with the $H_o = 0$ and the $B = 0$ lines (see Figure 16). However, the VSM method involves a calculated demagnetization factor, $D = H_d/4\pi M = 0.55$ and a correction must be applied to H_o to obtain H_i . In Figure 15, the lines corresponding to $H_i = 0$ and $B = 0$ are constructed, as shown, taking D into account. B_r and H_c are then obtained, as before, from the intersection of these lines with the hysteresis curve.

The agreement in B_r and H_c values obtained by the two methods was quite good. Apparently there is no loss of magnetization due to the demagnetizing field of approximately 4500 Oe incurred by open-circuiting the magnet after pulsed magnetization. The integrating fluxmeter method thus allows for rapid second quadrant measurements directly on TWT magnets, from which correlations can be made with peak axial field measurements in PPM stacks.

b. Magnetic Processing

(1) Magnetization

The magnetization of samarium-cobalt magnets presents unique problems due to the high coercive force of the material. It is clear that a pulsed method is more desirable than dc in terms of speed and cost if adequate fields of sufficient duration can be achieved to approach saturation. It was anticipated that fields in excess of 40 kOe, and more likely above 60 kOe, would be necessary to saturate samarium-cobalt, which is 2 to 4 times the intrinsic coercive force. The following program was planned to compare the efficiency of pulse with dc magnetizing:

- (a) Pulse magnetize several Sm-Co TWT magnets at various fields and pulse durations and determine the resultant magnetic properties.
- (b) Check the same magnets in dc fields varying up to 43 kOe, and at 100 kOe dc.

The integrating fluxmeter-hysteresis tracer described on page 28 was used to measure the remanence and coercive force of three Sm-Co TWT magnets as a function of pulse and dc magnetization parameters. Peak pulse fields up to 52 kOe, half-amplitude pulse durations of 2.3 and 10 msec. and dc fields of 43 and 100 kOe were used for magnetizing the three samples. Samples were demagnetized after each magnetization treatment and determination of second quadrant properties. The results are shown in Figure 17. The following indications are seen from this data:

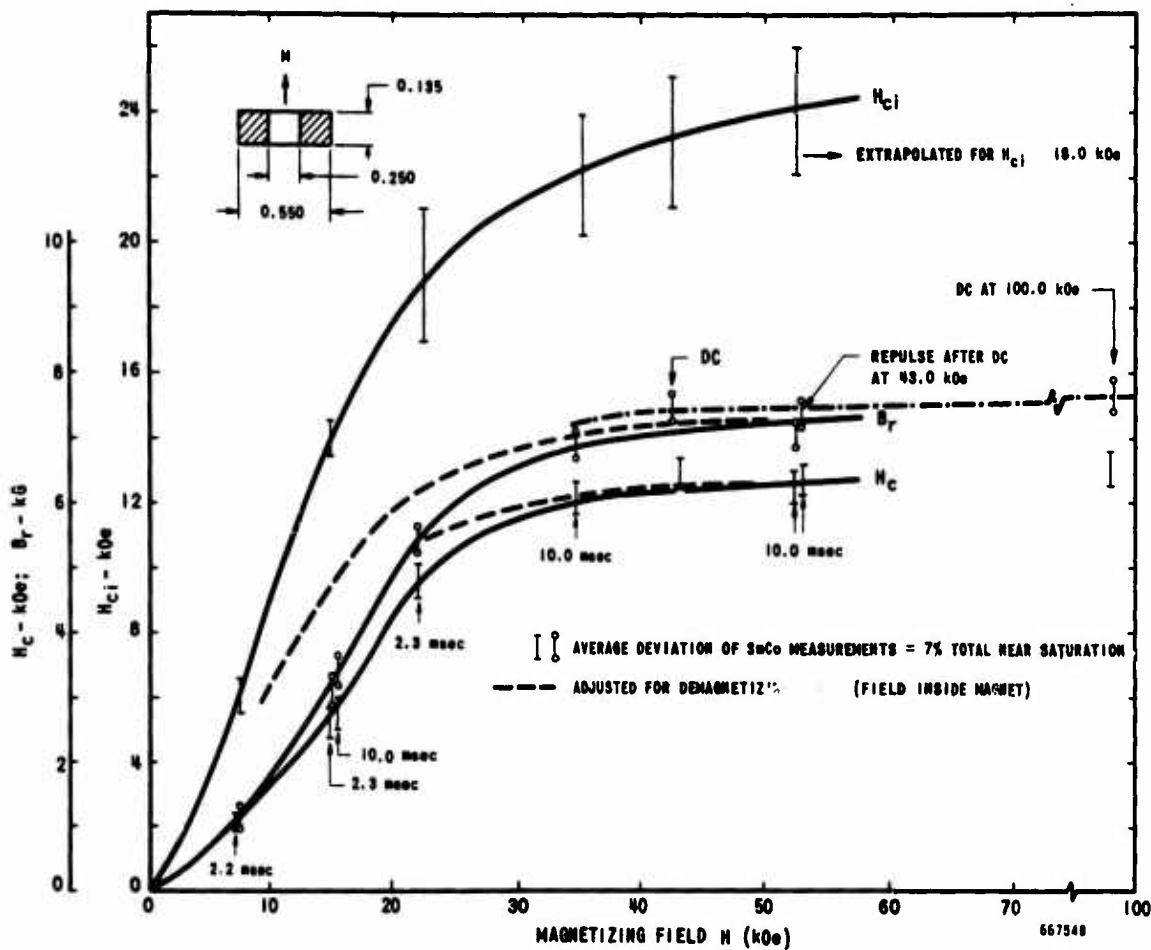


Figure 17. Pulse and DC Magnetization of Sm-Co TWT Magnets

- (a) The magnets are not completely saturated by a pulse field of 52 kOe and 10 msec duration.
- (b) DC magnetization at 100 kOe seems to give approximately 2% - 5% higher remanence and coercive force than pulse magnetization at up to 52 kOe.
- (c) Any difference between 2.3 and 10 msec pulses was not discernible and therefore lies within the 3% estimated uncertainty in the measurements.

Higher peak fields are needed to saturate samarium-cobalt magnets, and can be produced with short pulse durations. Very high field gradients of the order of 10,000 Oe/cm occur near the ends of the coil in the axial direction, and could put severe mechanical stress on the magnet, causing cracking. If eddy currents should attenuate the field inside the magnet, a longer pulse duration or a higher field will be required. This is a limiting design parameter for pulse coils. Several magnets were magnetized in a 100 kOe dc field and attempts were made to reproduce the second quadrant properties with pulse fields of sufficient intensity and duration.

It had previously been determined that a 100 kOe dc field is capable of saturating magnets, and basic magnetic properties so obtained were taken as a reference. Whatever the production magnetization technique, it should yield at least 95% of the maximum magnetic characteristics a material is capable of providing.

The maximum pulse magnetizing condition had been 52 kOe and 10 msec. In order to fully evaluate pulse and dc magnetization, additional pulsed field coils capable of higher fields were constructed.

A coil with a 0.600-in. ID which delivers a field of over 100 kOe with a pulse duration at half-peak amplitude of 4 msec was designed and constructed. The first coil delivered 165 kOe, but burst at 200 kOe because of over-heating, although it was water cooled. The cooling water temperature rise was monitored and indicated that 2 minutes were required for the temperature to drop to 30% of its peak value. Since the magneto-mechanical forces cause the copper to flow at around 100 kOe, fiberglass reinforcement was used between each winding. Two additional coils of this construction were built and are in operation. Due to the failure of the first model, these coils are now operated quite conservatively at up to 100 kOe and 4 msec.

Another coil design with a 1-3/4 in. bore was constructed (see Figure 18). It was completely embedded in 1-in. thick iron, which is a good safety feature against explosion. It delivers 80 kOe at 8 msec and can be pulsed every 30 seconds.

The smaller coil needs a pulsing supply with 7-1/2 kJ energy storage; the larger one requires 15 kJ. The peak currents employed are 3500 A for the smaller coil at 100 kOe and 4 msec, and 2000 A at 80 kOe and 8 msec for the larger coil. Figure 19 shows a typical current and field pulse obtained

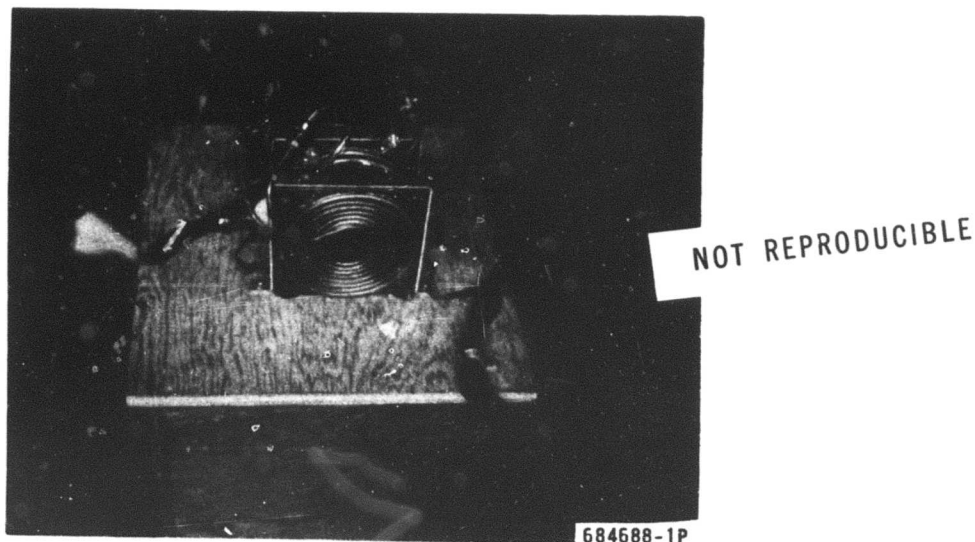


Figure 18. Pulse Magnetizing Coil, 1-3/4 in. ID, 80 kOe, 8 msec

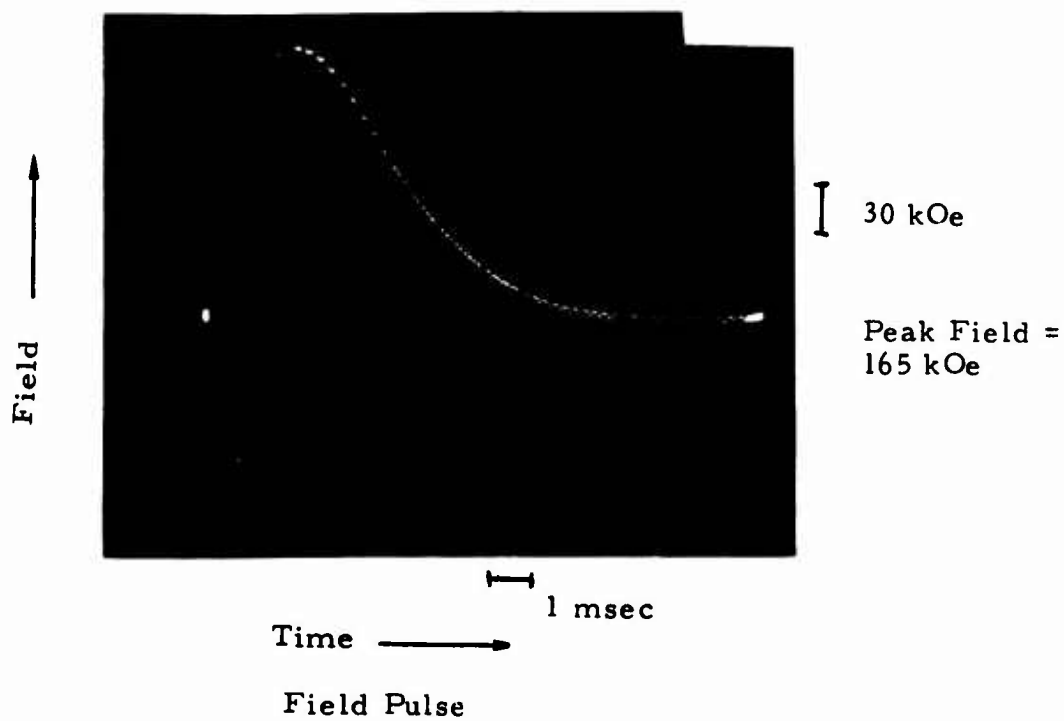
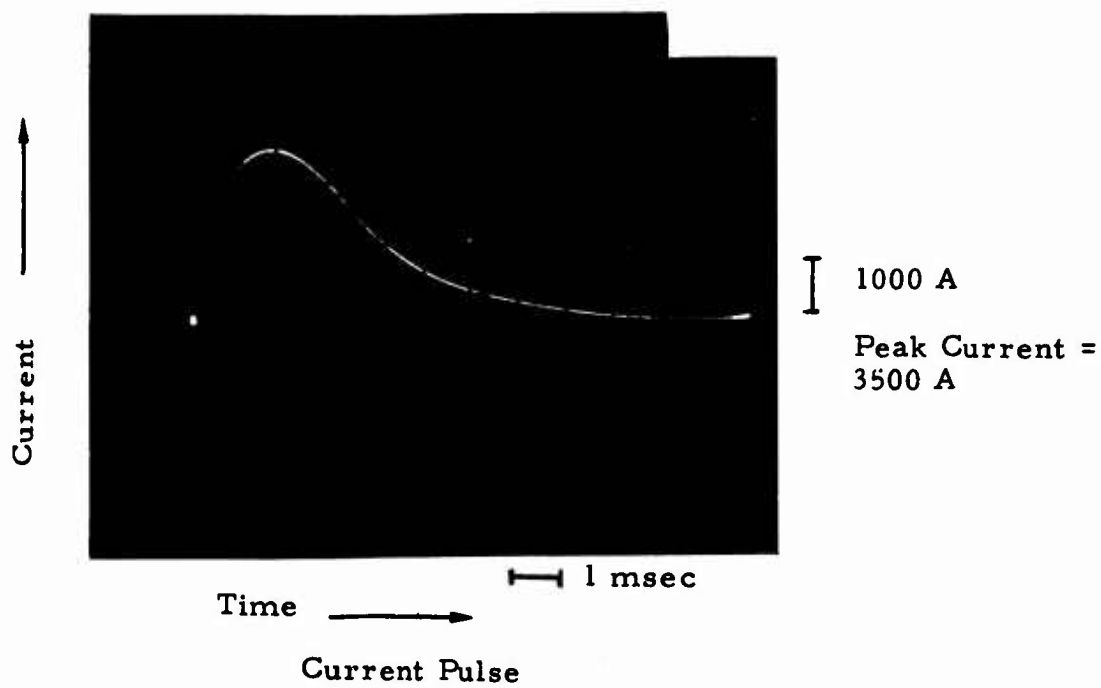


Figure 19. Typical Current and Field Pulses in 0.6 in. ID High Field Coil

with one of the 0.6-in. ID coils. The ripple in the magnetic field pattern is caused by the gaussmeter. Raytheon Model 8100 A with 3.2 mF capacitance and 3200 V peak voltage was the pulser used (see Figure 20). The pulser has a standard capacitor discharge circuit with thyatron switching and shunting tubes.

Additional tests were then performed to further determine the effectiveness of pulse magnetization. Other objectives in this series of tests were to make a comparison between laboratory fabricated magnets and magnets processed from a 5-lb melt and formed in the automatic press, and to determine the thermal stability of magnets.

Two sets of magnets were measured; set 1 consisted of 13 TWT magnets selected from several laboratory processed lots, and set 2 consisted of 20 magnets produced from a 5-lb melt and pressed in the automatic press at 100 kpsi. Axial peak fields, B_0^* , were measured on all 33 magnets before and after heating to 225°C for 2 one-hour cycles in a PPM stack. Second quadrant measurements were made on all 13 magnets from set 1, and 4 magnets from set 2. The four magnets have been identified in

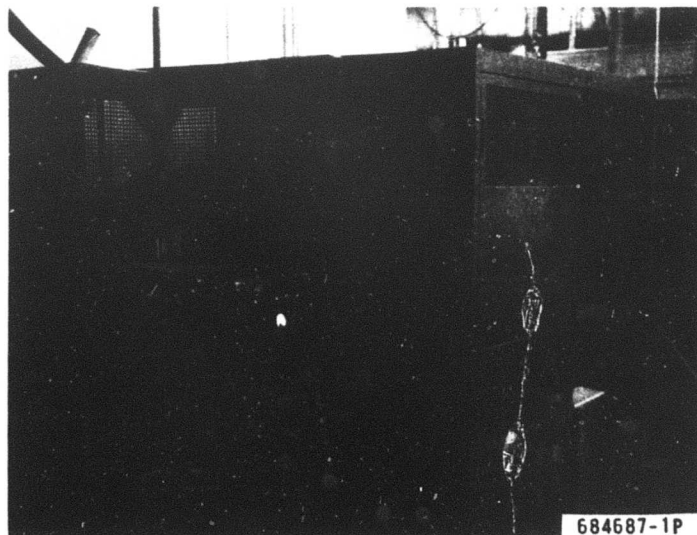


Figure 20. Raytheon 8100 A Pulser, 15 kJ

* This usage is consistent with that of tube engineers. In air, the induction B (gauss) is numerically equal to H (Oe).

Table VIII; the magnet numbers refer to magnets removed from the PPM stack, (see Table IX). Complete data on set 2 is included in this report (see Table VIII) since these were the first magnets to go completely through all processes evolved on this program. Data for the following magnetizing fields are shown in Figure 21: 20 kOe (8 msec), 30 kOe (8 msec), 50 kOe (8 msec) and 100 kOe (4 msec) pulsed, and 100 kOe dc. Set 2 was pulsed only at 50 kOe (8 msec) when second quadrant properties were obtained.

Figure 22 shows the dependence of basic magnetic properties (average values shown) on the magnetizing field. Although there is some loss in magnetic properties due to temperature cycling, the use of 50 kOe pulses rather than 100 kOe represents a very small degradation in B_r and H_c whether or not the magnets are heated. Further, it appears that 100 kOe, 4 msec pulse magnetizing is equivalent to 100 kOe dc in all basic magnetic properties. The electromagnet used at the time of the measurement did not provide a sufficiently large demagnetizing field to determine H_{ci} . Therefore, recoil B from 15 kOe was measured as an indication of the loss of magnetization at 15 kOe demagnetizing field; the recoil indicated $H_{ci} > 20,000$ Oe.

These magnets were typical of those produced in the laboratory for which H_{ci} averages around 20-25 kOe. The conclusion is that the 8 msec pulsed fields of approximately 50 kOe are sufficient to achieve over 97% of the magnetic properties achieved at 100 kOe dc. Little difference is observed at 50 kOe between the properties of set 2 and set 1. The automatic press-produced magnets are somewhat more stable with regard to B_r and H_c , and significantly more so in B_{recoil} .

Both set 1 and set 2 magnets were evaluated in PPM stack configuration. The average peak axial field was shown in Figure 21 as a function of the magnetizing field. Again, the equivalence of 100 kOe 4 msec pulse and 100 kOe dc magnetizing was demonstrated; it was also shown that 50 kOe pulsed fields are adequate for 97% saturation. The automatic-pressed magnets are at least equivalent to, if not better than, laboratory prepared magnets. For comparison, a short stack of Pt-Co TWT magnets was evaluated before and after heating. Clearly, the irreversible thermal loss due to heating was much greater for Pt-Co than for Sm-Co magnets (see Figure 21).

Based on the average magnetic values for the two sets of magnets, the temperature coefficient for irreversible loss of basic magnetic properties have been computed and these are shown in Table X. The temperature coefficient τ for some temperature interval, ΔT , is defined as

$$\tau = \frac{100(B_r \text{ (not heated)} - B_r \text{ (heated)})}{B_r \text{ (not heated)} \times (\Delta T)} \% / ^\circ \text{C} \quad (6)$$

Table VIII Properties of Magnets Fabricated In Automatic Press (Set 2).

Pulsed at 50 kOe

Magnet No.	B _r Gauss		H _c ' Oe		B _{recoil} from 15 kOe		B _o peak in Stack		(BH) _{max} MGOe	
	NH	H	NH	H	NH	H	NH	H	NH	H
5	7990	7660	7300	6900	4290	4260	3950	3650	15.7	13.7
6	7990	7900	7200	7000	(4500)*	(4760)*	3950	3675	15.7	14.3
10	7770	7750	7200	7000	4260	4290	3950	3650	14.9	14.1
16	7670	7770	7000	6950	4600	4620	3950	3700	14.4	13.9
Average	7860	7770	7180	6960	4380	4390	3950	3670	15.2	14.0
Difference	1.1%		3.1%		0.2%		7.0%		7.9%	

NH = Not Heated
H = Heated, two 1 hour periods at 225° C
* = Not used in Average

Table IX
Peak Axial Field, B_0 , in PPM Stacked TWT Magnets

- Pulse magnetized 50 kOe, 8 msec
- SmCo from automatic press (set 2)
- Temperature cycled at 225°C for two 1 hr periods.

Magnet No.	B_0 (G) SmCo		B_0 (G) PtCo	
	Before Heating	After Heating	Before Heating	After Heating
1	3650	3400	3225	2475
2	3725	3525	3375	2400
3	3800	3650	3275	2275
4	3800	3500	3325	2375
5	3950	3650	3350	2400
6	3950	3675	<u>3275</u>	<u>2350</u>
7	3800	3525	Avg. 3305	2385
8	4000	3750	28% Decrease	
9	3950	3650		
10	3950	3650		
11	3875	3700		
12	3950	3700		
13	3900	3625		
14	3825	3525		
15	4000	3725		
16	3950	3700		
17	3825	3500		
18	3875	3575		
19	3950	3750		
20	<u>4000</u>	<u>3750</u>		
	3880	3625		
	6.5% Decrease			

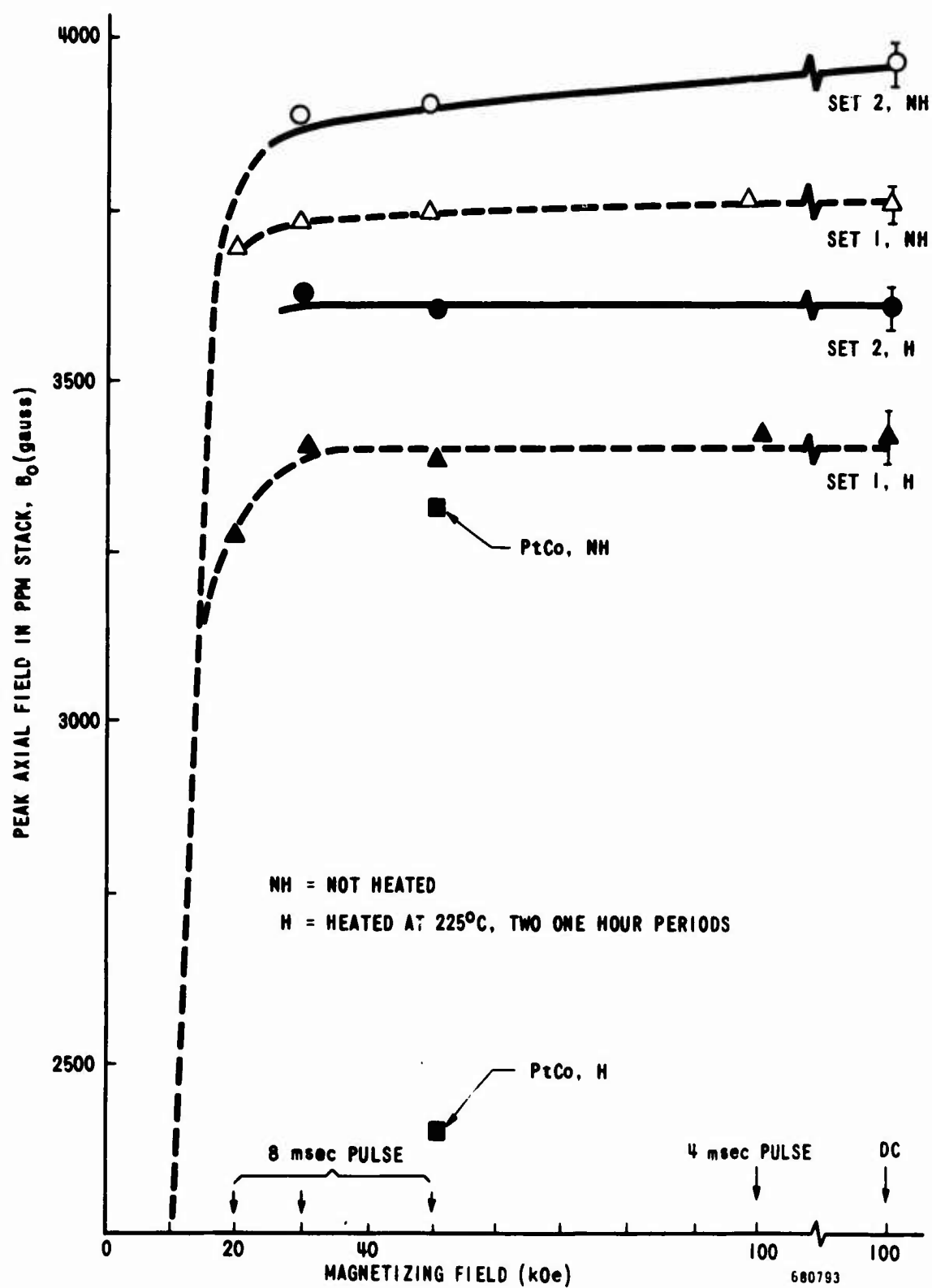


Figure 21. Peak Axial Field, B_0 , in PPM Stack vs Magnetizing Field

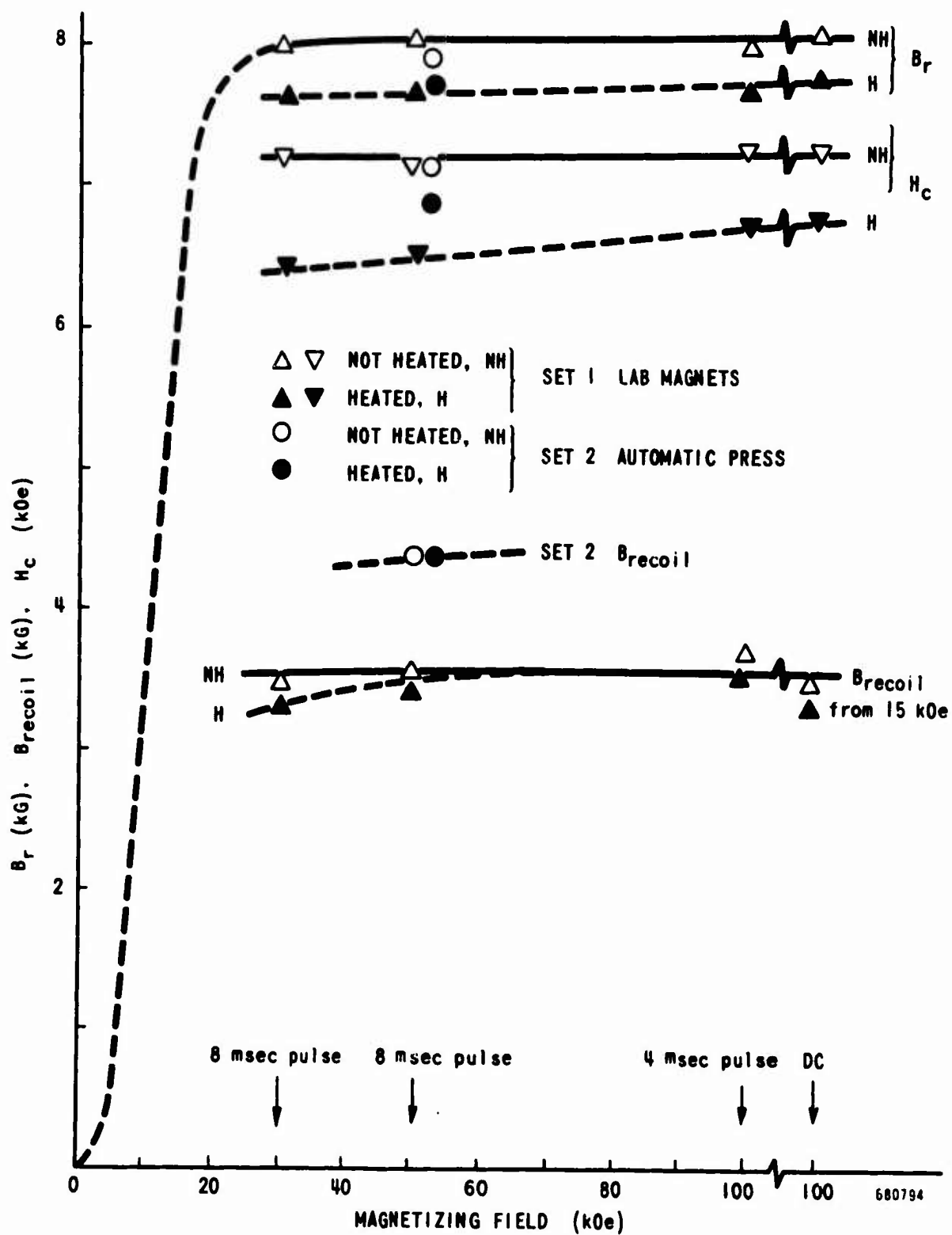


Figure 22. Remanence, B_r , Coercive Force, H_c , and B_{recoil} vs Magnetizing Field.

Table X
Irreversible Temperature Coefficients vs Magnetizing Field (%/°C)

Magnetizing Field	Lab Magnets (Set 1)			Automatic Press Magnets (Set 2)				
	B _r	H _c	B _{recoil}	B _{stack}	B _r	H _c	B _{recoil}	(BH) _{max}
50 kOe	0.019	0.046	0.012	0.041	0.006	0.014	0.000	0.029
100 kOe	0.016	0.031	0.000	0.041				0.035

Note that all measurements are made at room temperature. Temperature cycling to 225°C was done in a PPM stack corresponding to an estimated average operating point B/H ratio of -0.3.* Irreversible losses for the two magnetizing fields were not greatly different, and samples from the automatic press (set 2) exhibited a smaller irreversible loss in all properties than laboratory magnets (set 1).

Until the development of samarium-cobalt, platinum-cobalt was the hardest known permanent magnet material. It is interesting to note in some detail the difference in thermal stability between the two materials. A comparison of irreversible loss on temperature cycling in a PPM stack is made in Table IX for 50 kOe, 8 msec pulse magnetizing. The average axial peak field was decreased by 6.5% for Sm-Co magnets and 28% for Pt-Co after 2 one-hour cycles at 225°C. In terms of irreversible temperature coefficient, this corresponds to 0.033%/°C for Sm-Co and 0.14%/°C for Pt-Co. Subsequent recycling of Sm-Co magnets to 110°C after stabilizing at 225°C resulted in a reversible loss (measurements made as a function of temperature) of 0.031%/°C.

(2) Skin Depth

The use of pulsed fields raises the question of field penetration to achieve saturation throughout the magnet. The skin depth, δ , is given by

$$\delta = \sqrt{\frac{2}{\mu \sigma \omega}} \quad \text{in meters} \quad (7)$$

and the field at a depth x below the surface of the material is given by:

$$H_{(x)} = H_0 e^{-x/\delta} \quad (8)$$

where

$$\begin{aligned} \mu &= \text{permeability in henry/m} \\ \sigma &= \text{conductivity in mho/m} \\ \omega &= \text{angular frequency in sec}^{-1} \\ H_0 &= \text{field at the surface} \end{aligned}$$

Assuming the following values for Sm-Co magnet material,

$$\begin{aligned} \sigma &= 2 \times 10^6 \text{ mho/m} \\ \mu &= \mu_0 = 4\pi \times 10^{-7} \text{ henry/m} \\ \omega &= 300 \text{ sec}^{-1} \end{aligned}$$

associated with a 10 msec half-period pulse, a skin depth of $\delta = 0.052$ m is computed. Thus, at a depth of 0.100 in. the field is approximately 90% of the surface field. This corresponds to the situation of pulse magnetizing a

* This is based on our own experimental evidence and lies between values calculated from M. Schindler - IEEE Trans. Ed., Vol. 13, No. 12, Dec. 1966, pp. 942 - 949 and other theories which give B/H values of approx. -1.0

stack of QR1642 TWT magnets. If a pulse field of 80 kOe is used, then the smallest field seen at any point in a magnet would be approximately 70 kOe assuming a small demagnetizing field for a long stack. These fields are entirely adequate to provide at least 97% of saturation values of remanence and coercive force.

(3) Magnet Adjustment

After magnetization and thermal stabilization of a PPM - TWT magnet stack, it becomes necessary to determine which magnets are high and to adjust them into an acceptable range by demagnetization. This process has been time consuming and great improvement has been made by the use of the PPM magnet tester and adjuster described below (see Figures 23, 24, and 25).

The magnet is mounted on a cylindrical iron head containing a Hall probe for the measurement of the axial field. Measurements were made to verify that this field can be correlated with the axial field obtained in a PPM stack. If the reading is high, the magnet as mounted on the test head is then inserted into the iron clad coil (Figure 23) where it is demagnetized by self-repeating ringing ac pulses with automatically increasing peak field. This pulser is Raytheon-built and designed, using a modified F.W. Bell magnet processing unit.

When the test head B (Figure 23) indicates an acceptable reading, the pulser automatically turns off. An important feature is that the reading on test head B is the same inside and outside coil A, which simplifies the classification.

For calibration, six groups of 4 magnets with similar readings were measured: (a) in the PPM stack (groups in increasing order), (b) singly with 2 PPM shims, (c) on test head B outside, and (d) inside adjusting coil A.

Figure 26 shows that the readings (c) and (d) in the tester gave a closer correlation to the stack reading (a) than the reading (b) with single pole shoes, i.e., $\pm 1.5\%$ deviation versus $\pm 2.5\%$. In both cases, the pole shoes were centered within 0.005 in. in the magnet. In later measurements, with a better fixed Hall probe, the deviation was reduced to less than $\pm 1\%$.

The fact that (a) versus (c) is directly linear makes calibration for production set-ups simple.

For a new magnet geometry, it is sufficient to adjust a group of 6 magnets to a certain reading on the test head, stack them in a PPM stack and add 2 pairs of end magnets. The center 4 magnets of the group will give a point of the calibration line (through zero) of stack reading versus reading on test head.

By shim adjustment, the same readings on test head B, both in and outside the adjusting coil A were obtained. A maximum deviation of $\pm 1.5\%$ was obtained as shown in Figure 27.

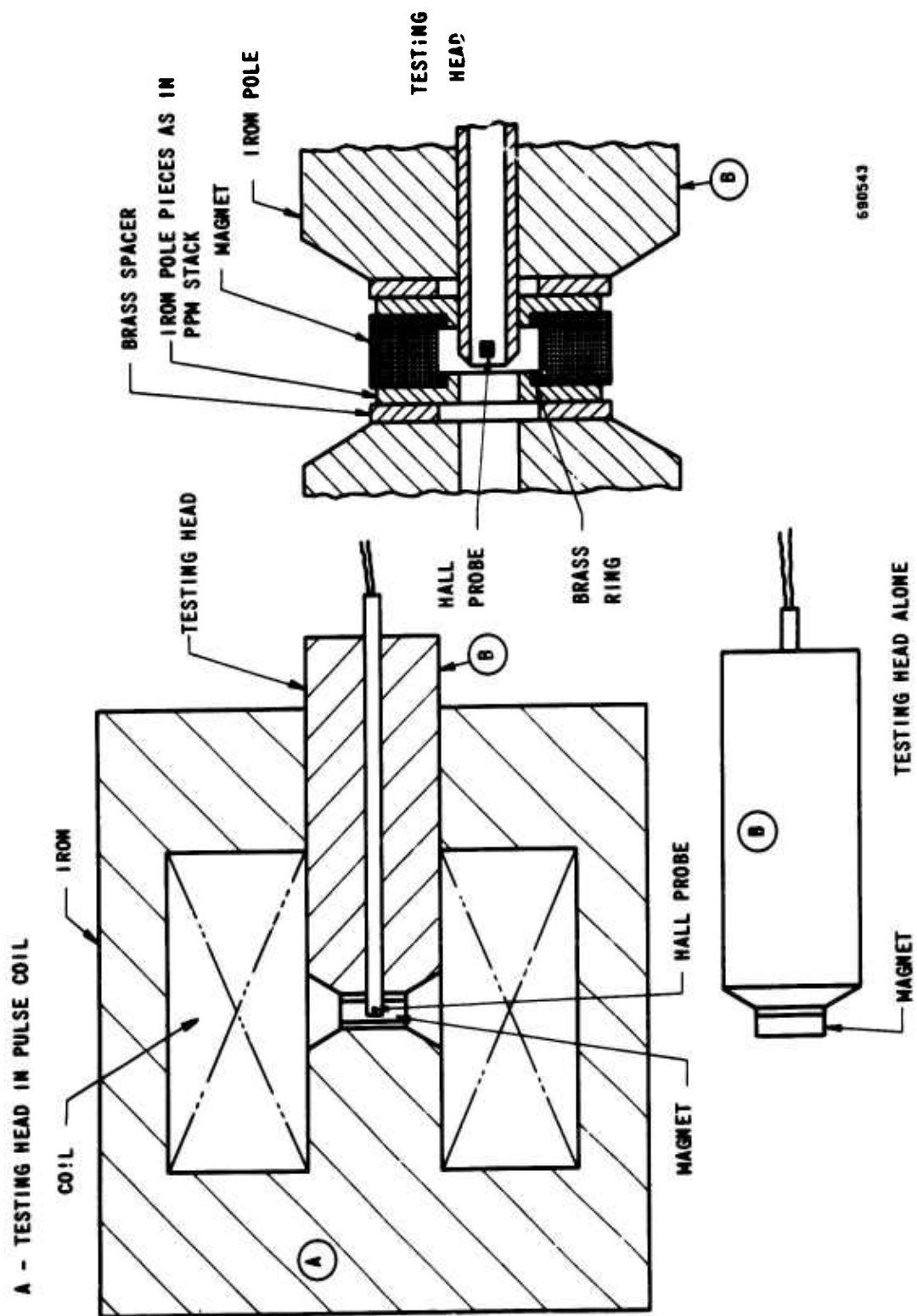


Figure 23. Testing and Adjusting Fixture

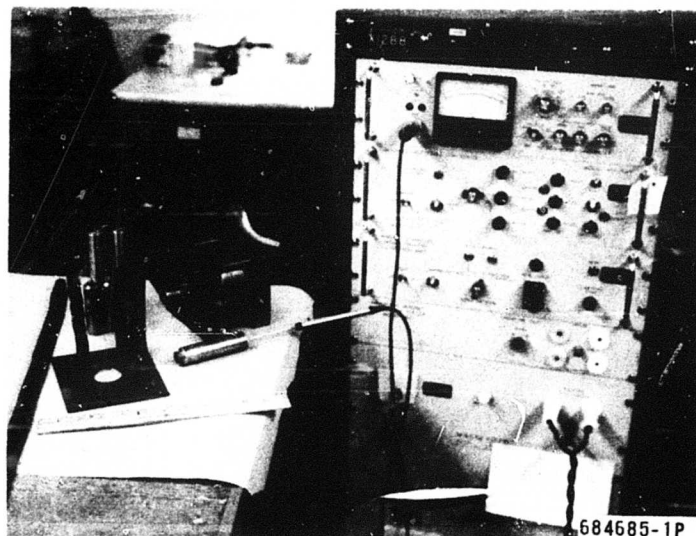


Figure 24. Tester-Adjuster with Coil, Measuring Head, and Power Supply

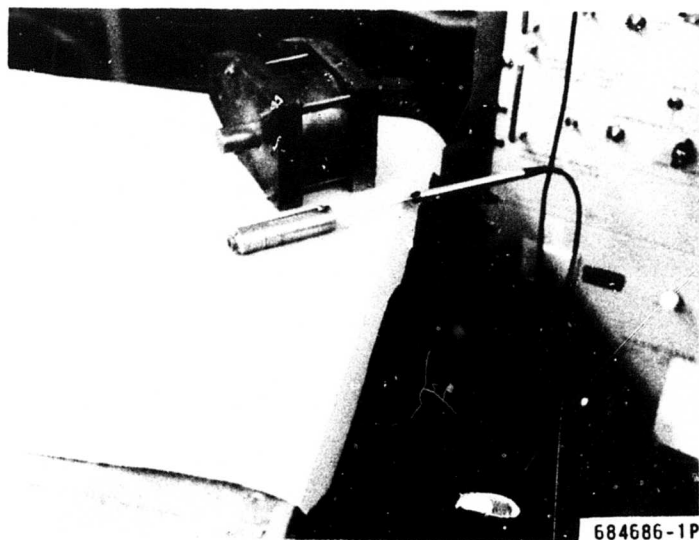


Figure 25. Adjusting Coil and Measuring Head

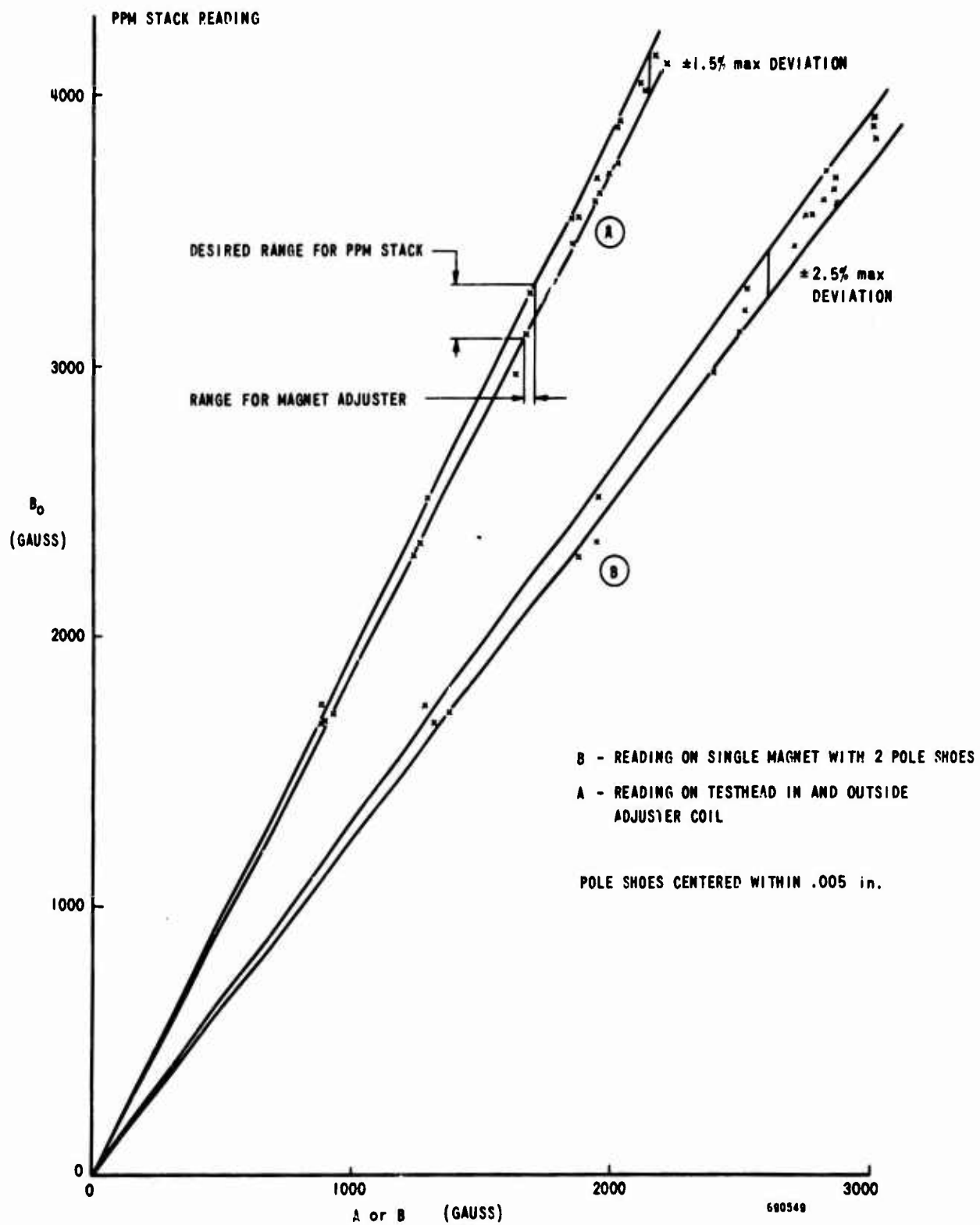


Figure 26. Calibration of Magnet Adjuster

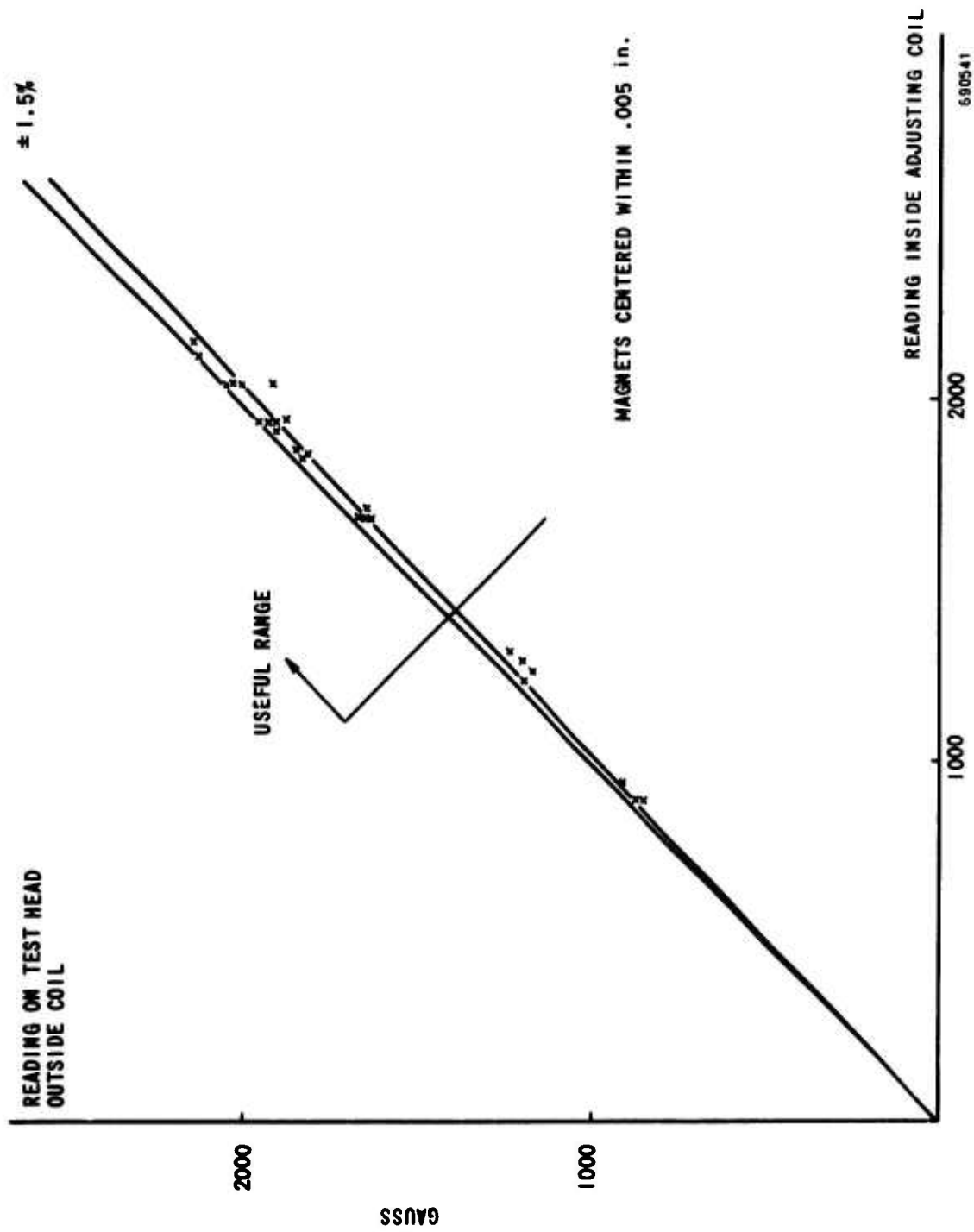


Figure 27. Reading on Test Head Outside and Inside Adjusting Coil

The demagnetizing field of magnets in a PPM stack varies considerably with radius and also has strong radial components. It seems best to use an adjusting and stabilizing fixture with a similar field distribution, such as that shown in Figure 23. With a resonant frequency of about 50 Hz, the skin depth in iron is 2 cm. The use of bulk iron instead of laminated iron for pole pieces and flux return path does not strongly affect the magnet field characteristics inside the bore. The coil without pole pieces gives about 5% higher peak fields when clad with 1 in. iron than the coil without any iron. Without iron poles, the coil delivers 22 kOe peak field; with the iron poles it is reduced to an estimated 15 kOe. The peak field can easily be increased to 40 kOe by changing capacitance and inductance but this would reduce the pulse repetition rate.

The same coil was used with other magnet fixtures, including flat iron poles with and without an air gap between magnet and iron, and also an ironless plastic holder which allows higher fields. All were much less accurate than the head in Figure 23. For more universal use with magnets of various sizes, the heads in Figure 23 but with flat iron shims instead of typical PPM shims with a rim have been used. The accuracy was a little worse than in Figure 26 ($\pm 3\%$).

The testing and adjusting fixture now in use has the advantage of classifying and adjusting in the same fixture and set-up. Semi-automatic feeding of magnets together with fully automatic push-button operation is possible.

c. Magnet Stability

(1) Introduction

Permanent magnets must be stabilized prior to use in order to avoid changes associated with the thermal and magnetic environment in use. It is general practice therefore to heat TWT magnets to a temperature in excess of any expected during use and in a demagnetizing field which simulates use. The demagnetizing field is obtained by stacking the magnets in a PPM configuration using actual pole pieces. The long term stability is also of interest; possible relevant factors include: (a) magnetization inhomogeneities due to the eddy current effect during pulse magnetization, (b) the effect of magnet shape on the variation of the demagnetizing field within one magnet, (c) inherent inhomogeneities in the magnet material, and (d) oxidation of Sm-Co.

The investigation of magnet stabilization procedures and magnet stability has included the following:

- Reversible and irreversible changes in magnetic properties due to heating as a function of temperature, demagnetizing field and magnet quality.

- Length of time and number of heat cycles required for adequate thermal stabilization
- Long term stability
- Low temperature exposure.

The principal results can be summarized as follows:

- Thermal stabilization takes place almost immediately after reaching any temperature up to 300°C. One heat cycle appears to be adequate.
- Magnets stabilized at 250°C were stable for 900 hr at 230°C and 50% relative humidity and for 830 hr at 80°C and 93% relative humidity.
- The irreversible loss of flux is close to zero at zero demagnetizing field, H_d , and increases linearly with increasing H_d . The temperature dependence of irreversible loss is much greater than linear, particularly at higher demagnetizing fields. The temperature coefficient varied from 0.023 to 0.40%/°C.
- The reversible loss of flux is almost independent of demagnetizing field and is very nearly linear with temperature. The temperature coefficient varied from 0.033% to 0.036%/°C between 25°C and 150°C and from 0.039% to 0.048%/°C between 25°C and 250°C.
- Sm-Co powder, with an average surface-to-volume ratio 100 times that of a QR1642 TWT magnet, gained weight at a rate of 0.15% for 1 hour at 250°C and 50% relative humidity.

(2) Reversible and Irreversible Thermal Effects

There is a variability in the axial field and irreversible thermal loss of PPM-stacked TWT magnets which is related to intrinsic magnetic properties. Attempts were made to correlate the reversible and irreversible thermal effects with 2nd quadrant properties and thermal processing. Typical irreversible loss in peak axial field is 10% after a 2-hour heating cycle at 225°C. Occasionally a set of PPM stack readings is obtained which shows much less degradation, and such magnets establish desirable property goals for achieving a higher yield. Such a set of six magnets showing a loss of 1.7% after 225°C heating was investigated in terms of 2nd quadrant properties and peak axial field after heat treatments at various temperatures up to 450°C. Table XI shows the average

Table XI. Low Irreversible Thermal Loss in a PPM Stack

<u>Treatment</u>	<u>Peak Axial Field (Avg.) (Gauss)</u>	<u>Irr. Coeff. RT-Temp %/°C</u>	<u>Loss %</u>
Magnetized	3520		
After 1 hr @ 225°C	3460	.008	1.7
After 1 hr @ 300°C	3415		
After 1 hr @ 300 repeat	3435	.010	2.6
Remagnetized	3510		
After 1 hr @ 225°C	3430		
Remagnetized	3520		
After 1 hr @ 450°C in N ₂	2795	.048	20.6
500 hr later	2820		
Remagnetized	3530		

peak axial field for the 6-magnet PPM stack with 2 end magnets at one end. It can be seen that all irreversible losses up to 450°C are recovered upon remagnetization. The 2nd quadrant properties of a typical magnet of this group are shown in Figure 28 as magnetized, after a 300°C heating and after a 450°C heating. Figure 29 summarizes the dependence of axial field and 2nd quadrant properties of remanence and coercive force as a function of the temperature to which the magnets were heated. These results clearly establish that Sm-Co magnets can be produced with property stability up to 300°C; stability in peak axial field, as might be expected, is accompanied by stability in other magnetic properties.

Magnets are not always produced with this degree of stability, and data obtained on other magnets illustrates the variability encountered during this program. For purposes of establishing more typical data, results obtained on a variety of magnets are reported below.

Magnets were derived from 3 different lots of samarium and the associated magnetic properties of B_r , H_c and H_{ci} were measured before and after temperature cycling. The results are shown in Figure 30. The experimental procedure was as follows:

- (a) Magnets individually magnetized - 52 kOe, 10 msec.
- (b) B_r , H_c , H_{ci} measured in hysteresis tracer.
- (c) Pulse demagnetized to less than 5% of original magnetization.

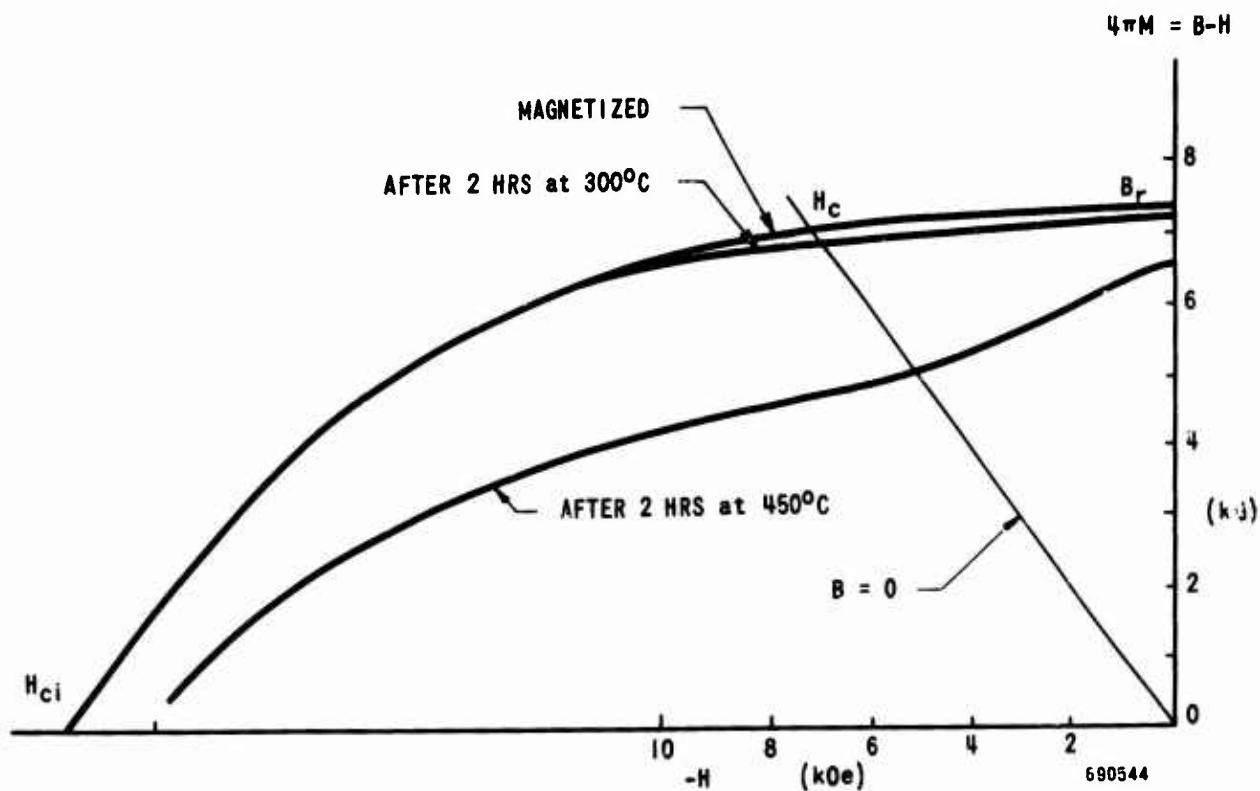


Figure 28. Sm-Co Magnets with Low Irreversible Thermal Loss measured at Room Temperature after Cycling in a PPM Stack to Indicated Temperature

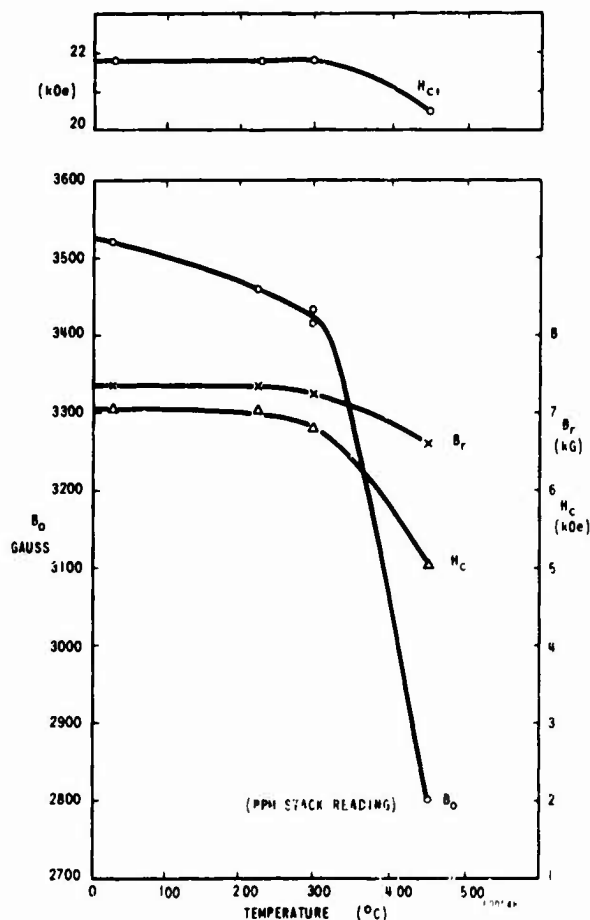


Figure 29. Magnetic Characteristics of Sm-Co Magnets with Low Irreversible Loss. Measured at Room Temperature after Cycling in a PPM Stack to Indicated Temperature.

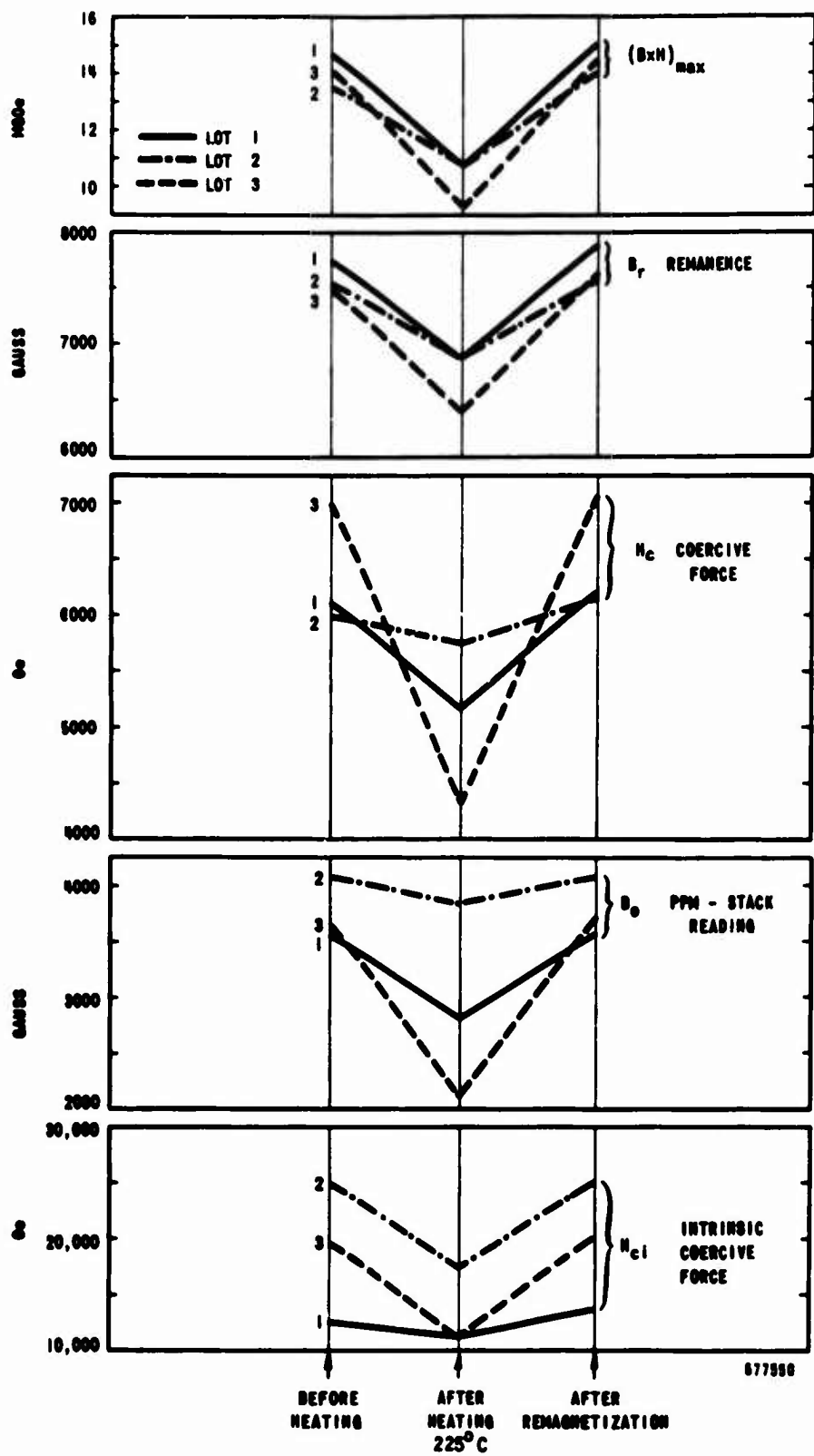


Figure 30. Thermal Stability of Sm-Co TWT Magnets Measured at Room Temperature.

- (d) Remagnetized individually and stabilized 1 hour at 225°C in PPM stack with standard end magnets.
- (e) Remeasured B_r , H_c , H_{ci} .
- (f) Demagnetized, remagnetized as before and remeasured B_r , H_c , H_{ci} .

The data in Figure 30 shows that the energy product $(BH)_{max}$ is not a good guide to stack performance of a TWT magnet; the intrinsic coercive force H_{ci} appears to correlate better with stack performance and thermal stability. Magnets from lot 3 held up best through temperature cycling and also had the best stack reading as well as high H_{ci} . It is not particularly surprising that material of higher H_{ci} is more resistant to elevated temperatures and to magnetic loadings such as in stack performance. These three lots of Sm-Co magnets were typical of magnet production quality during the initial phase of this program. Since then, the magnet quality has improved significantly.

In another case, four sets of magnets were measured, as follows:

- Set 1 12 production TWT magnets from a 5-lb melt, pressed on the automatic press.
- Set 2 12 laboratory TWT magnets, selected from several laboratory-produced lots.
- Set 3 4 production TWT magnets from a 5-lb melt but of marginal quality.
- Set 4 8 disc-shaped magnets from a 5-lb melt, of satisfactory magnetic quality but chosen for high irreversible loss.

The magnets of sets 1, 2, and 3 were standard ring-shaped TWT magnets 0.550 in. OD x 0.250 in. ID x 0.130 in. thick. Sets 1 and 2 were magnets of acceptable TWT quality while the magnets of set 3 were of marginal quality not meeting TWT acceptance requirements but close to it. The magnets of set 4 were solid discs 0.550 in. dia. x 0.125 in. long of acceptable quality. Data obtained from these samples are described in the following sections.

(a) Magnetic Measurements

Flux measurements were performed on all magnet sets using an integrating fluxmeter and a search coil surrounding the magnet under test. These measurements were done both at room and elevated temperatures on a hot plate. Special care was taken to achieve a uniform temperature in a magnet stack.

Axial field measurements for PPM stacked TWT magnets were performed for magnets of sets 1, 2, and 3 in a temperature-controlled furnace. The field was measured using a small search coil 0.140 in. OD and 0.040 in. long with 2500 turns of No. 52 wire and a recording fluxmeter.

The 2nd quadrant data of magnetization vs demagnetizing field were measured before and after baking under different conditions. An integrating fluxmeter hysteresis tracer was used to obtain the 2nd quadrant demagnetization curves on a recorder. Calibration was made with Ni standards for the magnetization and with a Hall probe for the demagnetizing field.

(b) Tests

Test No. 1 - Thermal Processing Time. PPM-stacked TWT magnets of sets 1, 2, and 3 were temperature-cycled to determine the thermal processing requirements for producing stable magnets. The results are shown in Figure 31. Two 15-minute heatings at 150° and 250°C, and two 60-minute heatings at 250°C indicated that in each case the first heating was sufficient to stabilize the peak axial field of PPM-stacked magnets. The magnetic measurements were made at room temperature. Further measurements at up to 4 hours heating at 150°C and 12 hours heating at 250°C showed that the field remained constant after a short initial period of several minutes to reach thermal equilibrium. Both the reversible and irreversible losses appear to be stabilized in this short period, based on the measurements performed in this segment. The total loss was magnetically recoverable in each case.

Other observers³ have also found that one heating cycle removes all irreversible loss for permanent magnet materials and that stability is reached quickly.

Test No. 2 - Effect of Thermal Processing on Second Quadrant Properties and Temperature Coefficients. Second quadrant measurements were made before and after various heat treatments for a magnet from each set (1 through 4). The data for a set 2 and a set 3 magnet are shown in Figures 32 and 33. The effects of heating a single magnet for 1 hour at 250° and 350°C are shown, as well as the effect of a PPM stack heating of the same magnet to 250°C. It can be seen that heating in a PPM stack has a greater effect on loss of magnet quality (particularly in the vicinity of $B = 0$) than does heating as a single magnet. The PPM stack configuration involves a larger demagnetizing field than an open-circuited magnet. It appears that H_{ci} was almost unchanged by heating to 350°C. The poorer magnets of set 3 (Figure 33) showed a greater loss of magnetization due to 250°C heating than the acceptable magnets of set 2 (Figure 32).

Test No. 3 - Thermal Flux Loss. A comprehensive set of measurements was made of the thermal loss of flux in TWT magnets of set 2 (production magnets of acceptable quality) as a function of the demagnetizing field

³

A. G. Clegg, M. McCaig, "The High Temperature Stability of Permanent Magnets of the Iron-Nickel-Aluminum System," Brit. J. Appl. Phys. Vol 9, p. 194 - 199, 1958.

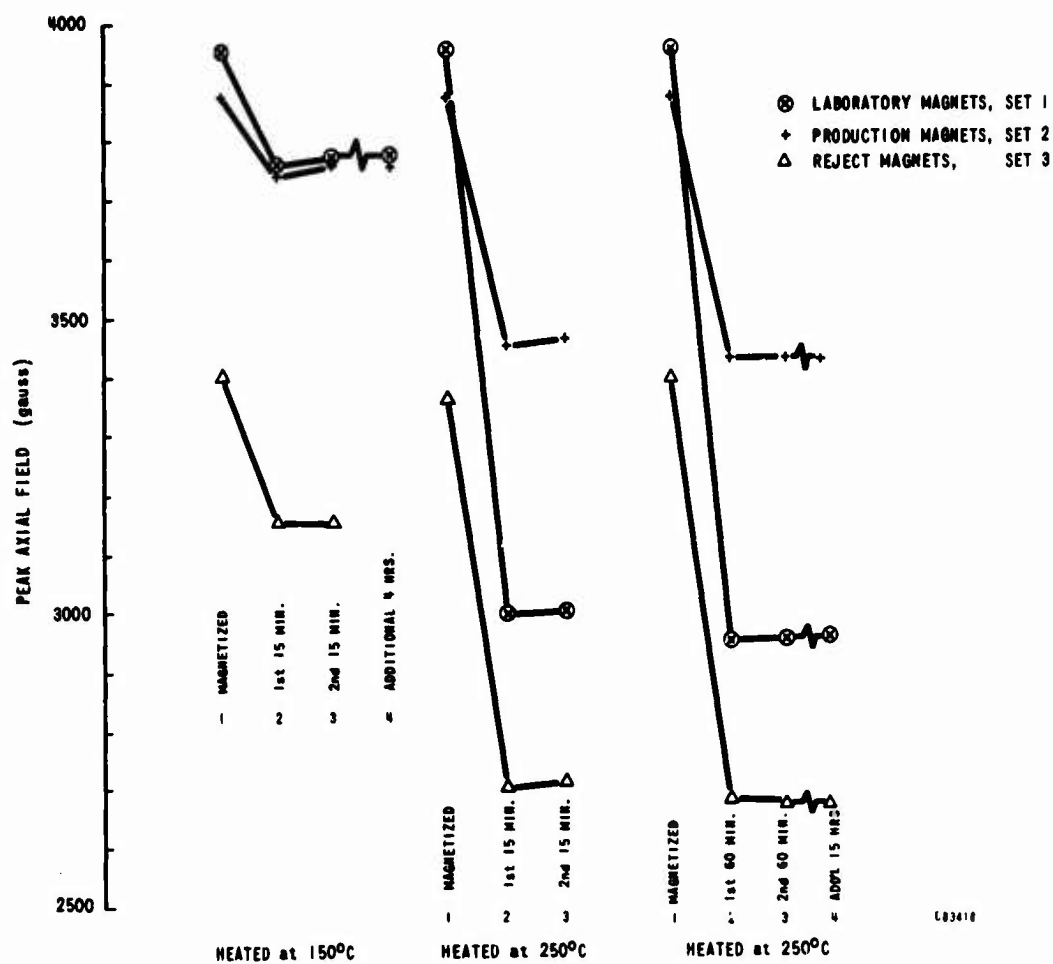


Figure 31. Thermal Processing of PPM Stacked Magnets, Measured at Room Temperature after Cycling to Temperature Indicated

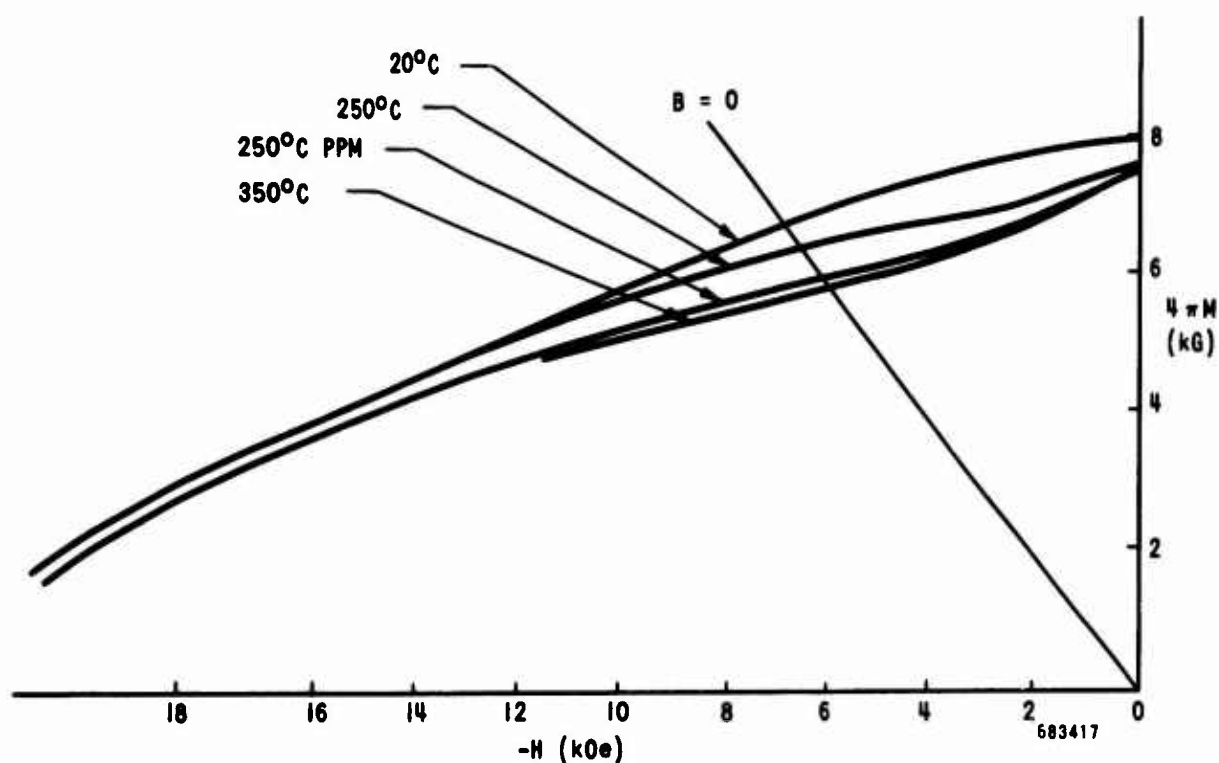


Figure 32. Magnetization $4\pi M$ vs Field H Measured at Room Temperature after Heating to Temperature Indicated on Curves. Single Magnets $B/H = -0.9$, PPM Stack $B/H = -0.3$. Production Magnets, Set 2.

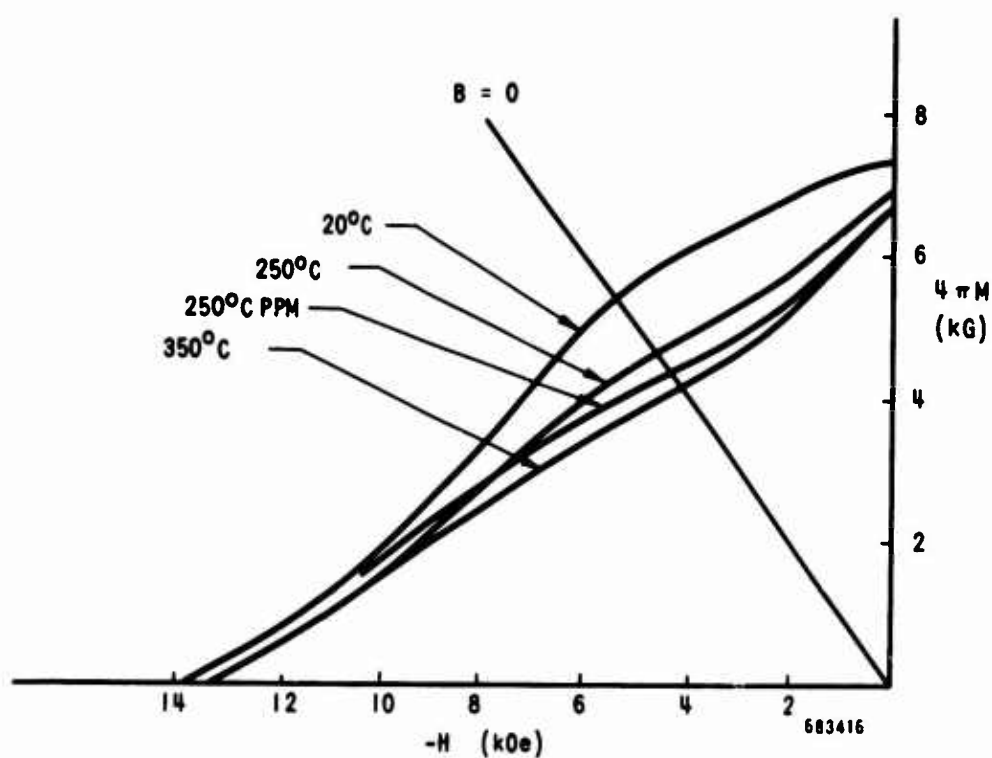


Figure 33. Magnetization $4\pi M$ vs Field H Measured at Room Temperature after Heating to Temperature Indicated on Curves. Single Magnets $B/H = -0.9$, PPM Stack $B/H = -0.3$. Marginal TWT Magnets, Set 3.

during heating at 150°C and 250°C. These measurements were performed on the hot plate and were taken at room temperature as well as at heating temperature. The results are shown in Figure 34. Since the demagnetizing field is proportional to the magnetization, $4\pi M$, of a permanent magnet, it will be lower at higher temperatures. The values plotted here are at room temperature, prior to heating. The demagnetizing field was varied by parallel stacking of magnets. Thus, four cases were measured: 1 magnet, 2 magnets, 4 magnets, and 8 magnets. In each case the flux of the same magnet was measured. The normalization of the flux was always made with respect to that obtained at room temperature after magnetizing in the magnet grouping indicated. Thus all measurements of reversible loss were made at temperature and are expressed as a percentage of room temperature flux after stabilization. Both the reversible and irreversible portions of the loss of flux can be obtained from the data shown in Figure 34. These were then plotted in % of loss of flux (reversible and irreversible separately) as a function of demagnetizing field, H_d , for two temperatures 150°C and 250°C and also as a function of temperature for several values of H_d . The demagnetizing field is specified at room temperature. These results are shown in Figures 35 through 38.

Figures 35 and 36 show the irreversible and reversible loss of flux as a function of H_d at 150°C and 250°C. The dependence appears to be linear in both cases. The irreversible loss varies more strongly with H_d than the reversible loss and goes to zero at $H_d = 0$ while reversible loss has a significant value at $H_d = 0$.

The temperature dependence of these losses is shown in Figures 37 and 38. The reversible loss (Figure 38) varies very nearly linearly with temperature while the irreversible loss varies at a more rapid rate, particularly at higher demagnetizing fields. Because of the approximately linear behavior of the reversible loss, it is convenient to define a temperature coefficient in $\%/^{\circ}\text{C}$ for the flux loss. Up to 150°C, this coefficient had the value 0.035%/°C at $H_d = 0.8$ kOe and 0.042%/°C at $H_d = 4.2$ kOe. The behavior of the irreversible and reversible losses shown here for Sm-Co magnets is qualitatively similar to that of Alnico-type magnets.

Test No. 4 - Thermal Processing of Disc Magnets. The flux loss was also measured for a disc-shaped magnet of set 4 (see Figure 39). The data was obtained with a flux coil surrounding the given magnet and heating was performed on a hot plate. Flux was measured at several intermediate temperatures between 25° and 300°C. After measurement at each of these intermediate temperatures, the magnet was cooled down to room temperature, re-measured and then heated to a higher temperature. The sequence in the single magnet case is shown by a set of numbers from 1 to 13. The same magnet was then placed in a stack of 8 magnet discs, heated to 250°C and cooled back to room temperature. The dashed curve of Figure 39 shows the data for this case. The case of 8 magnets has a larger L/D ratio and a computed demagnetizing field⁴ of 1.1 kOe. The single magnet case corresponds to a smaller L/D ratio of a demagnetizing field of 4.1 kOe.

⁴ Parker, R.T. and Studders, R.T., Permanent Magnets and Their Applications, Wiley and Sons, 1962, p. 163-169.

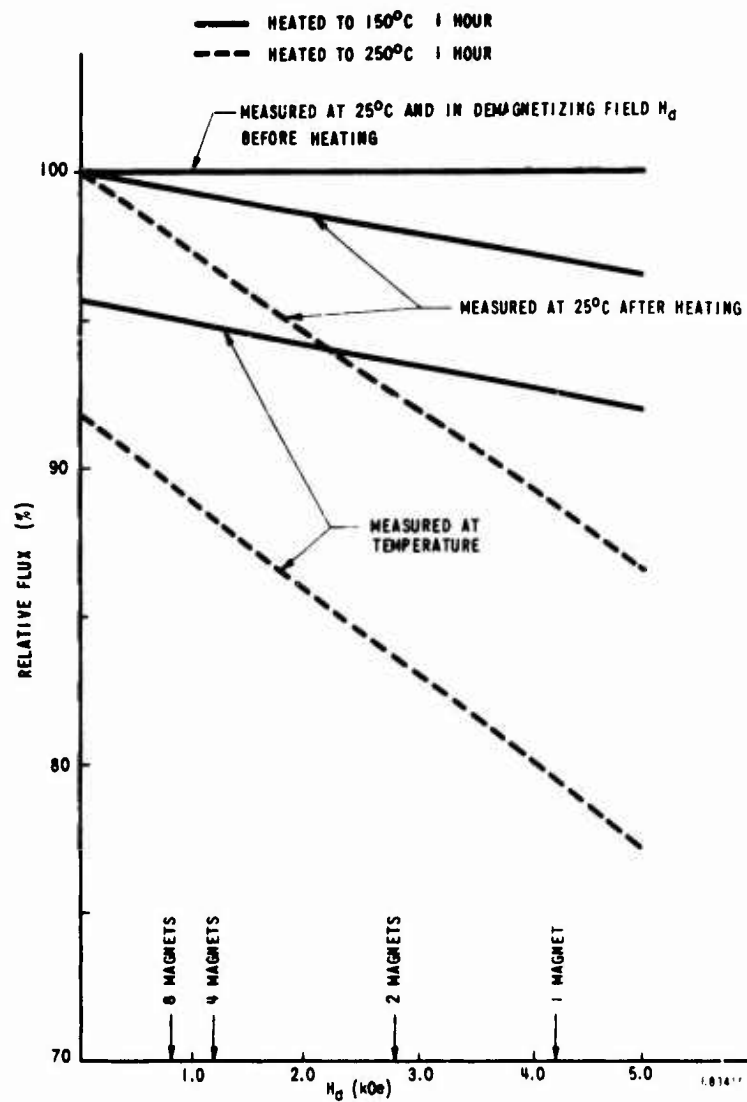


Figure 34. Thermal Loss of Flux in TWT Magnets vs Demagnetizing Field, H_d - Production Magnets, Set 2

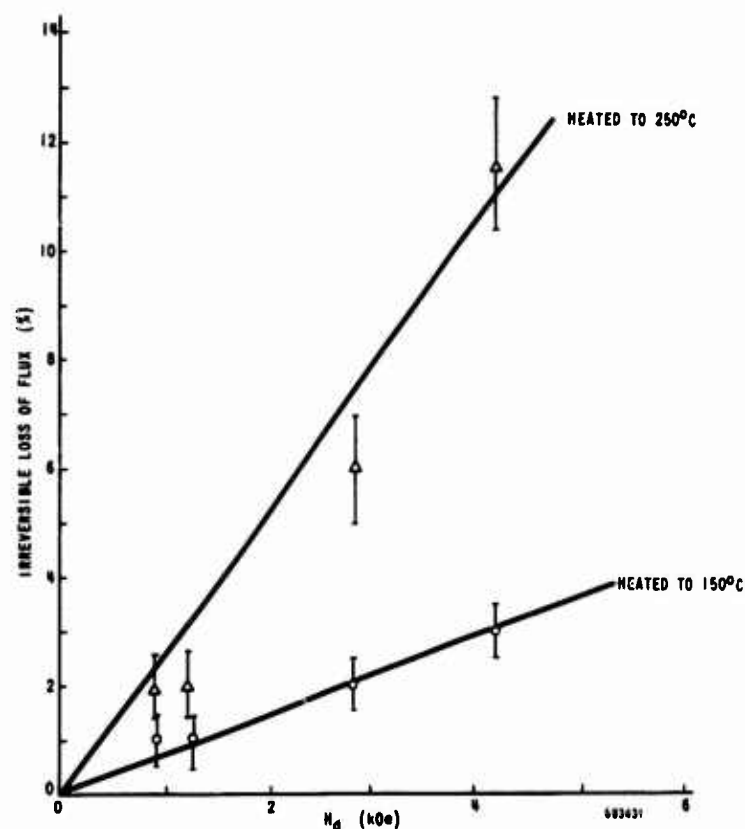


Figure 35. Irreversible Loss of Flux in TWT Magnets vs Demagnetizing Field, H_d - Production Magnets, Set 2.

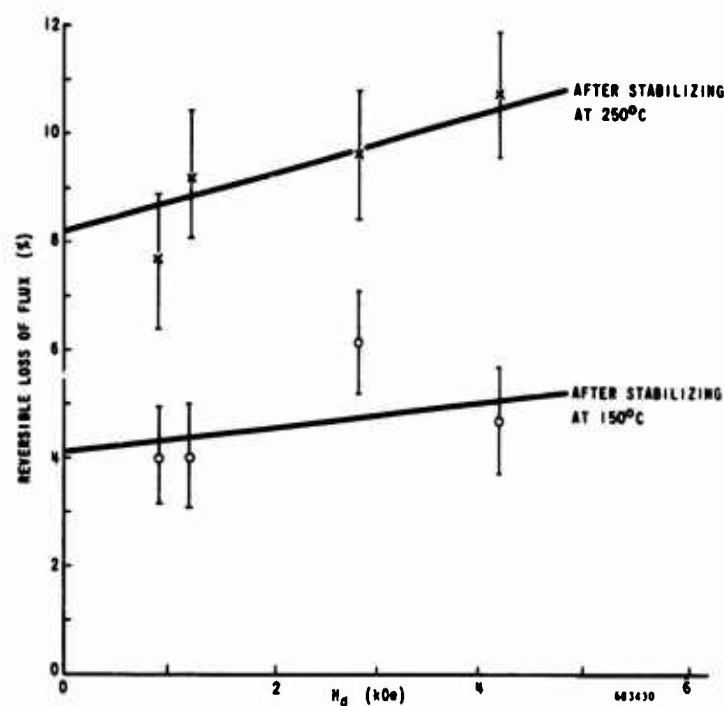


Figure 36. Reversible Loss of Flux in TWT Magnets vs Demagnetizing Field, H_d , - Production Magnets, Set 2.

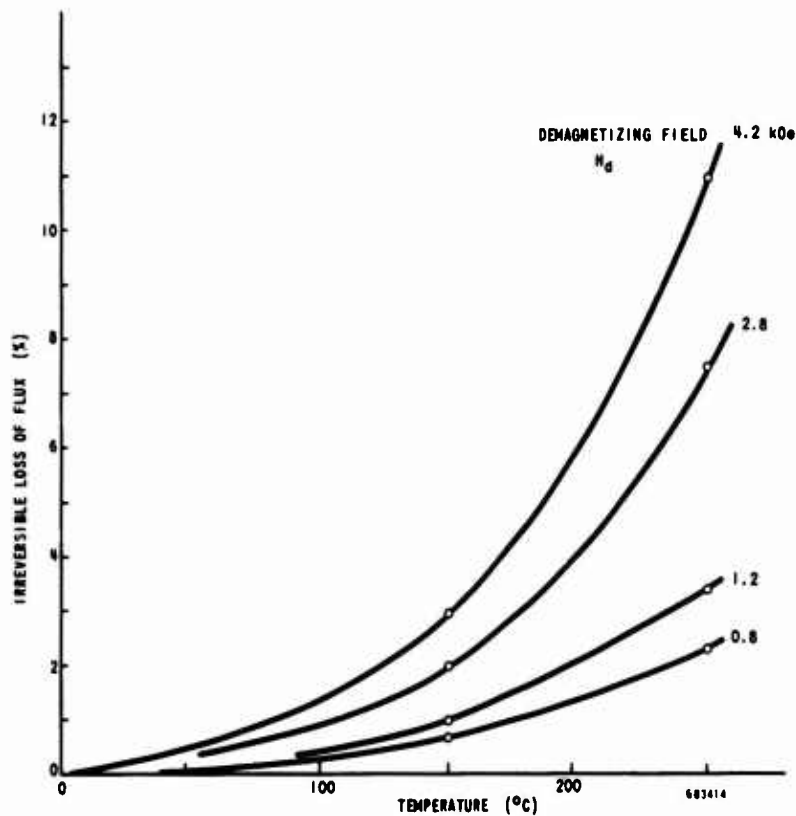


Figure 37. Irreversible Loss of Flux vs Temperature - Production Magnets Set 2.

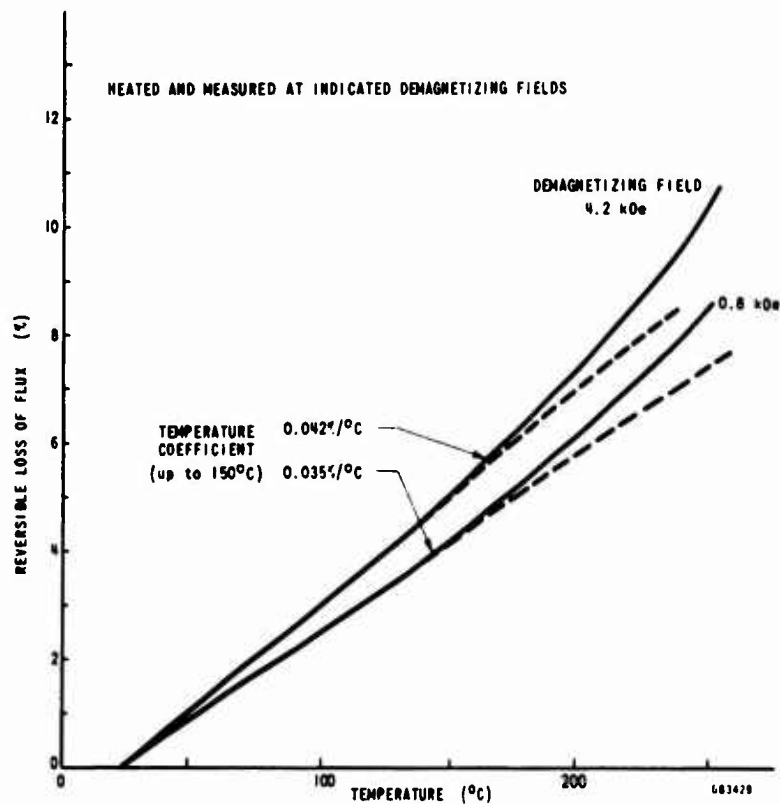


Figure 38. Reversible Loss of Flux vs Temperature for Various Demagnetizing Fields - Production Magnets, Set 2.

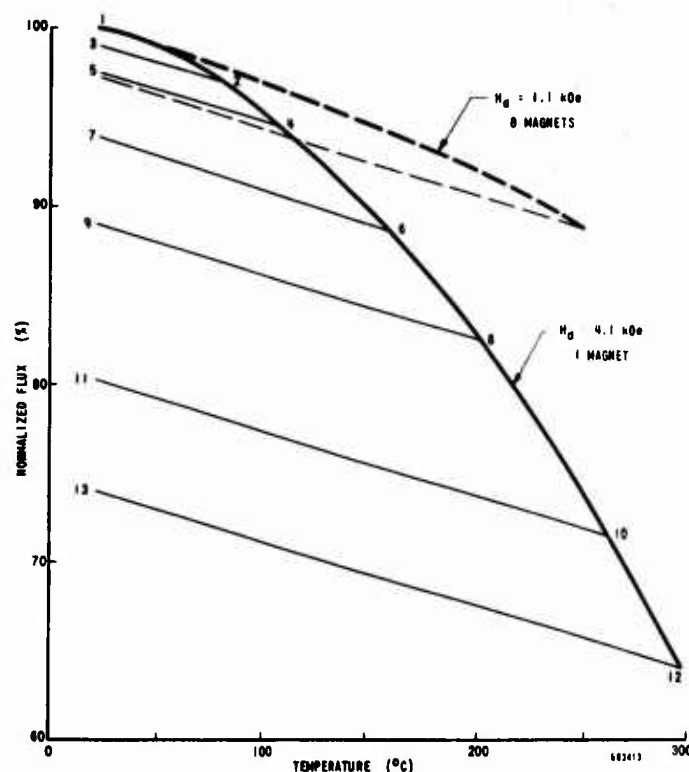


Figure 39. Flux Loss vs Temperature - Disc Magnets, Set 4

The reversible and irreversible losses were computed from the data of Figure 39 and then plotted as a function of temperature in the range 25°C to 300°C for the two demagnetizing fields 1.1 kOe and 4.1 kOe. (See Figures 40 and 41). Figure 40 demonstrates the almost linear behavior of the reversible loss, particularly at lower demagnetizing fields. Up to 150°C, the temperature coefficient was 0.036%/°C, which is quite similar to the range of values 0.035 to 0.042%/°C shown in Figure 38 for ring-shaped TWT magnets of set 2. The irreversible loss of flux shows a much stronger temperature dependence (Figure 41). The effect of the demagnetizing field is also much larger than for reversible loss. In general, the behavior of the disc-shaped magnets was similar to the ring-shaped TWT magnets of set 2.

Test No. 5 - Reversible Thermal Losses in PPM Stacks. Since Sm-Co magnets for TWT's are actually used in the PPM stack configuration, it was important to determine thermal losses when magnets are heated in that form. The magnets of sets 1, 2, and 3 were PPM stacked, heated to 255°C for 1 hour and then cooled slowly. The peak axial field was measured at temperature over the cooling interval 150° to 20°C with a small search coil, 0.140 in. dia., inserted into the stack. The heating and cooling was carried out in a thermally-controlled furnace. The data is shown in Figure 42. The temperature coefficient for reversible thermal loss for sets 1, 2, and 3 were found to be 0.039%/°C, 0.048%/°C, and 0.049%/°C, respectively. These values are slightly larger than those obtained in smaller demagnetizing fields as reported in Figures 38 and 40.

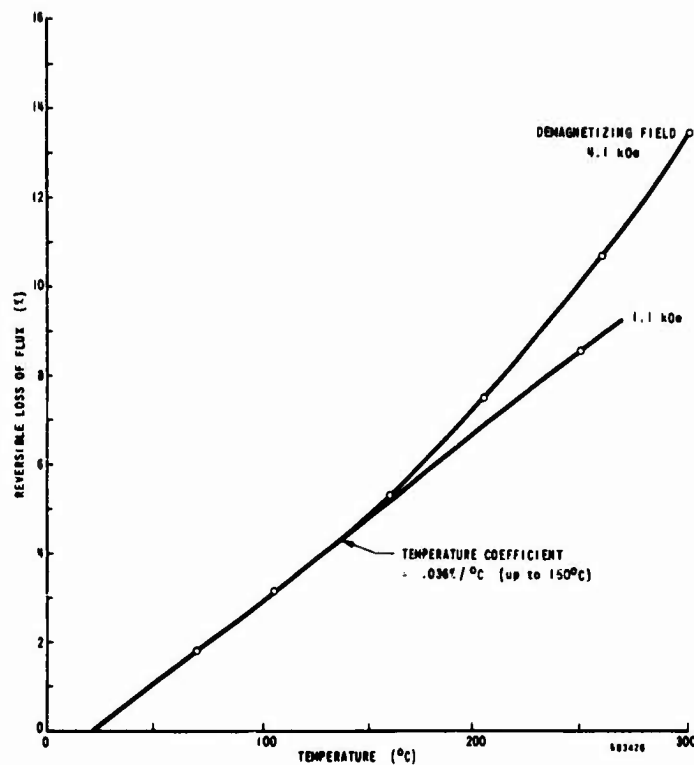


Figure 40. Reversible Loss of Flux vs Temperature - Disc Magnets, Set 4.

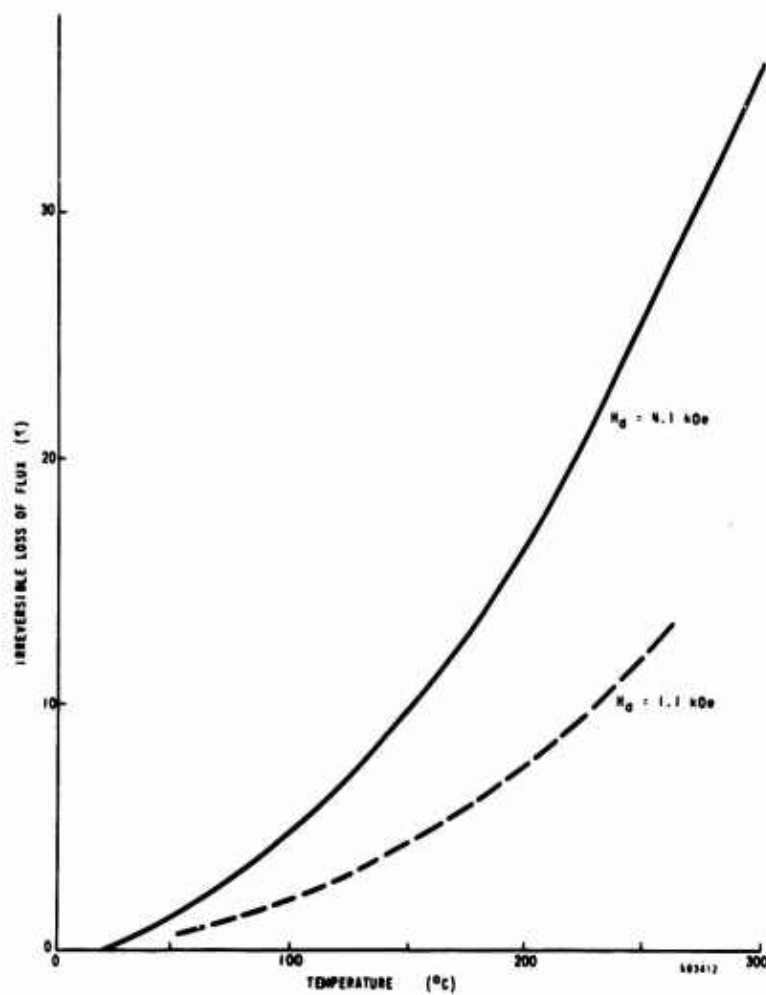


Figure 41. Irreversible Loss of Flux vs Temperature - Disc Magnets, Set 4

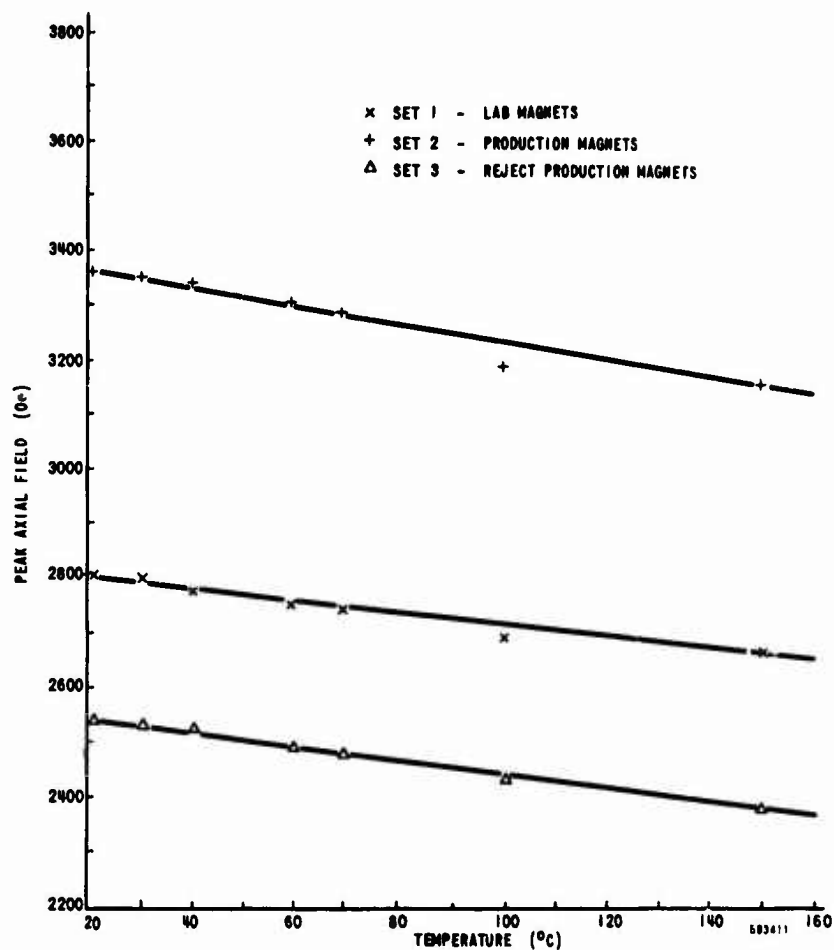


Figure 42. Reversible Thermal Losses of Peak Axial Field in a PPM Stack after Heating to 255°C for 1 Hour. Measured at Temperature During Cooling.

(c) Survey of Magnet Characteristics

Table XII shows the thermal behavior of different magnets in a PPM stack, all under the same conditions. The demagnetizing field was 4.1 kOe and the temperature 150°C. These data were extracted from all the measurements reported here. When the field and temperature deviated from the above values, the losses were corrected to 150°C and 4.1 kOe, according to the dependence reported in section (b) above.

The irreversible losses depend very strongly on the magnet alloy type, although specific alloy characteristics have not yet been identified. There seems to be no connection to the intrinsic coercive force or remanence. To be acceptable for PPM stacks, the irreversible losses must be small because the higher demagnetizing fields (6 kOe) increase the losses considerably. The reversible losses also change with alloy type, but to a much lesser extent. Magnets with low irreversible losses have a quite uniform reversible coefficient of 0.031%/°C in the temperature interval room temperature to 150°C. Acceptable magnets with higher irreversible losses have a coefficient as high as 0.038%/°C.

Table XII Survey of Magnet Characteristics.

Set	B _r	H _c	H _{ci}	Loss ΔB/B by heating from RT to 150°C		T-Coeff. $\frac{\Delta B}{B \Delta T}$ between RT and 150°C		H-Coeff $\frac{\Delta B}{B \Delta H}$ at 150°C, between 0 and 4.1 kOe		Magnet Quality Rating
	RT			Irrev. %	Rev. %	Irrev. %/°C	Rev. %/°C	Irrev. %/kOe	Rev. %/kOe	
	Heated at 250°C									
	kG	kOe	kOe							
1	7.9 7.9	7.1 6.7	17 17	4.4	4.0	0.034	0.031	1.07	----	Acceptable for PPM
2	8.0 7.6	6.8 6.4	23 22	3.0	4.0	0.023	0.031	0.74	0.034	
3	7.4 7.0	5.3 4.7	14 13	7.3	4.9	0.056	0.038	1.78	----	Not acceptable for PPM but accept- able for other use.
4	7.6 7.4	6.9 6.2	21 21	10	4.9	0.078	0.038	2.44	0.071	

Heating Temperature 150°C
Demagnetizing Field 4.1 kOe

The irreversible losses are proportional to the demagnetizing field. A much weaker dependence is found in the reversible losses. For magnets acceptable in TWT's, H_c drops considerably less during heating than for magnets acceptable for general use (lower demagnetizing field) which may have higher irreversible losses.

(3) Long Term Stability

Long term stability of magnets has been investigated in various thermal and demagnetizing environments. Results have been obtained on two PPM stacks of 14 split magnets, each with pole pieces brazed in place. These magnets had previously been thermally cycled in a PPM stack for 2 one-hour cycles at 225°C. After this initial stabilization, the stacks were cycled to 200°C (approximate anticipated use temperature) with oven power on for 20 hours and off for 4 hours, for a total elapsed time of 750 hours. Cycling contrasted to continuous exposure at temperature simulates to a certain extent actual conditions in tube use. Axial peak fields were measured and the average decrement (14 positions measured) for one stack was 3.5% and the other 3.9%. These figures include losses due to pole piece oxidation, actual demagnetization of magnets, probably some slight surface oxidation of magnets, and mechanical changes. Magnet stacks in tubes are completely potted and protected from oxidation. Further tests are required to determine actual long-term demagnetization in thermal environments, but these results indicate samarium-cobalt is quite stable.

Another test was made without cycling. The magnets were not split, and the pole pieces not brazed in place as in the above cycling experiment. Two PPM stacks were used. The first stack consisted of magnets from sets 1, 2, and 3, identified on page 57. This stack, after being heated to 250°C for 1 hour was exposed to 230°C and normal relative humidity for 900 hours. No measurable change was found in stack readings or hysteresis curves (see Table XIII and Figure 43). The temperature was monitored by a thermocouple attached to the PPM stack. The second stack was made of magnets from sets 1 and 2. It was exposed for 830 hours to 80°C and 95% relative humidity. This is equivalent to extreme tropical conditions. The result is shown in Table XIV. Here, too, no measurable degradation was found.

Table XIII

QR1642 Axial Field Test at 230°C, Normal Humidity
Room Temperature Measurements

Alloy	Set No. 1	Set No. 2	Set No. 3
Magnetized	3940	3915	3350
After 1 hr at 250°C	3600	3220	2780
After 500 hrs at 230°C	3620	3240	2740
After 900 hrs at 230°C	(3580)		

Table XIV

Long Term Humidity Test
(80°C, 95% Relative Humidity)

Alloy	Stack Reading at Room Temperature	
	Set 1 (6 pairs)	Set 2 (6 pairs)
Magnetized	3840	3965
After 1 hr at 225°C	3475	3325
After 500 hr at 80°C, 95% H	3485	3315
After 830 hr at 80°C, 95% H	3490	3345

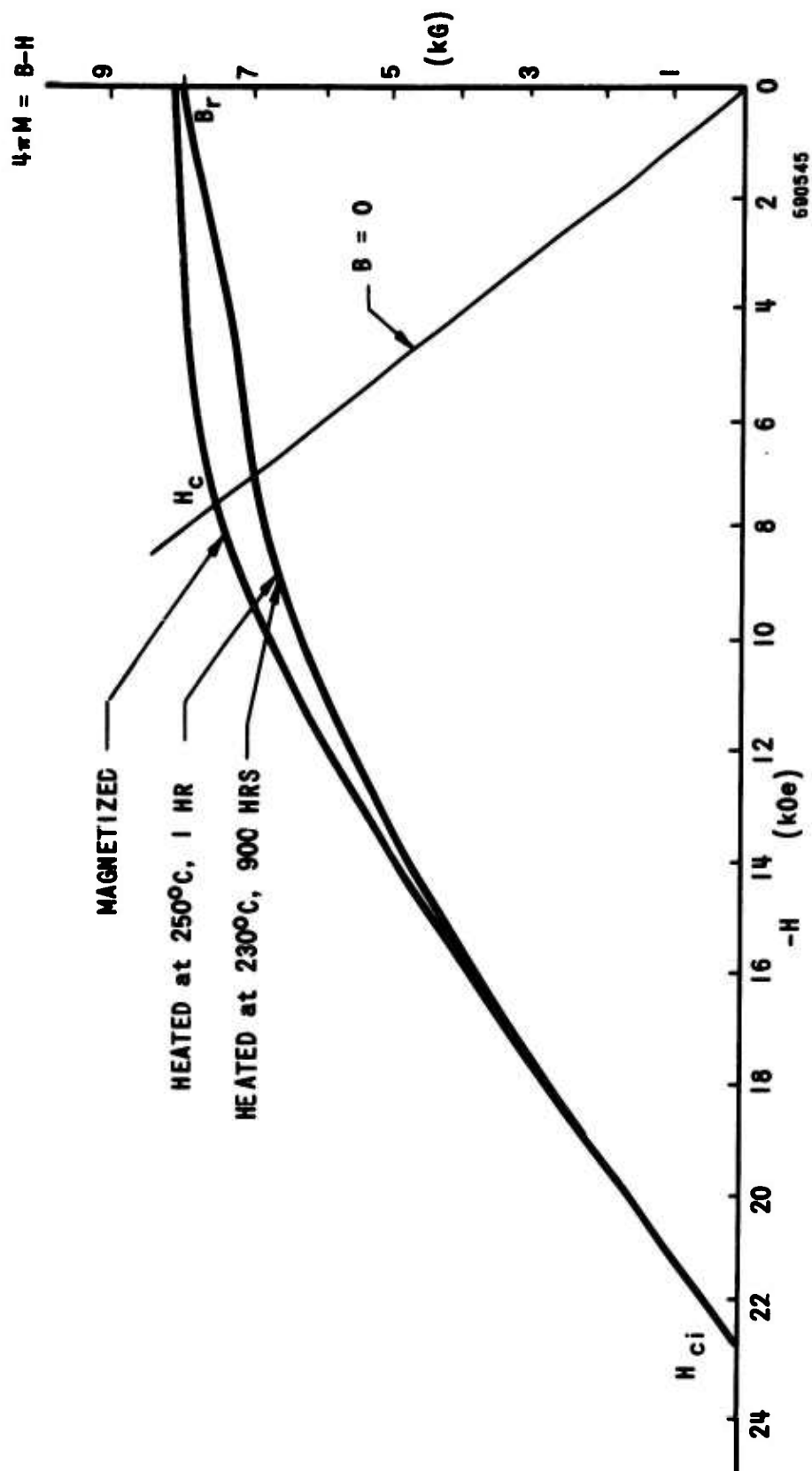


Figure 43. Effect of Long Term Heating in a PPM Stack, Set 2. Measured at Room Temperature after Cycling at Indicated Temperature.

(4) Low Temperature Exposure

The same PPM stacks used for the long term stability tests above were exposed to and measured at low temperatures. The stacks were immersed in fine dry ice snow for 2 hours, and in liquid nitrogen for 20 minutes. Prior to that, the stack was heated to 225°C for one hour. No irreversible changes were found (Table XV).

The reversible thermal loss of a disc magnet from set 4 is shown in Figure 44. For this purpose a magnet (heated to 225°C for 1 hr) was mounted on top of a copper cylinder and thermal contact was made with silicone grease. The temperature was measured with a thermocouple close to the top of the copper cylinder. The flux was measured with a 0.620 in. ID coil. The magnet had an OD of 0.550 in. and a length of 0.190 in. giving a B/H ratio of -0.93. The flux increased with decreasing temperature with a coefficient in the range 0.04 to 0.06%/°C (see Table XVI). The higher temperature coefficient found here at low temperatures has also been found in Alnico-type permanent magnet materials by others.⁵ They have also observed no irreversible change at low temperatures.

Table XV

Axial Peak Field after Low Temperature Exposure

Treatment	Axial Field Reading at Room Temperature		
	Set 1	Set 2	Set 3
Magnetized	3945	3975	3375
After baking to 225°C, 1 hr	3575	3350	2880
After 1 hr in Dry Ice	3620	3380	2895
After 20 minutes in liquid nitrogen	3615	3380	2905

⁵ R. K. Tenzer, "Effects of Temperature Variation on the Remanence of Permanent Magnets", Proc. 1957 Conf. on Magnetism and Magnetic Materials, pp. 203-211.

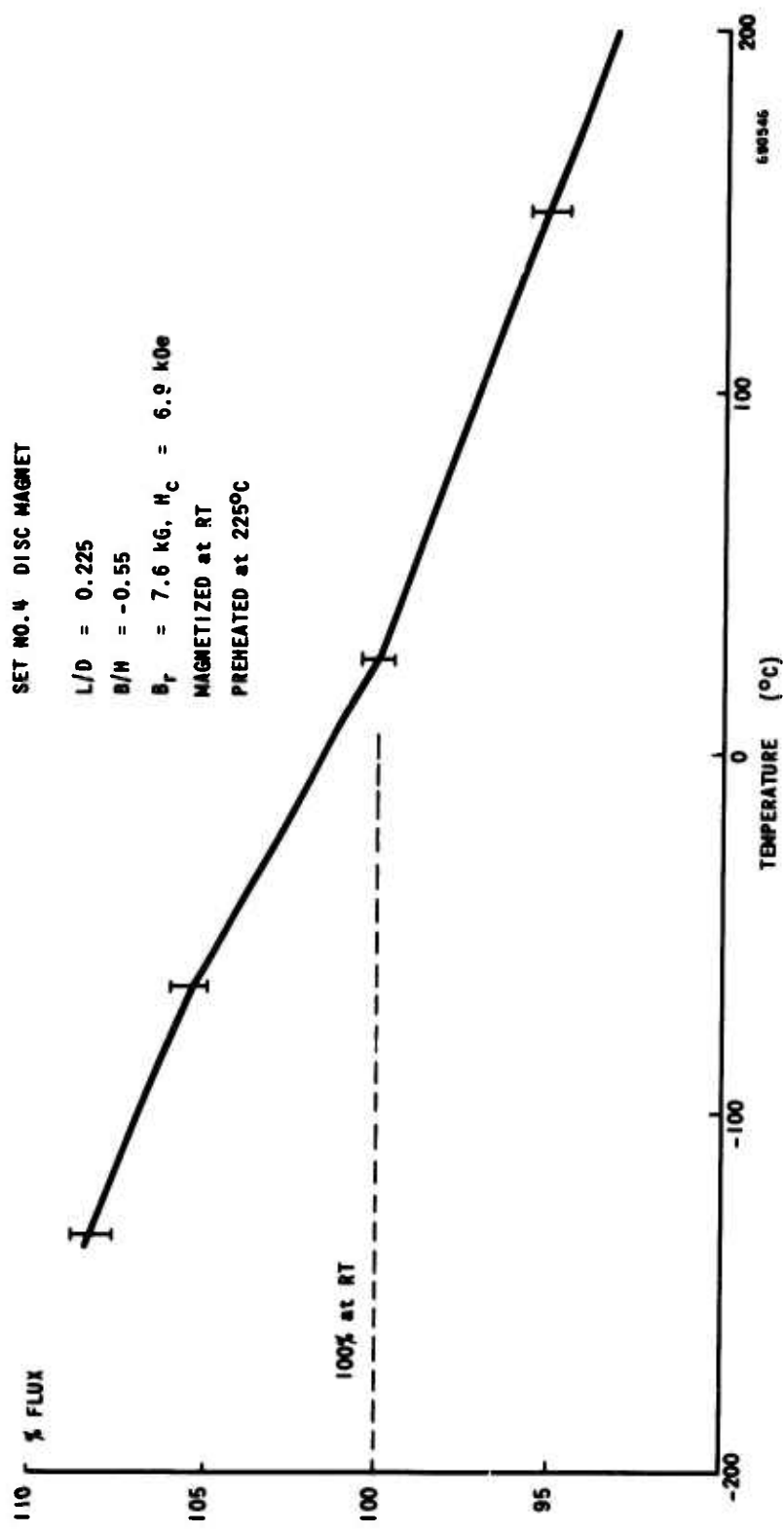


Figure 44. Reversible Flux Change at Low Temperatures

Table XVI
Temperature Coefficient at Low Temperatures

Temperature (°C)	Flux %	Rev. Coefficient (%/°C) to Room Temp.
+ 150	95.3	.038
+ 25	100.0	
- 65	105.5	.058
- 135	108.2	.048

(5) Oxidation Rate

In previous sections thermal stability was determined by various magnetic property measurements. No measurable changes were detected for periods of up to 900 hr at 230°C. As an additional measurement of stability, oxidation rates were determined.

The rate of oxidation is extremely slow, and to amplify weight gain, a sintered magnet was ground into powder. The higher surface to volume ratio, S/V, increases the amount of oxidation for a given period of time.

Figure 45 shows the particle size distribution, $n(r)$. The oxidation rate is proportional to the surface area and the weight gain, the weight being proportional to the volume. Therefore, the weight gain in % is proportional to S/V. The S/V ratio of a particle is

$$S/V = 4\pi r^2 / (4/3 \pi r^3) = 3/r. \quad (9)$$

The average S/V ratio of a powder with a distribution $n(r)$ is

$$\frac{\int_0^{\infty} (3/r)n(r) dr}{\int_0^{\infty} n(r) dr} \quad (10)$$

$S/V = 29 \text{ mm}^{-1}$. From Figure 45 we integrate graphically and obtain

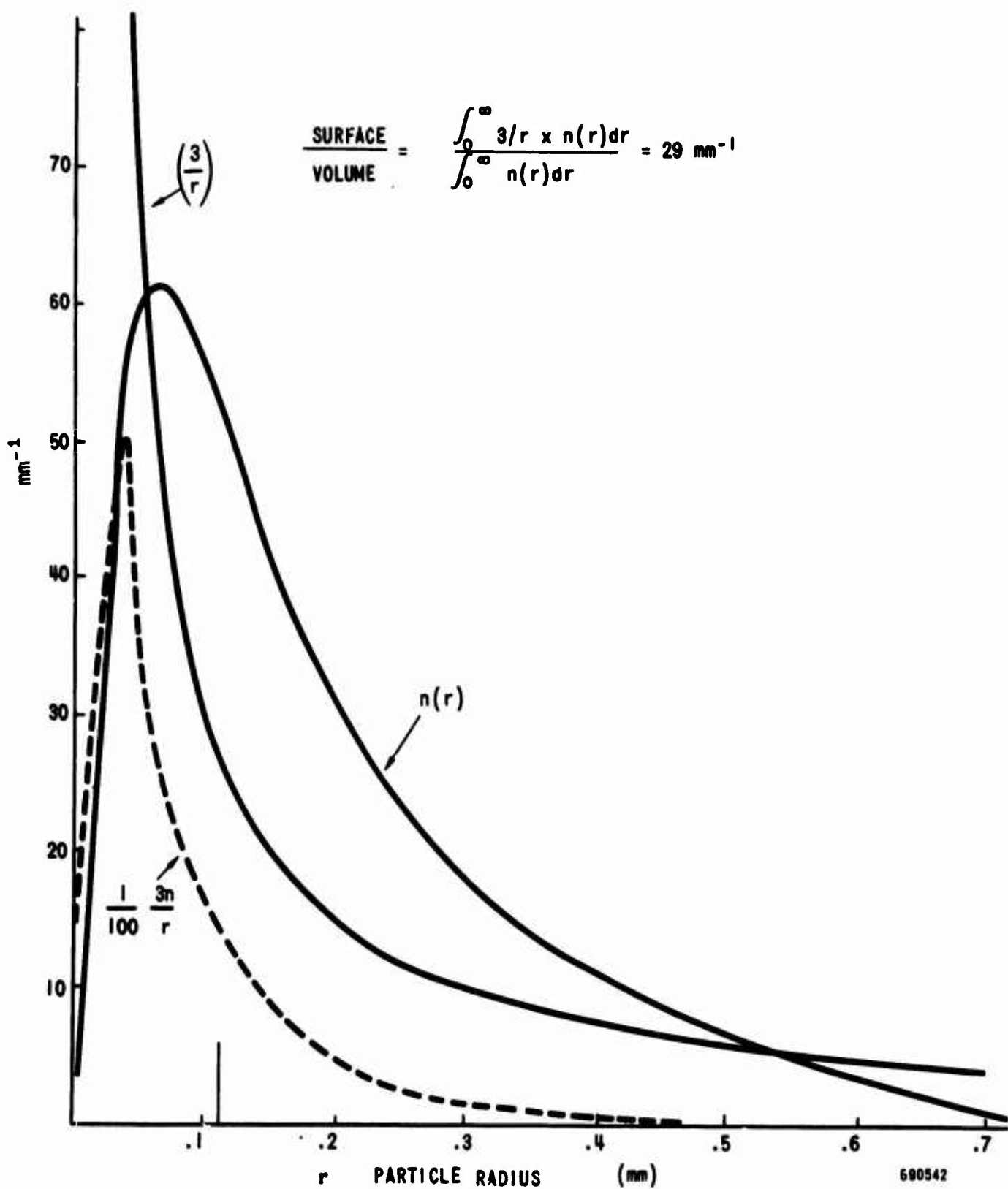


Figure 45. Powder Characteristics for Oxidation Test

For a QR1642 magnet, we obtain

$$S/V = \frac{1}{2L} + \frac{1}{D_0 - D_1} = 0.28 \text{ mm}^{-1}. \quad (11)$$

Therefore, the S/V ratio of the powder is 100 times larger than that of the magnet. Figure 46 shows an initial rate of weight change of 0.34%/hr for powder at 250°C in air. This measurement was made with a DuPont Thermobalance. Prior to that, the powder was ground and stored in toluene. Immediately before the measurement, it was heated in vacuum. We assume that the rate of oxidation can be represented by

$$X = a e^{-bt} \quad (12)$$

By analysis of the experimental data we obtain for the powder

$$X_{\text{powder}} = 0.34 e^{-1.2t} \%/\text{hr} \quad (13)$$

where t = time in hours. It can be shown that for a magnet we obtain

$$X_{\text{magnet}} = X_{\text{powder}} \frac{(S/V)_{\text{magnet}}}{(S/V)_{\text{powder}}} = 0.0034 e^{-1.2t} \quad (14)$$

For infinite time, we obtain a total weight increase of

$$\Delta W = \int_0^{\infty} X(t) dt = 0.0028 \%$$

for a QR1642 magnet which is negligible.

9. PACKAGING AND SHIPPING

Shipped magnets, magnetized or not, are kept in matched pairs when split. Each split pair is put together in the attracting mode and pressed into a P.V.C. multi-cavity shipping insert. These inserts are stacked in layers with foam insulation between them, and placed in a plexiglass container. The hinged lid is closed and taped. These containers, which hold as many as 50 magnet pairs, are overpacked in conventional PPP636 shipping cartons with foam insulation. When magnetic shielding for air shipping is required, MIL-S-4473C, which simply states that the field at 7 ft from any surface shall be 0.00525 gauss maximum, is followed. The magnets in the attracting mode are already partially keepered, thus reducing the leakage field. If further reduction in leakage is required, sufficient layers of 26 gage low carbon steel (annealed) complying with QQ-636 is wrapped around the foam.

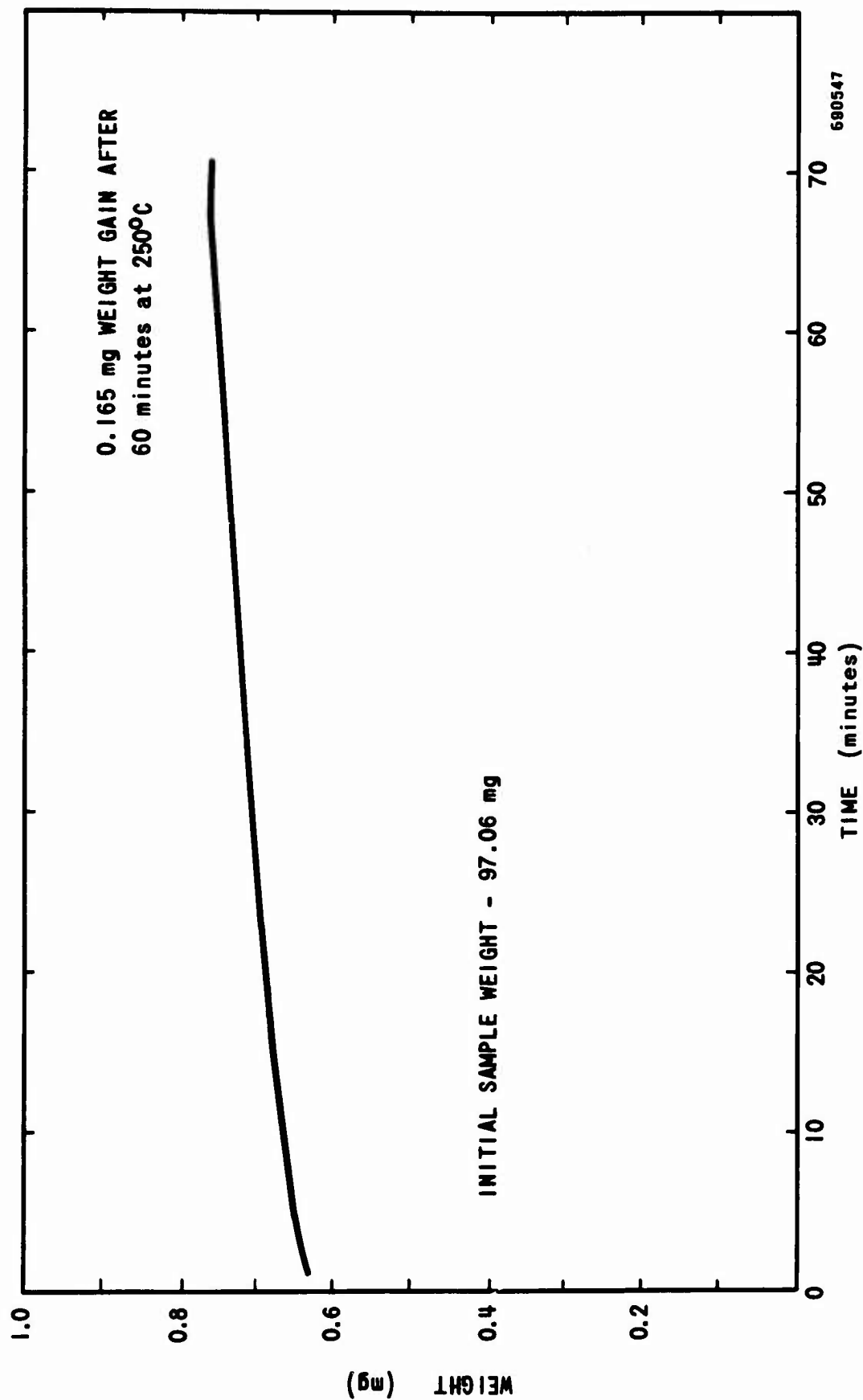


Figure 46. Weight Gain of Sm-Co Powder Sample at 250°C, 50% Relative Humidity

SECTION IV

MEASUREMENTS OF PPM STACKS AND COMPARISON WITH THEORY

During this program, we became aware of certain magnetic circuit design problems associated with PPM structures for TWT's. In some cases measured peak axial fields differed from those calculated. Magnets that produced high fields tended to reduce the peak field of neighboring magnets with low fields. Furthermore, the magnetization losses after heating a PPM stack were considerably higher than the losses after heating a single magnet although, according to some theories,^{6, 7, 8} a single magnet has a B/H ratio similar to one in a PPM stack (QR1642, B/H = -0.9 single and -1.0 in a stack. Raytheon's estimate of the average B/H in a stack is -0.3. In an attempt to understand all this, several PPM design theories^{7, 8, 9} were tested by actually measuring hysteresis curves and peak axial fields using QR1642 TWT magnets of different quality. Further effort should include varying the magnet dimensions. There is a lack of experimental evidence covering a wide range of magnetic and geometric parameters. The tests reported here primarily concern the variation of magnetic parameters and represent a preliminary experimental assessment of PPM design theories.

A PPM stack consisting of 5 groups of 4 magnets each was tested. The magnets within each group had similar magnetic characteristics but varied from group to group. A 2nd quadrant hysteresis curve was taken for a typical magnet of each group. The operating point and axial field calculations were then performed for several theories, namely Sterrett and Heffner⁷ (SH), Sterzer and Siekanowicz⁸ (SS), and Schindler⁹ (S), (see Table XVII). The values of B_m/H_m were -0.91 for the SS theory, -0.95 for the SH theory and +0.13 for the S theory. The average value of the ratio H_p (calculated)/ H_p (measured) was $1.16 \pm .03$, $1.02 \pm .02$ and $.94 \pm .08$ respectively. All these theories are seen to be in rough agreement with measured axial fields; however, SH provides the closest agreement.

⁶ K. K. N. Chang, "Optimum Design of Periodic Magnet Structures for Electron Beam Focusing," RCA Review Vol. 16, March 1955, p. 65.

⁷ T. E. Sterrett and H. Heffner, "The Design of Periodic Focusing Structures," IRE Trans. Ed., Jan. 1958, p. 35.

⁸ F. Sterzer and W. W. Siekanowicz, "The Design of Periodic Permanent Magnets for Focusing of Electron Beams," RCA Review, Vol. 18, p. 39 March 1957.

⁹ M. T. Schindler, "An Improved Procedure for the Design of PPM Assemblies for TWT's", IEEE Trans ED, Vol. 13, No. 12, Dec. 1966, pp. 942 - 949.

Table XVII
Comparisons of Calculated and Measured PPM Characteristics
of QR1642 TWT Magnets.

Magnet Group	Measured Values				Calculated Values			
	B_r	H_c	H_{ci}	Average Peak Axial Field, H_p	H_p			
					SS	SH	S	R
No.	G	Oe	kOe	Oe	Oe	Oe	Oe	Oe
1	4420	3750	21	2000	2250	2020	2170	
2	5930	3000	4.1	2100	2560	2300	1640	
3	5970	3700	5.3	2450	2780	2500	2010	
4	7550	5250	14	3125	3630	3300	2960	
5	7900	6200	20	3500	3960	3450	3490	3450

In addition to the more complete comparisons between experiment and theory described above, a computer calculation developed at Raytheon¹⁰ (designated R) which plots the equipotentials and flux lines, was made for the magnets of Group 5 (see Table XVII). The B/H ratio is non-uniform and was found to vary from -0.2 to -3.6. The highest demagnetizing fields are found near the ID of the magnet. The SS and SH theories assume uniform B/H over the entire magnet and imply a lower demagnetizing field than given by effective values based on either S or R theories (non-uniform B/H).

It is believed that the present theories do not take proper account of the demagnetizing field of neighboring magnets. This added demagnetizing field can be expected to affect the axial field much less than it does the value of B_m/H_m . Our best estimate of the average B_m/H_m for the QR1642 PPM magnets is approximately -0.3. This is based on indirect evidence we have relative to irreversible thermal losses and approximate probe measurements of off-axis axial fields in PPM-stacked magnets.

It is believed that there are some shortcomings in present theories. Proper account should be taken of the influence of neighboring magnets in determining the B/H value and the axial field. In addition, further measurements for varying parameters of magnet geometry should be made in pursuance of these issues.

10. W.J. Harold, "Calculations of Equipotentials and Flux Lines in Axially Symmetrical Permanent Magnet Assemblies By Computer", Intermag Conference, Denver, Colorado, April, 1971. To be published.

SECTION V

MICROWAVE DEVICE APPLICATION OF SAMARIUM-COBALT MAGNETS

1. OBJECTIVE

The objective of this phase of the program was to demonstrate the superior functional characteristics of Raytheon QR1642 traveling-wave amplifier focused with samarium-cobalt magnets.

The characteristics of this TWT are as follows: 4% duty cycle, 3 kW, broadband, 8.0 - 12.0 GHz, grid pulsed, 12 dB gain, air-cooled, periodic permanent magnet focused, transparent, 2.0 dB insertion loss max. This is an air-cooled tube that is required to operate with ambient temperatures from -54 to +80°C and air inlet temperatures from -10° to +80°C. Additional environmental requirements are altitude, shock, and vibration. Typical specifications include: altitude, 70,000 ft; shock, 30 G; and vibration at frequencies from 2 - 500 cycles to 5 G. Complete specifications of this device are given in Appendix A.

The periodic permanent magnet focusing circuit for the QR1642 consists of 14 torroided magnets 0.550 in. OD x 0.247 in. ID x 0.130 in. thick, magnetized through the 0.130 in. dimension. Magnets are stacked (NNSSNNSS), separated by pole pieces designed to produce peak magnetic fields along the beam axis of 3000 to 3400 gauss. A typical pole design is illustrated in Figure 47. A photograph of the QR1642 is shown in Figure 48. The view includes a number of focusing magnets with several sub-assemblies.

The power level of this tube is high enough to create temperature increases that obviously eliminate consideration of focusing with ferrites or alnicos. The periodicity and field requirements at X-band require the thin magnetic design and very high coercive force. Therefore, no comparison was made between these and samarium-cobalt magnets. Platinum-cobalt is the only other permanent magnet that could possibly be considered, but, as already demonstrated in an earlier section, it is not as stable in a PPM stack as samarium-cobalt after temperature cycling to 225°C. Samarium-cobalt was used to focus the QR1642 and temperature increases were noted as a function of power and duty cycle. This demonstrated the power/duty cycle point beyond which only samarium-cobalt would continue to focus the tube.

2. ENVIRONMENTAL TESTING OF THE QR1642 TRAVELING-WAVE AMPLIFIER TUBE

Five QR1642 tubes were subjected to operational tests at extreme temperatures; the environmental test procedure is included in Appendix B. Four tubes successfully completed these evaluation tests. One tube (No. 5) was lost during the evaluation program because of a defective rf transition. A photograph of the test station is shown in Figure 49. The data obtained on these five tubes, Serials Nos. 1, 2, 3, 4 and 5 are included in Tables XVIII - XXXV and in Figures 50 - 68 found on pages 88 - 110.

- A. THESE DIAMETERS TO BE CONCENTRIC WITH REFERENCE DIAMETER "Z" WITHIN 0.001.
- B. THESE SURFACES TO BE PERPENDICULAR TO AXIS OF REFERENCE DIAMETER "Z" WITHIN 0.001.
- C. ALL SURFACES TO HAVE A 63 MICROINCH FINISH OR BETTER.
- D. MATERIAL : ARMCO IRON

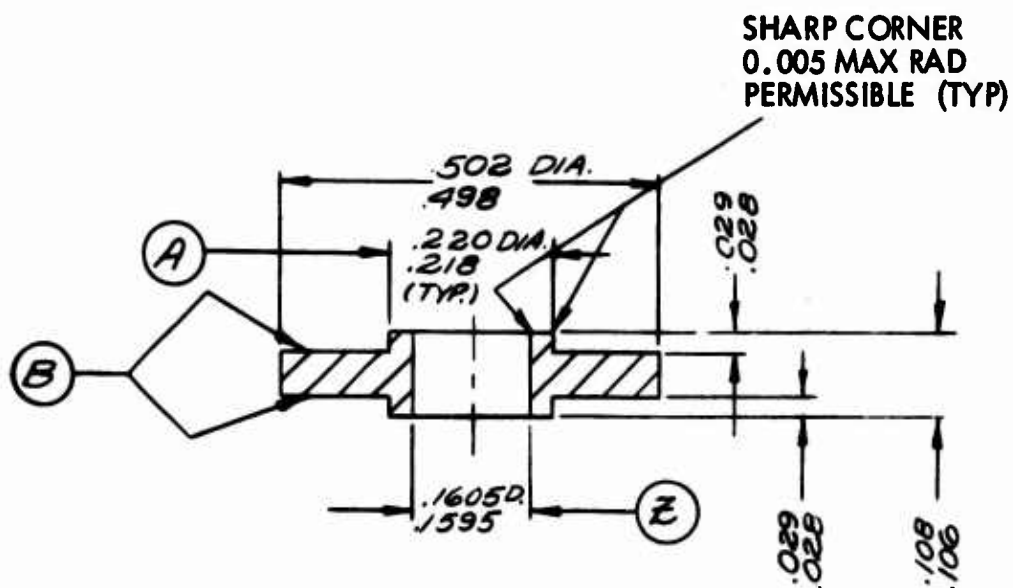
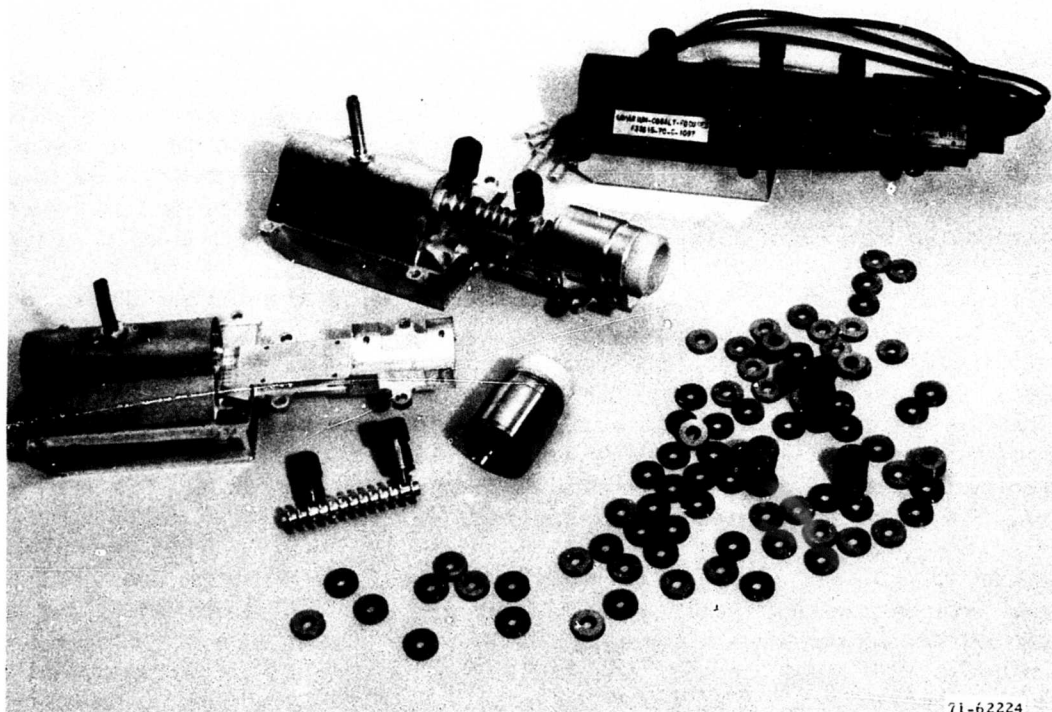
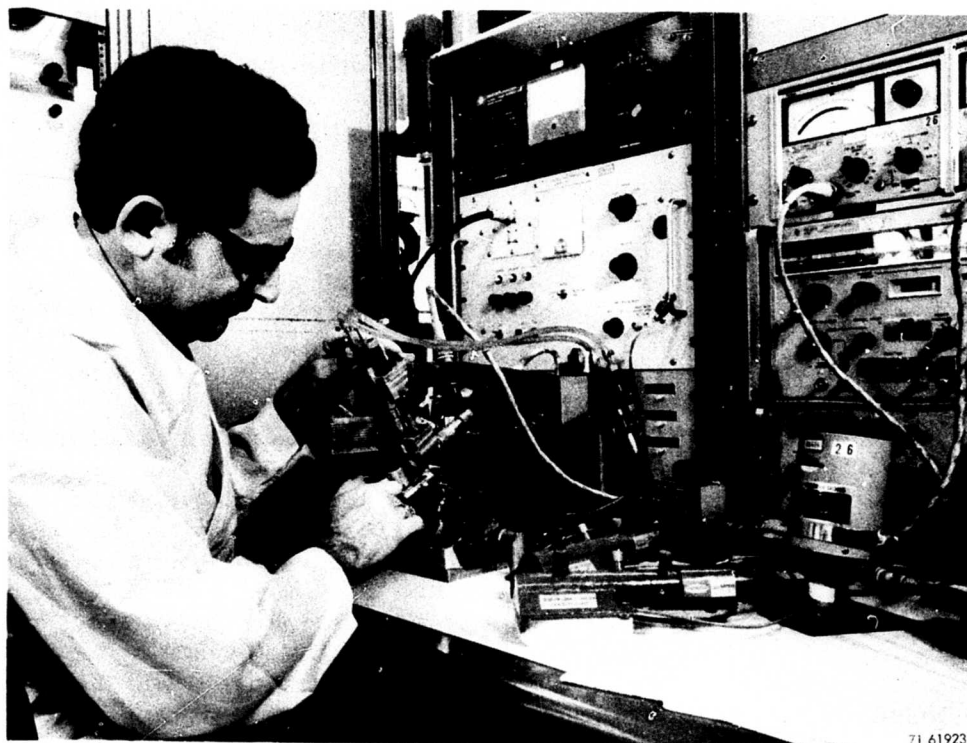


Figure 47. Pole Design for Periodic Permanent Magnet Circuit for the QR1642 TWT



71-62224

Figure 48. Photograph of QR1642



71 61923

Figure 49. Environmental Test Station

On each tube tested, data was obtained at two input power drive levels, 158 watts (52 dBm) and 250 watts (54 dBm), after environmental testing. The environmental test was designed to reflect actual operational conditions which would stress the TWT. The TWT must maintain specified microwave performance while operating in high and low temperature environments and have no irreversible detrimental changes. The test samples were resubmitted to initial test conditions after environmental testing and subjected to comparative analysis of their performance. The data shows no irreversible degradation of performance.

Tables XVIII, XXII, XXVI, XXX and XXXIV show the output power performance prior to environmental testing. Tables XXI, XXV, XXIX and XXXIII show performance of the TWT after completion of the environmental test. This performance data is plotted in Figures 50 - 57. These plots show that the peak power output as a function of frequency did not degrade because of the environmental tests. Figures 58 and 59 show performance data of tube No. 5 before environmental testing. Comparison analysis could not be made because the product was lost during environmental testing.

Tables XIX, XXIII, XXXI, and XXXV show data taken with the TWT operating at mid-band frequency, saturated output power in an 80°C ambient. The temperature of the samarium-cobalt magnets, the beam focusing system of the TWT, was monitored. The output power and helix shell currents were recorded as the duty cycle was increased. The TWT thermally stabilizes within 0.25-hour and the additional 0.75-hour of operation at each duty cycle level shows no degradation in tube performance. The maximum temperature of the samarium-cobalt magnet outside diameter is plotted as a function of duty cycle in Figures 60, 62, 64, 66 and 68. The same type of information was obtained while the TWT was operating in a -55°C ambient. The maximum temperature as a function of duty cycle is shown in Figures 61, 63, 65 and 67 while the microwave performance is listed in Tables XX, XXIV, XXVIII, and XXXII.

One test sample, Serial No. 5, was a catastrophic failure when the output window was fractured during the 80°C ambient environmental test. The defect was traced to an rf transition which had no Teflon insulation between its center conductor and outer conductor. Rf breakdown caused sufficient heating to melt the Teflon in the output of the tube, caused arcing across the output window, and resulted in loss of tube vacuum.

In summary, the data obtained during this evaluation shows no significant change in performance. This clearly indicates no loss in beam transmission or magnetic field. Extrapolating the data shows that some of these samples could operate at an additional 2% increase in duty cycle before the magnet focusing system stabilizing temperature is exceeded; accordingly, Pt-Co could not be used to focus this TWT operating at 4% duty cycle under the environmental conditions of the above tests. Figure 69 shows that the QR1642 TWT would have been restricted to operation at lower duty cycles if the Pt-Co magnets had been utilized to focus the electron beam. Operating this device at higher duty cycles would subject the Pt-Co magnets to temperatures which would cause irreversible losses in beam focusing properties and destroy the TWT performance.

DATA SHEET A

T AND A STEP NO. 4.1 SERIAL NO. 1 DATE 1-29-71 OPER. PER.
DUTY CYCLE 4.4% PULSE WIDTH 5.5 μSEC PRF 8000

LABEL VALUES	RECORD
E_k <u>10.5</u>	i_{ws} (no rf) <u>.149</u>
i_{beam} <u>1.35</u>	
e_c <u>136</u>	

FREQ	pi WATTS	po kW	pi WATTS	po kW	FREQ	pi WATTS	po kW	pi WATTS	po kW
					10.0	158	2.72	250	3.09
					10.2	158	2.68	250	2.87
					10.4	158	2.61	250	2.84
8.0	158	2.66	250	2.89	10.6	158	2.88	250	2.16
8.2	158	2.77	250	2.97	10.8	158	2.42	250	2.72
8.4	158	3.12	250	3.38	11.0	158	2.34	250	2.64
8.6	158	3.03	250	3.18	11.2	158	2.30	250	3.08
8.8	158	2.67	250	3.82	11.4	158	2.22	250	2.81
9.0	158	3.23	250	3.31	11.6	158	2.26	250	2.86
9.2	158	3.19	250	3.34	11.8	158	1.85	250	2.23
9.4	158	3.00	250	3.16	12.0	158	2.21	250	2.57
9.6	158	2.64	250	2.89					
9.8	158	2.88	250	2.96					

REMARKS

680788 2a

Table XVIII. QR1642 No. 1 Step 4.1

REVISIONS:

NAME	DATE		RAYTHEON	LEXINGTON MASS. 02173
APPROVED				
83			CODE 49956	SH

PRINTED IN U.S.A.

FORM NO. 10-6707 0000 VELLUM
10-6708 FILM

DATA SHEET B

T AND A STEP NO. 4.3 SERIAL NO. 1 DATE 2-15-71 OPER. _____

DUTY CYCLE 4.4% PULSE WIDTH 5.5 μSEC PRF 8000 FREQ 9.8 GHz $p_i = 250$ WATTS

LABEL VALUES	RECORD
E_k <u>10.5</u>	i_{ws} (no rf) <u>.115</u>
i_{beam} <u>1.32</u>	$T_{chamber}$ <u>80°C</u>
ec _____	

TIME HRS	po kW	i_{beam} A	i_{ws} A	T1	T2	T3	T4	T5	T6	du
0		1.32	.115	80	80	80	80	80	80	2%
0.25	3.44	1.32	.246	110	110	105	115	110	100	
0.50	3.44	1.32	.246	110	110	110	115	110	102	
0.75	3.44	1.32	.246	110	110	110	115	110	102	
1.00	3.44	1.32	.246	110	110	110	115	110	102	
0		1.32	.115	110	110	110	115	110	102	3%
0.25	3.27	1.32	.278	130	128	132	140	132	120	
0.50	3.27	1.32	.278	130	130	135	140	135	125	
0.75	3.27	1.32	.278	130	130	135	140	135	125	
1.00	3.27	1.32	.278	130	130	135	142	135	125	
0		1.32	.132	142	135	135	135	135	130	4%
0.25	2.95	1.32	.265	160	155	165	180	170	150	
0.50	2.95	1.32	.275	160	160	172	190	180	160	
0.75	2.95	1.32	.275	160	160	175	190	180	160	
1.00	2.95	1.32	.280	162	162	177	192	182	165	

680788-1

Table XIX. QR1642 No. 1 Step 4.3

REVISIONS:

NAME _____	DATE _____	84	RAYTHEON	LEXINGTON MASS. 02173
APPROVED _____				
			CODE 49956	SH

DATA SHEET B

T AND A STEP NO. 4.6 SERIAL NO. 1 DATE 2-17-71 OPER. _____

DUTY CYCLE 4.4% PULSE WIDTH 5.5 μSEC PRF 8000 FREQ 9.8 GHz pi = 250 WATTS

LABEL VALUES	RECORD
E _k 10.5	i _{ws} (no rf) .115
i _{beam} 1.32	T _{chamber} -55°C
ec _____	

TIME HRS	po kW	i _{beam} A	i _{ws} A	T1	T2	T3	T4	T5	T6	du
0		1.32	.115	-55	-55	-55	-55	-55	-55	2%
0.25	3.00	1.32	.244	+35	+35	+35	+40	+35	+30	
0.50	3.00	1.32	.244	+35	+35	+35	+40	+40	+30	
0.75	3.00	1.32	.244	+35	+35	+35	+40	+40	+30	
1.00	3.00	1.32	.244	+35	+35	+35	+40	+40	+30	
0		1.32	.131	+45	+45	+45	+45	+45	+30	3%
0.25	2.95	1.32	.246	+60	+60	+65	+68	+60	+50	
0.50	2.95	1.32	.246	+60	+60	+65	+70	+60	+50	
0.75	2.95	1.32	.246	+60	+60	+65	+70	+60	+50	
1.00	2.95	1.32	.246	+60	+60	+65	+70	+60	+50	
0		1.32	.131	+65	+65	+65	+70	+65	+55	4%
0.25	2.95	1.32	.264	+80	+80	+85	+90	+85	+70	
0.50	2.95	1.32	.264	+80	+80	+85	+92	+85	+70	
0.75	3.00	1.32	.264	+85	+85	+90	+95	+90	+75	
1.00	3.00	1.32	.264	+85	+85	+92	+100	+95	+80	

680788-1

Table XX. QR1642 No. 1 Step 4.6

REVISIONS:

NAME	DATE	85	RAYTHEON	LEXINGTON MASS. 02173
APPROVED				
			CODE 49956	SH

DATA SHEET A

T AND A STEP NO. 4.9 SERIAL NO. 1 DATE 2-18-71 PER.
 DUTY CYCLE 4.4% PULSE WIDTH 5.5 μSEC PRF 8000

LABEL VALUES	RECORD
E _k <u>10.5</u>	i _{ws} (no rf) <u>.141</u>
i _{beam} <u>1.35</u>	
ec <u>138</u>	

FREQ	pi WATTS	po kW	pi WATTS	po kW	FREQ	pi WATTS	po kW	pi WATTS	po kW
					10.0	158	2.73	250	3.03
					10.2	158	2.54	250	2.69
					10.4	158	2.31	250	2.60
8.0	158	2.69	250	2.89	10.6	158	2.90	250	3.10
8.2	158	2.64	250	2.94	10.8	158	2.33	250	2.57
8.4	158	2.82	250	3.02	11.0	158	2.38	250	2.62
8.6	158	2.74	250	2.83	11.2	158	2.50	250	2.87
8.8	158	2.50	250	2.66	11.4	158	2.36	250	2.70
9.0	158	3.28	250	3.24	11.6	158	2.43	250	2.67
9.2	158	3.20	250	3.32	11.8	158	1.80	250	2.17
9.4	158	2.80	250	2.91	12.0	158	2.08	250	2.40
9.6	158	2.42	250	2.63					
9.8	158	2.60	250	2.73					

REMARKS

680788 2a

Table XXI, QR1642 No. 1 Step 4.9

REVISIONS:

NAME	DATE	86	RAYTHEON	LEXINGTON MASS. 02173
APPROVED				
			CODE 49956	SH

DATA SHEET A

T AND A STEP NO. 4.1 SERIAL NO. 2 DATE 1-29-71 OPER.
DUTY CYCLE 4.4% PULSE WIDTH 5.5 μSEC PRF 8000

LABEL VALUES	RECORD
E _k 10.3	i _{ws} (no rf) .134
i _{beam} 1.35	
ec 131	


FREQ	pi WATTS	po kW	pi WATTS	po kW	FREQ	pi WATTS	po kW	pi WATTS	po kW
					10.0	158	2.82	250	2.96
					10.2	158	2.58	250	2.68
					10.4	158	2.53	250	2.64
8.0	158	2.90	250	3.05	10.6	158	2.84	250	2.94
8.2	158	3.02	250	3.09	10.8	158	2.44	250	2.55
8.4	158	3.26	250	3.42	11.0	158	2.48	250	2.66
8.6	158	3.11	250	3.10	11.2	158	2.75	250	2.99
8.8	158	2.65	250	2.78	11.4	158	2.48	250	2.68
9.0	158	3.14	250	3.13	11.6	158	2.54	250	2.62
9.2	158	3.10	250	3.16	11.8	158	2.02	250	2.22
9.4	158	2.92	250	2.93	12.0	158	2.31	250	2.44
9.6	158	2.68	250	2.74					
9.8	158	2.75	250	2.76					

REMARKS

680788 2a

Table XXII, QR1642 No. 2 Step 4.1

REVISIONS:

NAME	DATE	87		LEXINGTON MASS. 02173
APPROVED				CODE 49956 SH

DATA SHEET B

T AND A STEP NO. 4.3 SERIAL NO. 2 DATE 2-10-71 OPER.

DUTY CYCLE 4.4% PULSE WIDTH 5.5 μSEC PRF 8000 FREQ 9.8 GHz pi = 250 WATTS

LABEL VALUES	RECORD
E _k 10.5	i _{ws} (no rf) .128
i _{beam} 1.32	T _{chamber} 80°C
ec	

TIME HRS	po kW	i _{beam} A	i _{ws} A	T1	T2	T3	T4	T5	T6	du
0		1.32	.128	85	83	83	83	80	80	2%
0.25	3.15	1.32	.196	100	95	100	95	100	90	
0.50	3.15	1.32	.196	103	100	105	100	105	95	
0.75	3.15	1.32	.196	103	100	105	100	105	95	
1.00	3.15	1.32	.196	103	100	105	100	105	97	
0		1.32	.132	103	100	105	100	105	100	3%
0.25	2.98	1.32	.207	120	120	125	125	130	116	
0.50	2.98	1.32	.207	120	120	125	125	130	116	
0.75	2.98	1.32	.207	125	120	130	125	132	116	
1.00	2.98	1.32	.220	125	120	130	128	135	120	
0		1.32	.132	130	125	135	135	140	130	4%
0.25	2.94	1.32	.230	145	145	156	155	160	140	
0.50	2.94	1.32	.230	145	145	160	160	165	145	
0.75	2.94	1.32	.280	155	152	170	175	174	150	
1.00	2.94	1.32	.280	158	155	175	175	180	155	

680788-1

Table XXIII. QR1642 No. 2 Step 4.3

REVISIONS:

NAME	DATE	88	RAYTHEON	LEXINGTON MASS. 02173
APPROVED			CODE 49956	SH

DATA SHEET B

T AND A STEP NO. 4.6 SERIAL NO. 2 DATE 1-29-71 OPER.

DUTY CYCLE 4.4% PULSE WIDTH 5.5 μSEC PRF 8000 FREQ 9.8 GHz pi = 250 WATTS

LABEL VALUES	RECORD
E _k 10.5	i _{ws} (no rf) .132
i _{beam} 1.32	T _{chamber} -55°C
ec	

TIME HRS	po kW	i _{beam} A	i _{ws} A	T1	T2	T3	T4	T5	T6	du
0		1.32	.132	-55	-55	-55	-55	-55	-55	2%
0.25	3.15	1.32	.196	+50	+55	+60	+60	+60	+50	
0.50	3.15	1.32	.196	+50	+55	+60	+60	+60	+50	
0.75	3.15	1.32	.196	+50	+55	+60	+60	+60	+50	
1.00	3.15	1.32	.196	+50	+50	+60	+60	+60	+50	
0		1.32	.132	+35	+35	+40	+40	+40	+35	3%
0.25	3.06	1.32	.212	+55	+55	+55	+60	+65	+50	
0.50	3.06	1.32	.212	+57	+57	+65	+60	+65	+50	
0.75	3.06	1.32	.212	+65	+65	+72	+68	+72	+58	
1.00	3.06	1.32	.212	+60	+60	+68	+65	+68	+55	
0		1.32	.132	+70	+67	+75	+75	+80	+65	4%
0.25	3.06	1.32	.230	+75	+75	+90	+90	+98	+75	
0.50	3.06	1.32	.230	+85	+82	+98	+98	+105	+75	
0.75	3.06	1.32	.230	+80	+80	+100	+100	+105	+80	
1.00	3.06	1.32	.230	+80	+80	+100	+100	+105	+80	

580788-1

Table XXIV. QR1642 No. 2 Step 4.6

REVISIONS:

NAME	DATE	89	RAYTHEON	LEXINGTON MASS. 02173
APPROVED			CODE 49956 SH	

DATA SHEET A

T AND A STEP NO. 4.9 SERIAL NO. 2 DATE 2-18-71 PER.
DUTY CYCLE 4.4% PULSE WIDTH 5.5 μSEC PRF 8000

LABEL VALUES	RECORD
E_k <u>10.3</u>	i_{ws} (no rf) <u>.139</u>
i_{beam} <u>1.35</u>	
ec <u>128</u>	

FREQ	pi WATTS	po kW	pi WATTS	po kW	FREQ	pi WATTS	po kW	pi WATTS	po kW
					10.0	158	2.68	250	2.77
					10.2	158	2.30	250	2.35
					10.4	158	2.37	250	2.44
8.0	158	2.76	250	2.89	10.6	158	2.70	250	2.87
8.2	158	2.86	250	2.91	10.8	158	2.32	250	2.42
8.4	158	2.99	250	3.14	11.0	158	2.38	250	2.48
8.6	158	2.93	250	2.89	11.2	158	2.61	250	2.80
8.8	158	2.54	250	2.62	11.4	158	2.30	250	2.57
9.0	158	3.03	250	3.00	11.6	158	2.38	250	2.46
9.2	158	2.94	250	2.98	11.8	158	1.94	250	2.18
9.4	158	2.71	250	2.71	12.0	158	2.19	250	2.34
9.6	158	2.50	250	2.53					
9.8	158	2.60	250	2.59					

REMARKS

680788 2a

Table XXV. QR1642 No. 2 Step 4.9

REVISIONS:

NAME	DATE	90	RAYTHEON	LEXINGTON MASS. 02173
APPROVED				
			CODE 49956	SH

DATA SHEET A

T AND A STEP NO. 4.1 SERIAL NO. 3 DATE 2-25-71 PER. DW
DUTY CYCLE 4.4% PULSE WIDTH 5.5 μSEC PRF 8000

LABEL VALUES	RECORD
E_k <u>10.3</u>	i_{ws} (no <u>.152</u>
i_{beam} <u>1.35</u>	
e_c <u>115</u>	

FREQ	pi WATTS	po kW	pi WATTS	po kW	FREQ	pi WATTS	po kW	pi WATTS	po kW
					10.0	158	2.90	250	3.02
					10.2	158	2.46	250	2.60
					10.4	158	2.50	250	2.61
8.0	158	2.89	250	2.92	10.6	158	2.90	250	3.05
8.2	158	2.96	250	3.05	10.8	158	2.22	250	2.39
8.4	158	3.03	250	3.08	11.0	158	2.25	250	2.47
8.6	158	2.87	250	2.86	11.2	158	2.50	250	2.80
8.8	158	2.66	250	2.64	11.4	158	2.34	250	2.52
9.0	158	3.29	250	3.25	11.6	158	2.24	250	2.53
9.2	158	3.28	250	3.30	11.8	158	1.88	250	2.17
9.4	158	2.80	250	2.88	12.0	158	1.93	250	2.29
9.6	158	2.58	250	2.57					
9.8	158	2.70	250	2.76					

680788 2a

REMARKS
Table XXVI. QR1642 No. 3 Step 4.1

REVISIONS:

NAME	DATE
APPROVED	

91

RAYTHEON	LEXINGTON MASS. 02173
CODE 49956	SH

DATA SHEET B

T AND A STEP NO. 4.3 SERIAL NO. 3 DATE 1-20-70 OPER.

DUTY CYCLE 4.4% PULSE WIDTH 5.5 μSEC PRF 8000 FREQ 9.8 GHz pi = 250 WATTS

LABEL VALUES	RECORD
E_k 10.5	i_{ws} (no rf) .152
i_{beam} 1.32	$T_{chamber}$ 80°C
ec	

TIME HRS	po kW	i_{beam} A	i_{ws} A	T1	T2	T3	T4	T5	T6	du
0	--	1.32	.152	80	80	80	80	80	80	2%
0.25	2.95	1.32	.279	115	105	100	100	105	100	
0.50	2.90	1.32	.279	115	105	105	102	105	100	
0.75	2.90	1.32	.279	115	105	105	102	105	100	
1.00	2.90	1.32	.279	115	105	105	102	105	100	
0	--	1.32	.152	130	110	105	105	105	110	3%
0.25	2.70	1.32	.295	142	125	123	123	127	120	
0.50	2.75	1.32	.290	142	130	128	125	130	120	
0.75	2.75	1.32	.290	142	130	128	125	130	120	
1.00	2.75	1.32	.290	142	130	128	125	130	120	
0	--	1.32	.152	155	130	128	125	130	130	4%
0.25	2.65	1.32	.305	170	150	148	148	155	140	
0.50	2.65	1.32	.305	170	150	150	150	155	140	
0.75	2.65	1.32	.305	180	165	165	162	170	142	
1.00	2.65	1.32	.305	184	172	168	165	172	144	

680788-1

Table XXVII. QR1642 No. 3 Step 4.3

REVISIONS:

NAME	DATE	92	RAYTHEON	LEXINGTON MASS. 02173
APPROVED				
			CODE 49956	SH

DATA SHEET B

T AND A STEP NO. 4.6 SERIAL NO. 3 DATE 3-31-71 OPER. _____

DUTY CYCLE 4.4% PULSE WIDTH 5.5 μSEC PRF 8000 FREQ 9.8 GHz $p_i = 250$ WATTS

LABEL VALUES	RECORD
E_k <u>10.5</u>	i_{ws} (no rf) <u>.152</u>
i_{beam} <u>1.32</u>	$T_{chamber}$ <u>-55°C</u>
ec _____	

TIME HRS	p_o kW	i_{beam} A	i_{ws} A	T1	T2	T3	T4	T5	T6	du
0		1.32	.152	-55	-55	-55	-55	-55	-55	2%
0.25	2.8	1.32	.275	+50	+40	+37	+35	+37	+35	
0.50	2.8	1.32	.275	+40	+30	+30	+30	+30	+30	
0.75	2.85	1.32	.275	+40	+30	+30	+30	+30	+30	
1.00	2.85	1.32	.275	+40	+30	+30	+30	+30	+30	
0		1.32	.162	+40	+30	+30	+30	+30	+30	3%
0.25	2.75	1.32	.285	+70	+60	+60	+60	+60	+55	
0.50	2.75	1.32	.285	+70	+60	+60	+60	+60	+55	
0.75	2.75	1.32	.285	+72	+60	+60	+60	+60	+55	
1.00	2.75	1.32	.285	+75	+65	+62	+60	+60	+55	
0		1.32	.164	+75	+65	+62	+62	+60	+55	4%
0.25	2.75	1.32	.300	+80	+70	+65	+65	+65	+60	
0.50	2.75	1.32	.300	+80	+70	+65	+65	+65	+60	
0.75	2.75	1.32	.300	+85	+75	+70	+70	+65	+65	
1.00	2.75	1.32	.300	+85	+80	+75	+72	+70	+65	

680788-1

Table XXVIII, QR1642 No. 3 Step 4.6

NAME	DATE	93	RAYTHEON	LEXINGTON MASS. 02173
APPROVED			CODE 49956	SH

10-0706 YELLOW
FORM NO. 10-0707 ORANGE YELLOW
10-0708 PINK

PRINTED IN U.S.A.

REVISIONS:

DATA SHEET A

T AND A STEP NO. 4.9 SERIAL NO. 3 DATE 3-8-71 OPER. DW
 DUTY CYCLE 4.4% PULSE WIDTH 5.5 μSEC PRF 8000

LABEL VALUES	RECORD
E_k <u>10.3</u>	i_{ws} (no rf) <u>.151</u>
i_{beam} <u>1.35</u>	
ec <u>113</u>	

FREQ	pi WATTS	po kW	pi WATTS	po kW	FREQ	pi WATTS	po kW	pi WATTS	po kW
					10.0	158	2.83	250	2.96
					10.2	158	2.22	250	2.48
					10.4	158	2.51	250	2.60
8.0	158	2.81	250	2.72	10.6	158	2.77	250	2.99
8.2	158	3.02	250	3.17	10.8	158	2.07	250	2.33
8.4	158	3.15	250	3.26	11.0	158	2.09	250	2.38
8.6	158	2.64	250	2.58	11.2	158	2.60	250	2.84
8.8	158	2.39	250	2.38	11.4	158	2.40	250	2.55
9.0	158	3.32	250	3.20	11.6	158	2.17	250	2.46
9.2	158	3.32	250	3.33	11.8	158	1.95	250	2.20
9.4	158	2.80	250	2.88	12.0	158	2.17	250	2.44
9.6	158	2.56	250	2.54					
9.8	158	2.67	250	2.70					

REMARKS
 Table XXIX. QR1642 No. 3 Step 4.9

680788 2a

REVISIONS:

NAME	DATE	94	RAYTHEON	LEXINGTON MASS. 02173
APPROVED				
			CODE 49956	SH

DATA SHEET A

T AND A STEP NO. 4.1 Serial NO. 4 DATE 3-24-71 PER. DW
 DUTY CYCLE 4.4% PULSE WIDTH 5.5 μSEC PRF 8000

LABEL VALUES	RECORD
E _k <u>10.3</u>	i _{ws} (no rf) <u>.148</u>
i _{beam} <u>1.35</u>	
ec <u>165</u>	

FREQ	pi WATTS	po kW	pi WATTS	po kW	FREQ	pi WATTS	po kW	pi WATTS	po kW
					10.0	158	2.64	250	2.70
					10.2	158	2.25	250	2.36
					10.4	158	2.43	250	2.47
8.0	158	2.67	250	2.75	10.6	158	2.57	250	2.78
8.2	158	2.42	250	2.46	10.8	158	2.31	250	2.42
8.4	158	2.58	250	2.67	11.0	158	2.35	250	2.44
8.6	158	2.85	250	2.78	11.2	158	2.59	250	2.76
8.8	158	2.69	250	2.65	11.4	158	2.37	250	2.48
9.0	158	2.83	250	2.78	11.6	158	2.08	250	2.34
9.2	158	2.92	250	2.92	11.8	158	2.26	250	2.39
9.4	158	2.65	250	2.68	12.0	158	2.00	250	2.18
9.6	158	2.50	250	2.48					
9.8	158	2.55	250	2.60					

680788 2a

REMARKS
 Table XXX. QR1642 No. 4 Step 4.1

REVISIONS:

NAME	DATE	95	RAYTHEON	LEXINGTON MASS. 02173
APPROVED				
			CODE 49956	SH

DATA SHEET B

T AND A STEP NO. 4.3 SERIAL NO. 4 DATE 3-25-71 OPER. _____

DUTY CYCLE 4.4% PULSE WIDTH 5.5 μSEC PRF 8000 FREQ 9.8 GHz P_i = 250 WATTS

LABEL VALUES	RECORD
E_k <u>10.5</u>	I_{ws} (no rf) <u>.162</u>
I_{beam} <u>1.35</u>	$T_{chamber}$ <u>80°C</u>
ec _____	

TIME HRS	P_o kW	I_{beam} A	I_{ws} A	T1	T2	T3	T4	T5	T6	du
0	--	1.35	.160	80	80	80	80	80	80	2%
0.25	2.25	1.35	.295	110	100	100	100	98	85	
0.50	2.25	1.35	.295	110	100	100	100	100	87	
0.75	2.25	1.35	.295	112	105	105	100	100	87	
1.00	2.25	1.35	.295	112	107	105	102	102	87	
0	--	1.35	.160	128	110	110	110	110	92	3%
0.25	2.25	1.35	.290	130	115	110	110	110	100	
0.50	2.25	1.35	.290	130	115	110	110	110	100	
0.75	2.25	1.35	.290	130	115	110	110	110	100	
1.00	2.25	1.35	.290	130	115	110	110	110	100	
0	--	1.35	.160	150	130	120	120	120	115	4%
0.25	2.2	1.35	.290	155	130	125	125	135	115	
0.50	2.2	1.35	.290	155	130	125	125	135	115	
0.75	2.2	1.35	.290	155	130	125	125	135	115	
1.00	2.2	1.35	.290	155	135	125	125	135	115	

680788-1

Table XXXI, QR1642 No. 4 Step 4.3

REVISIONS:

NAME	DATE	96	RAYTHEON	LEXINGTON MASS. 02173
APPROVED			CODE 49956 SH	

DATA SHEET B

T AND A STEP NO. 4.6 SERIAL NO. 4 DATE 3-25-71 OPER. _____

DUTY CYCLE 4.4% PULSE WIDTH 5.5 μSEC PRF 8000 FREQ 9.8 GHz P_i = 250 WATTS


LABEL	VALUES	RECORD
E_k	<u>10.5</u>	i_{ws} (no rf) <u>.160</u>
i_{beam}	<u>1.35</u>	$T_{chamber}$ <u>-55°C</u>
ec	_____	

TIME HRS	P_o kW	i_{beam} A	i_{ws} A	T1	T2	T3	T4	T5	T6	Δu
0		1.35	.160	-55	-55	-55	-55	-55	-55	2%
0.25	2.2	1.35	.290	+50	+40	+32	+32	+30	+25	
0.50	2.2	1.35	.290	+50	+40	+32	+32	+30	+25	
0.75	2.2	1.35	.290	+50	+40	+32	+32	+32	+25	
1.00	2.2	1.35	.290	+50	+40	+32	+32	+32	+25	
0		1.35	.160	+65	+52	+40	+40	+40	+35	3%
0.25	2.2	1.35	.290	+72	+65	+45	+45	+45	+35	
0.50	2.2	1.35	.290	+72	+65	+45	+45	+45	+35	
0.75	2.2	1.35	.290	+72	+65	+45	+45	+45	+35	
1.00	2.2	1.35	.290	+72	+65	+45	+45	+55	+35	
0		1.35	--	+82	+75	+55	+55	+65	+50	4%
0.25	2.2	1.35	.290	100	80	70	+70	80	60	
0.50	2.2	1.35	.290	100	80	70	70	80	60	
0.75	2.2	1.35	.290	100	80	70	70	80	60	
1.00	2.2	1.35	.290	100	80	70	70	80	60	

680788-1

Table XXXII, QR1642 No. 4 Step 4.6

REVISIONS:

NAME	DATE	97	 LEXINGTON MASS. 02173
APPROVED			
CODE 49956		SH	

DATA SHEET A

T AND A STEP NO. 4.9 SERIAL NO. 4 DATE 3-26-71 OPER. DW
DUTY CYCLE 4.4% PULSE WIDTH 5.5 μSEC PRF 8000

LABEL VALUES	RECORD
E _k <u>10.3</u>	i _{ws} (no rf) <u>.146</u>
i _{beam} <u>1.35</u>	
ec <u>166</u>	

FREQ	pi WATTS	po kW	pi WATTS	po kW	FREQ	pi WATTS	po kW	pi WATTS	po kW
					10.0	158	2.68	250	2.72
					10.2	158	2.35	250	2.41
					10.4	158	2.39	250	2.46
8.0	158	2.55	250	2.76	10.6	158	2.62	250	2.75
8.2	158	2.54	250	2.53	10.8	158	2.26	250	2.36
8.4	158	2.67	250	2.73	11.0	158	2.36	250	2.48
8.6	158	2.71	250	2.65	11.2	158	2.61	250	2.78
8.8	158	2.61	250	2.54	11.4	158	2.36	250	2.46
9.0	158	2.97	250	2.92	11.6	158	2.06	250	2.34
9.2	158	2.94	250	2.91	11.8	158	2.18	250	2.29
9.4	158	2.66	250	2.65	12.0	158	1.79	250	2.08
9.6	158	2.45	250	2.41					
9.8	158	2.56	250	2.60					

680788 2a

REMARKS
Table XXXIII. QR1642 No. 4 Step 4.9

REVISIONS:

NAME	DATE	98	RAYTHEON	LEXINGTON MASS. 02173
APPROVED				
			CODE 49956	SH

DATA SHEET A

T AND A STEP NO. 4.1 SERIAL NO. 5 DATE 2-26-71 PER. DW
DUTY CYCLE 4.4% PULSE WIDTH 5.5 μSEC PRF 8000

LABEL VALUES	RECORD
E _k 10.3	i _{ws} (no rf) .134
i _{beam} 1.35	
ec 161	

FREQ	pi WATTS	po kW	pi WATTS	po kW	FREQ	pi WATTS	po kW	pi WATTS	po kW
					10.0	158	2.49	250	2.64
					10.2	158	2.64	250	2.78
					10.4	158	2.60	250	2.74
8.0	158	2.76	250	2.64	10.6	158	2.75	250	2.90
8.2	158	3.03	250	2.96	10.8	158	2.31	250	2.55
8.4	158	2.76	250	2.80	11.0	158	2.65	250	2.76
8.6	158	2.15	250	2.24	11.2	158	2.60	250	2.86
8.8	158	2.47	250	2.43	11.4	158	2.30	250	2.49
9.0	158	3.10	250	3.06	11.6	158	2.67	250	2.98
9.2	158	3.02	250	3.03	11.8	158	2.38	250	2.77
9.4	158	2.80	250	2.84	12.0	158	2.35	250	2.58
9.6	158	2.59	250	2.64					
9.8	158	2.57	250	2.57					

REMARKS

680788 2a

Table XXXIV. QR1642 No. 5 Step 4.1

NAME	DATE
APPROVED	

RAYTHEON	LEXINGTON MASS. 02173
CODE 49956	SH

DATA SHEET B

T AND A STEP NO. 4.3 SERIAL NO. 5 DATE 3-8-71 OPER. _____

DUTY CYCLE 4.4% PULSE WIDTH 5.5 μ SEC PRF 8000 FREQ 9.8 GHz p_i = 250 WATTS

LABEL VALUES	RECORD
E_k <u>10.5</u>	i_{ws} (no rf) <u>.134</u>
i_{beam} <u>1.32</u>	$T_{chamber}$ <u>80°C</u>
ec _____	

TIME HRS	p_o kW	i_{beam} A	i_{ws} A	T1	T2	T3	T4	T5	T6	du
0		1.32	.134	85	85	85	92	95	95	2%
0.25	2.57	1.32	.230	90	100	100	102	102	102	
0.50	2.57	1.32	.230	90	100	100	102	102	105	
0.75	2.57	1.32	.230	90	100	100	100	102	105	
1.00	2.57	1.32	.230	90	100	100	100	102	105	
0		1.32	.142	100	105	100	110	115	120	3%
0.25	2.55	1.32	.246	105	115	115	120	120	125	
0.50	2.55	1.32	.246	110	120	120	125	125	130	
0.75	2.55	1.32	.246	112	125	122	127	130	130	
1.00	2.60	1.32	.246	115	125	125	127	130	130	
0		1.32	.162	125	130	125	140	145	155	4%
0.25	2.65	1.32	.162	125	130	146	150	155	160	
0.50	2.65	1.32	.162	125	130	146	150	155	160	
0.75	2.65	1.32	.162	125	130	146	150	155	160	
1.00	2.65	1.32	.162	125	130	146	150	155	160	

680788-1

Table XXXV. QR1642 No. 5 Step 4.3

REVISIONS:

NAME _____	DATE _____	100	RAYTHEON	LEXINGTON MASS. 02173
_____	_____			_____
APPROVED _____	_____		CODE 49956	SH

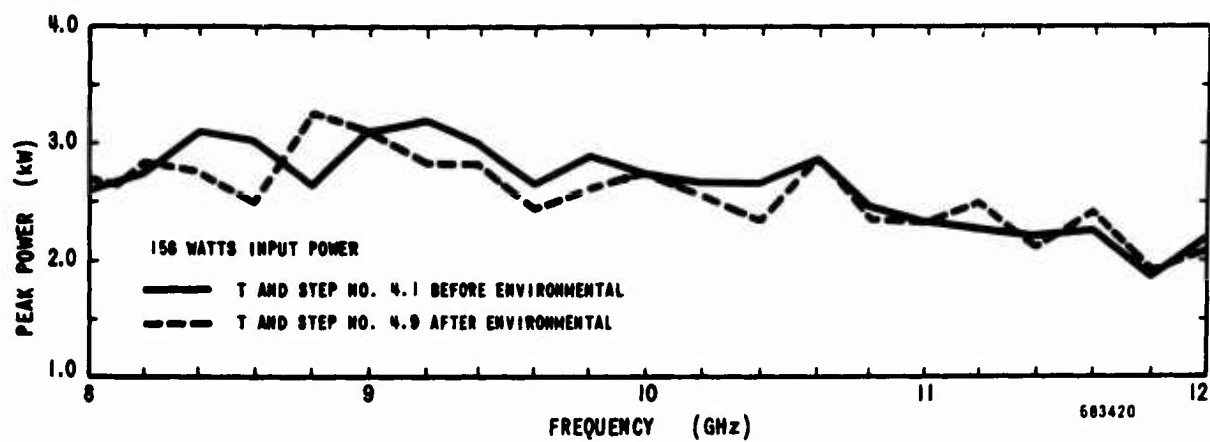


Figure 50. QR1642 No. 1 Peak Power vs Frequency Before and After Environmental Testing

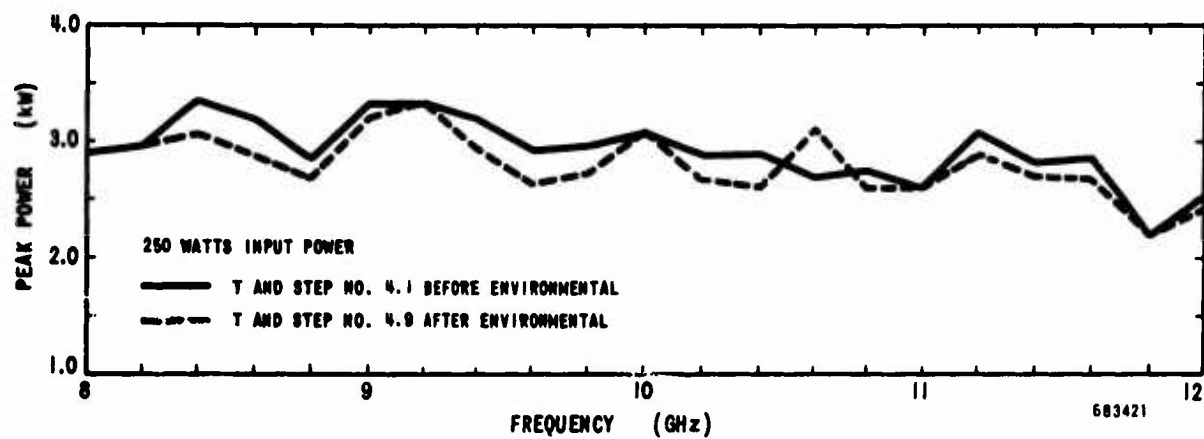


Figure 51. QR1642 No. 1 Peak Power vs Frequency Before and After Environmental Testing

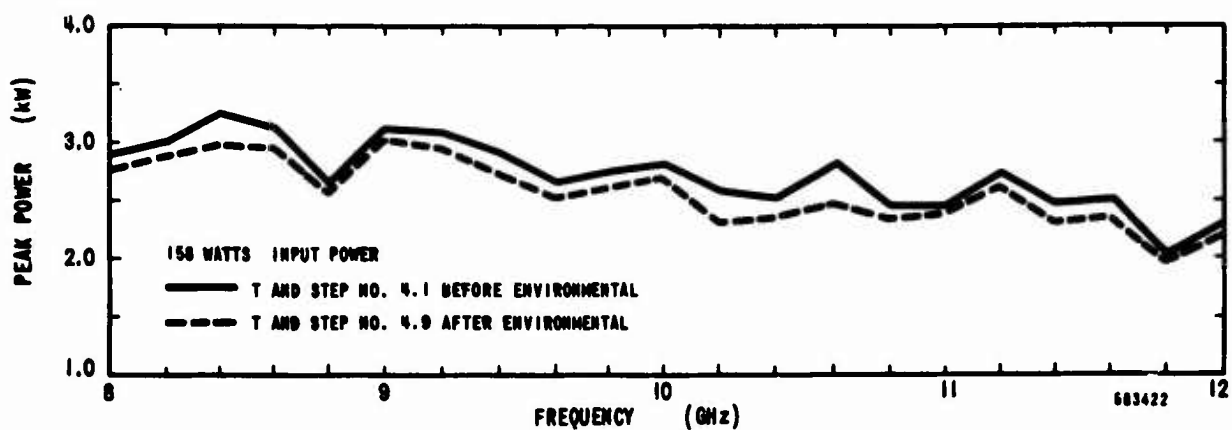


Figure 52. QR1642 No. 2 Peak Power vs Frequency Before and After Environmental Testing

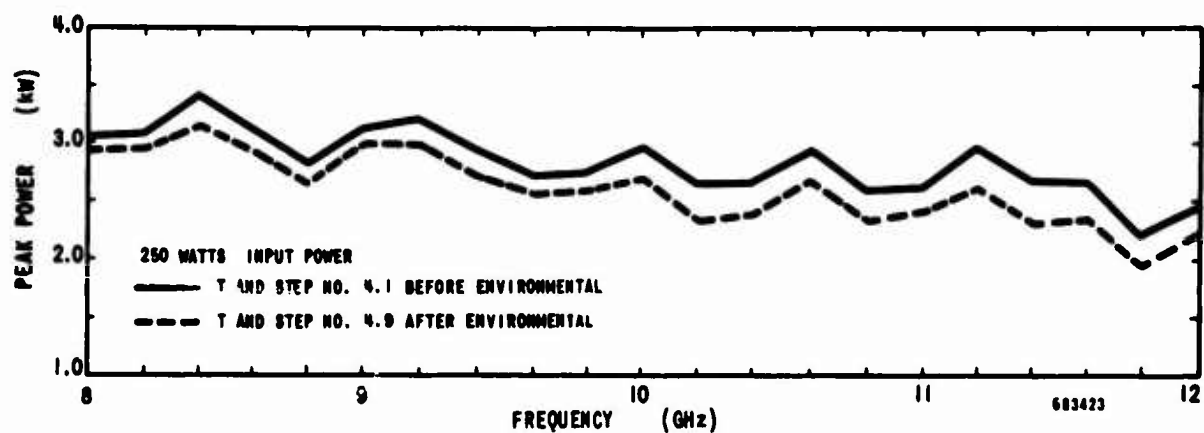


Figure 53. QR1642 No. 2 Peak Power vs Frequency Before and After Environmental Testing

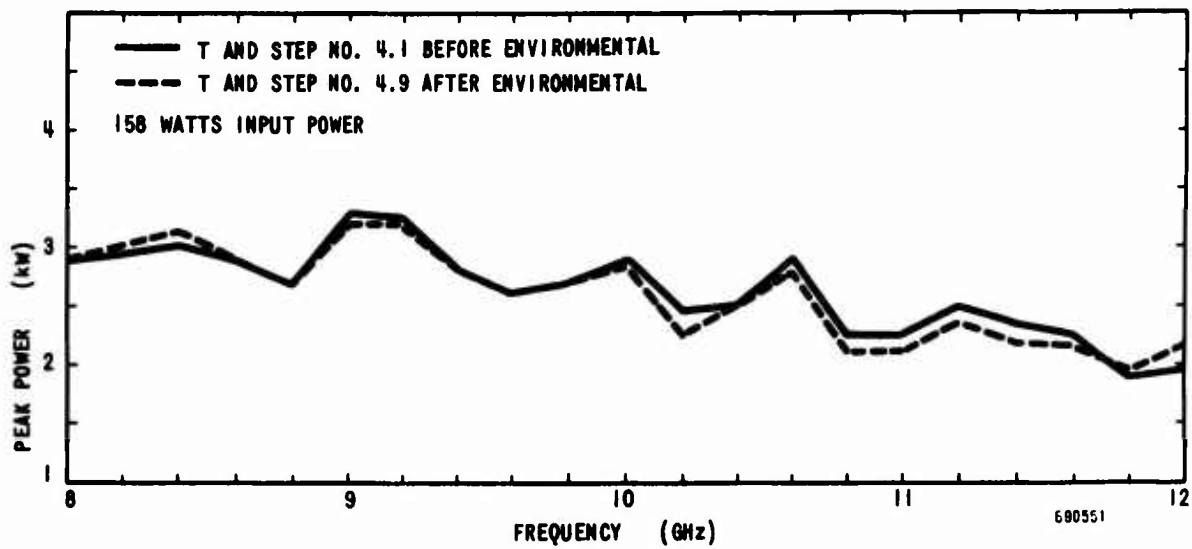


Figure 54. QR1642 No. 3 Peak Power vs Frequency before and after Environmental Testing

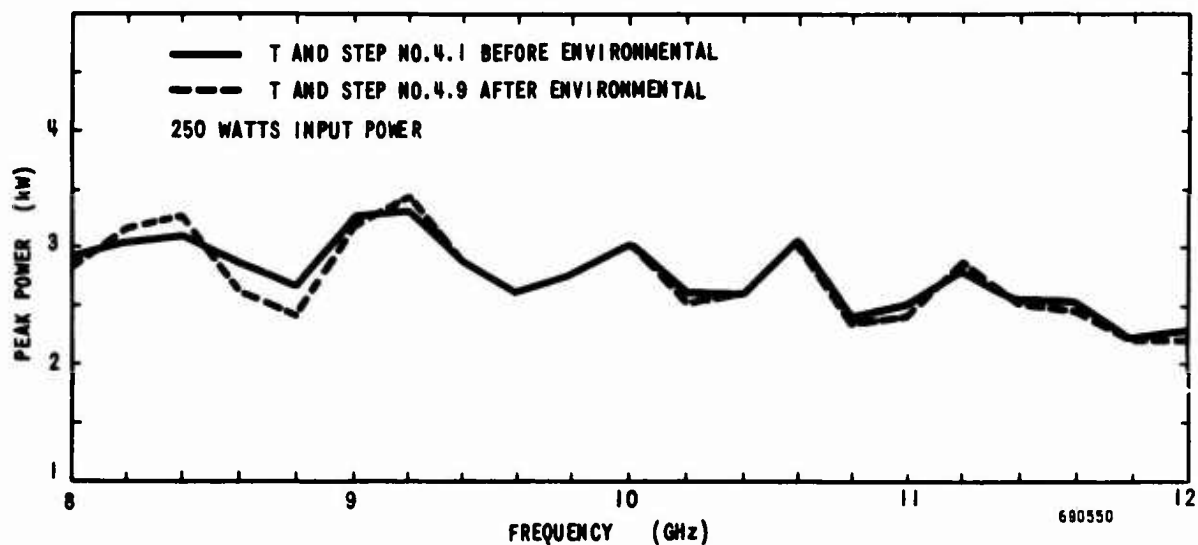


Figure 55. QR1642 No. 3 Peak Power vs Frequency before and after Environmental Testing

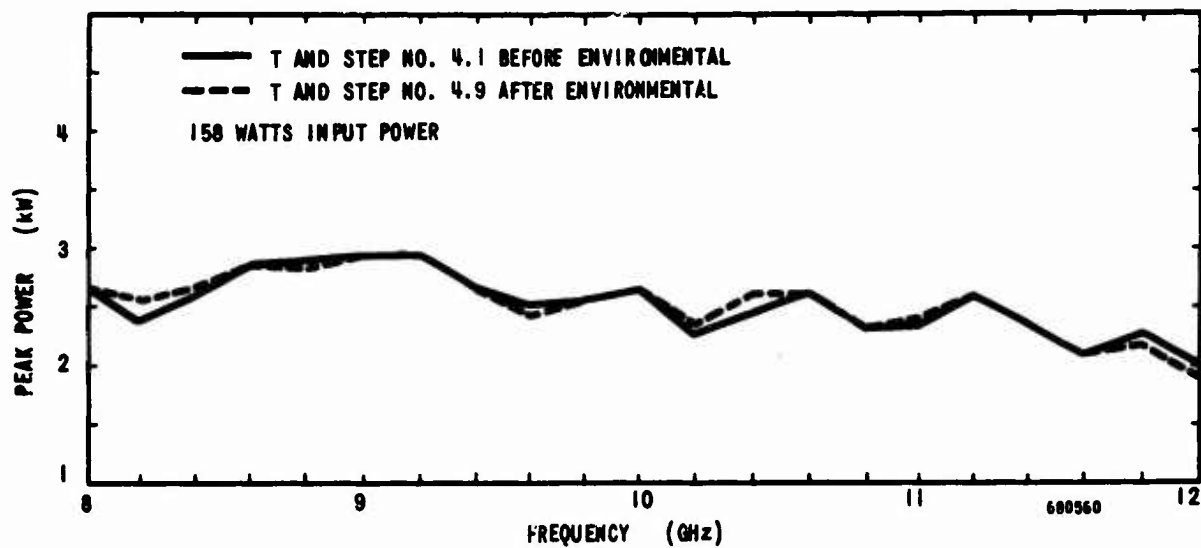


Figure 56. QR1642 No. 4 Peak Power vs Frequency before and after Environmental Testing

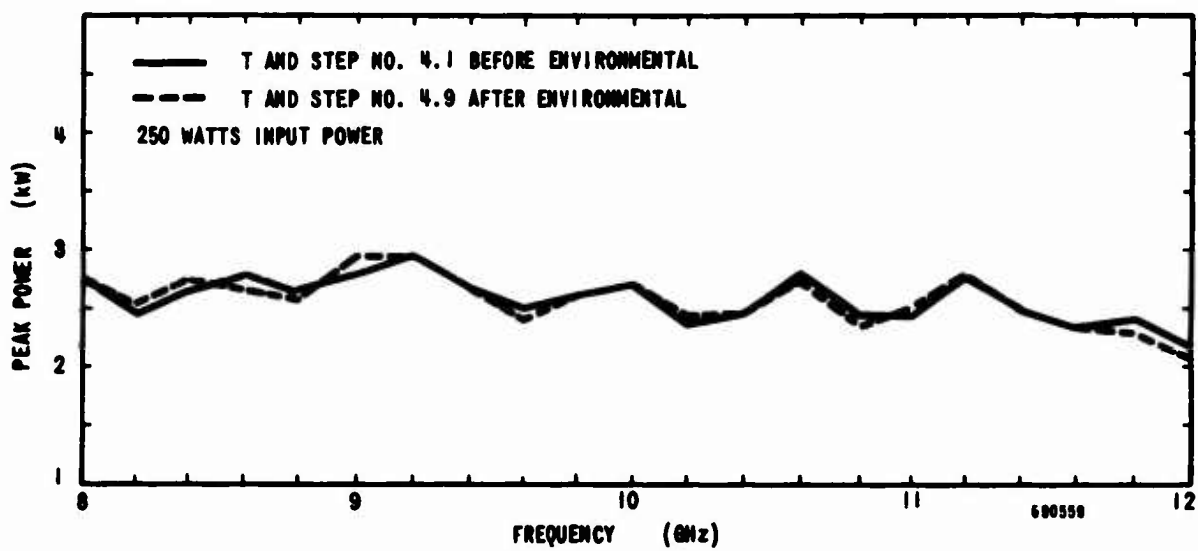


Figure 57. QR1642 No. 4 Peak Power vs Frequency Before and After Environmental Testing

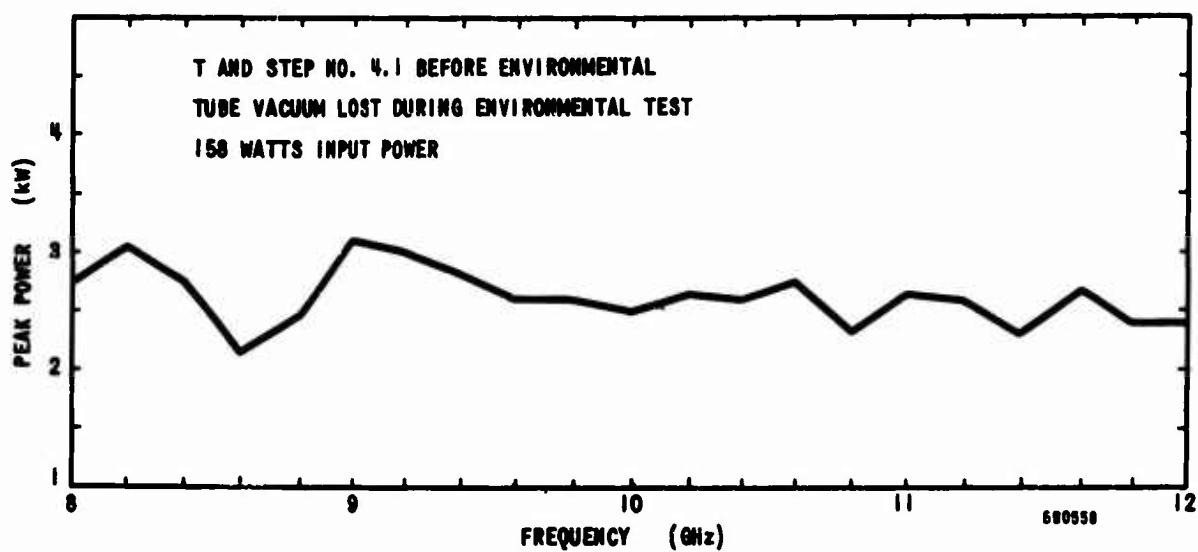


Figure 58. QR1642 No. 5 Peak Power vs Frequency Before Environmental Test

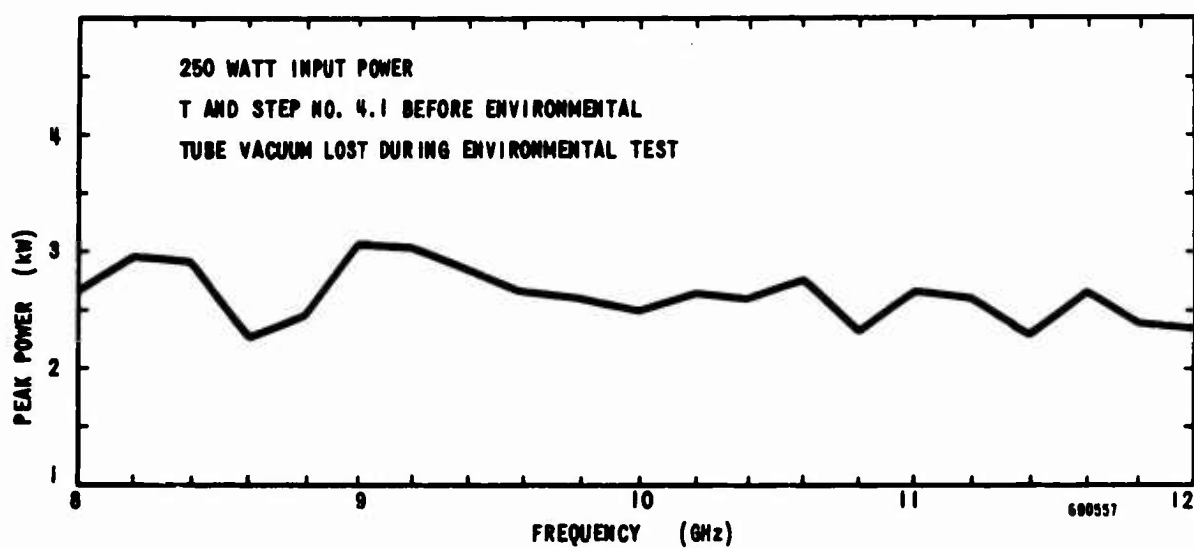


Figure 59. QR1642 No. 5 Peak Power vs Frequency Before Environmental Test

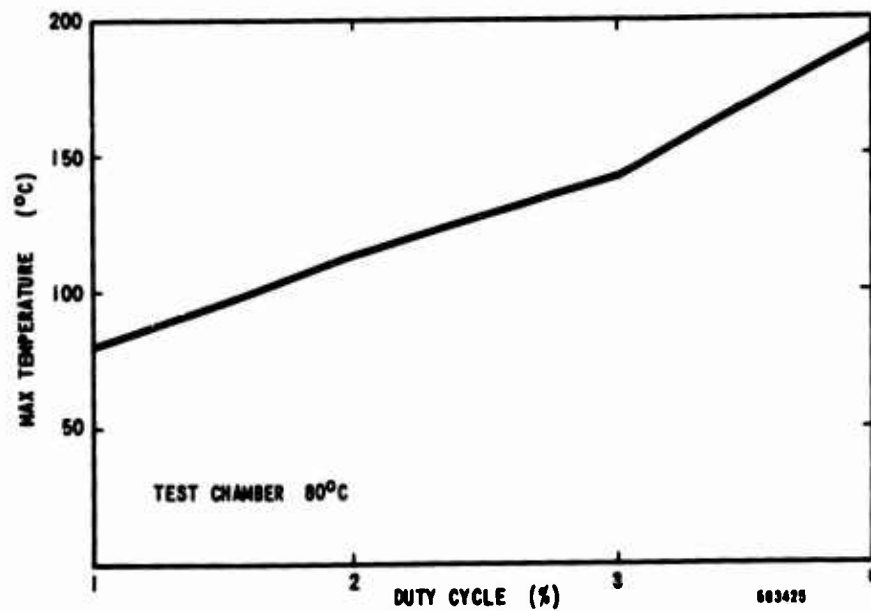


Figure 60. QR1642 No. 1 Maximum Temperature on OD of Magnets after 3 Hours vs Duty Cycle

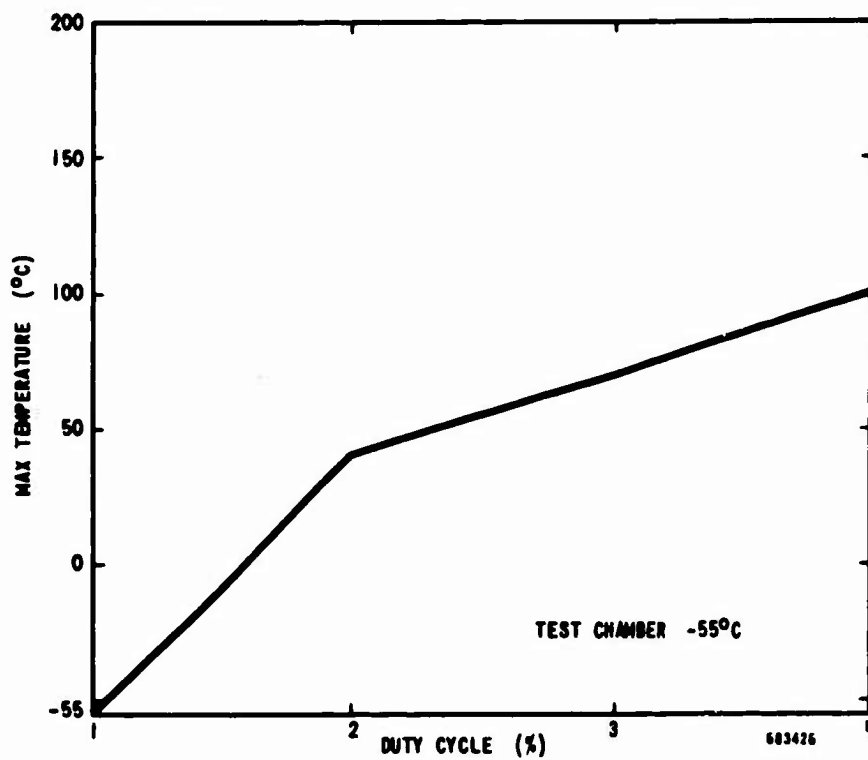


Figure 61. QR1642 No. 1 Maximum Temperature on OD of Magnets after 3 Hours vs Duty Cycle

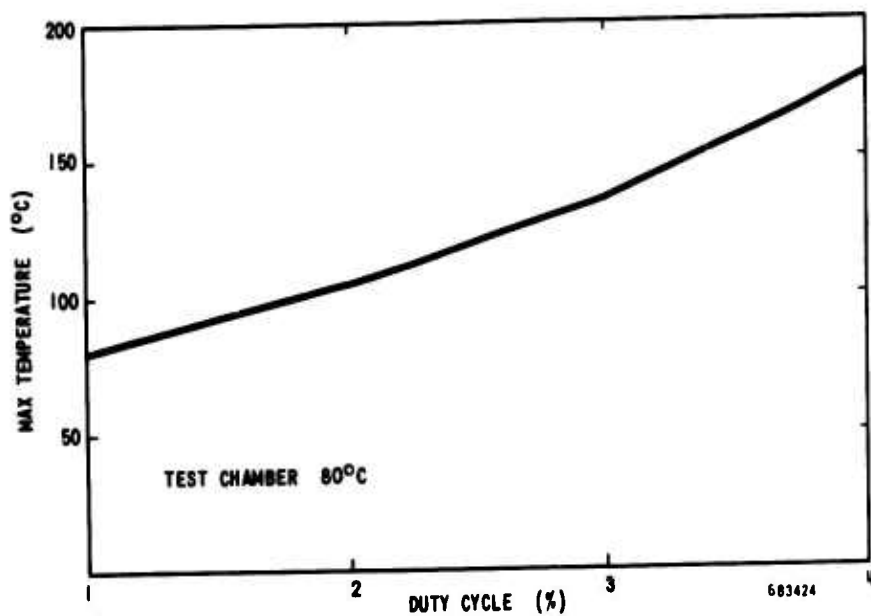


Figure 62. QR1642 No. 2 Maximum Temperature on OD of Magnets after 3 Hours vs Duty Cycle

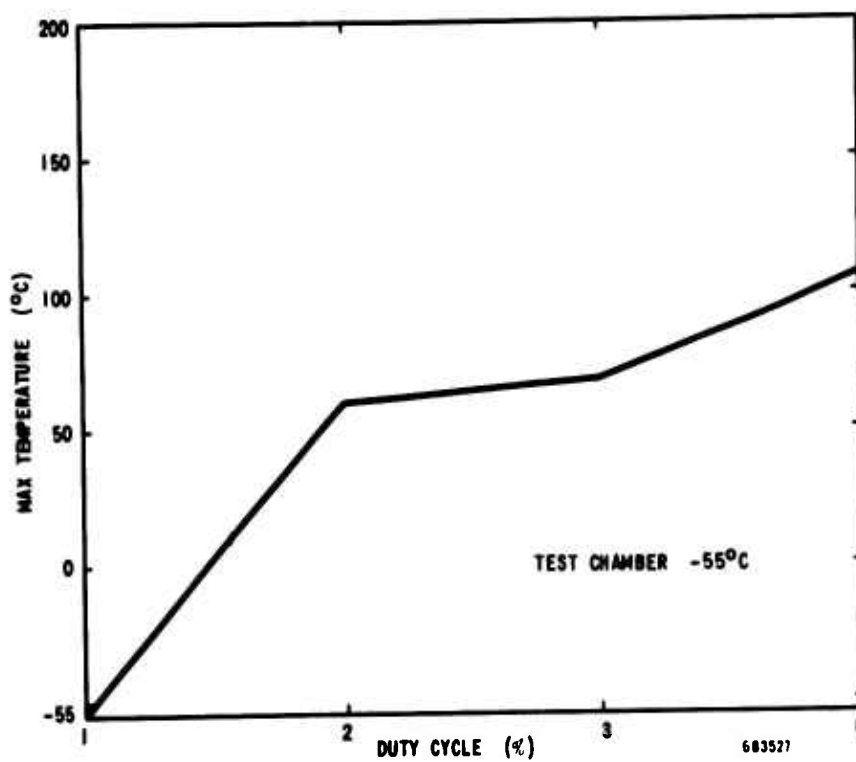


Figure 63. QR1642 No. 2 Maximum Temperature on OD of Magnets after 3 Hours vs Duty Cycle

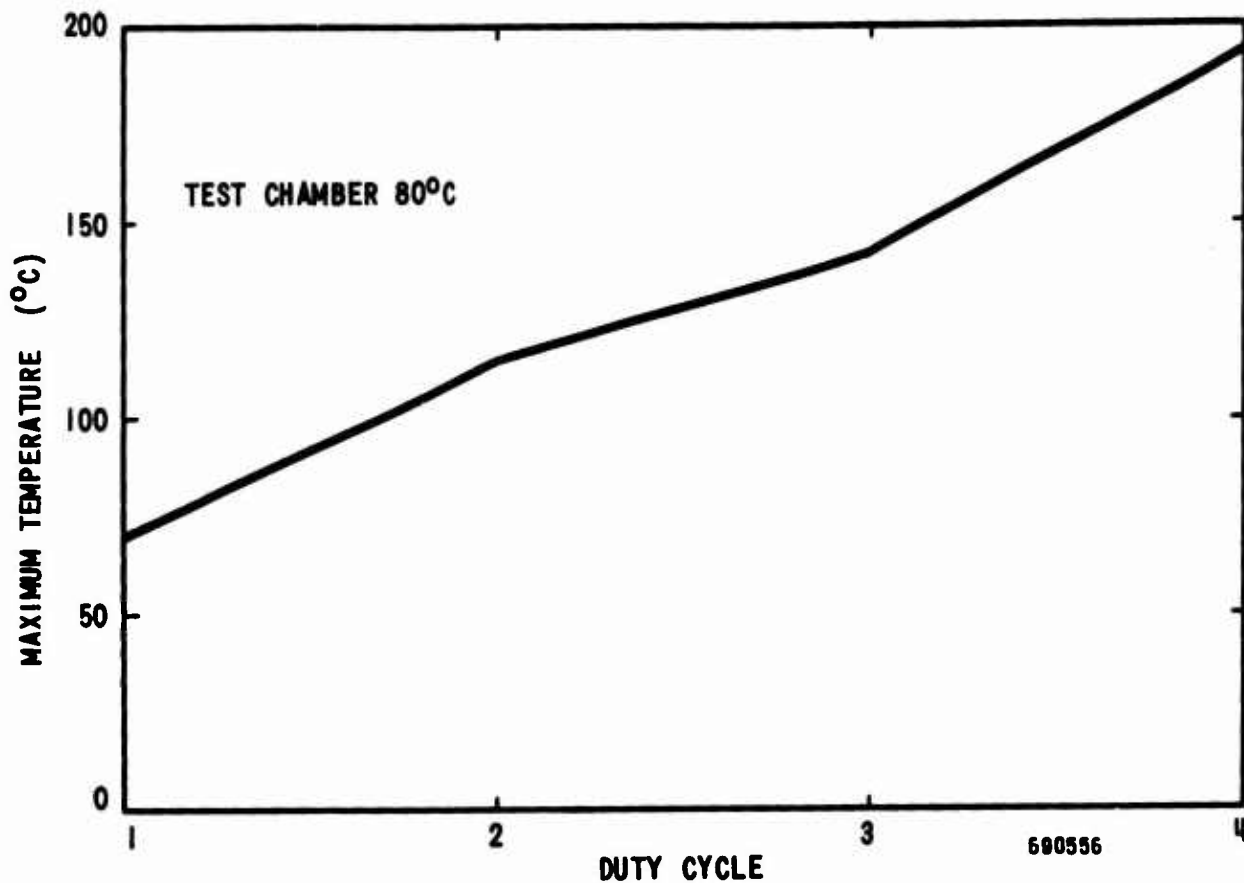


Figure 64. QR1642 No. 3 Maximum Temperature on OD of Magnets After 3 Hours vs Duty Cycle

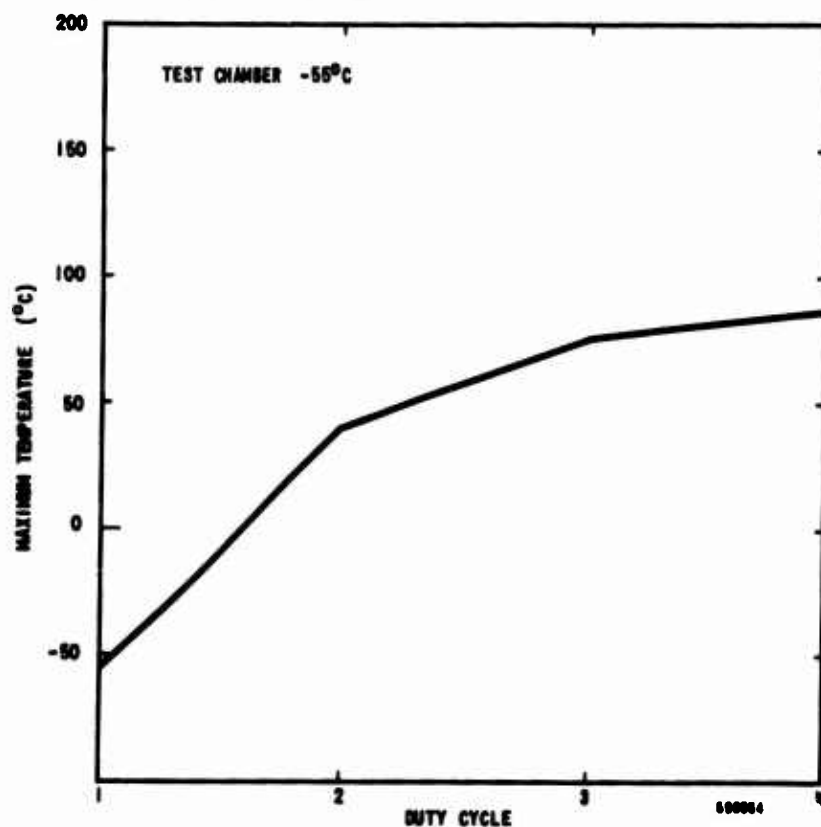


Figure 65 QR1642 No. 3 Maximum Temperature on OD of Magnets After 3 Hours vs Duty Cycle

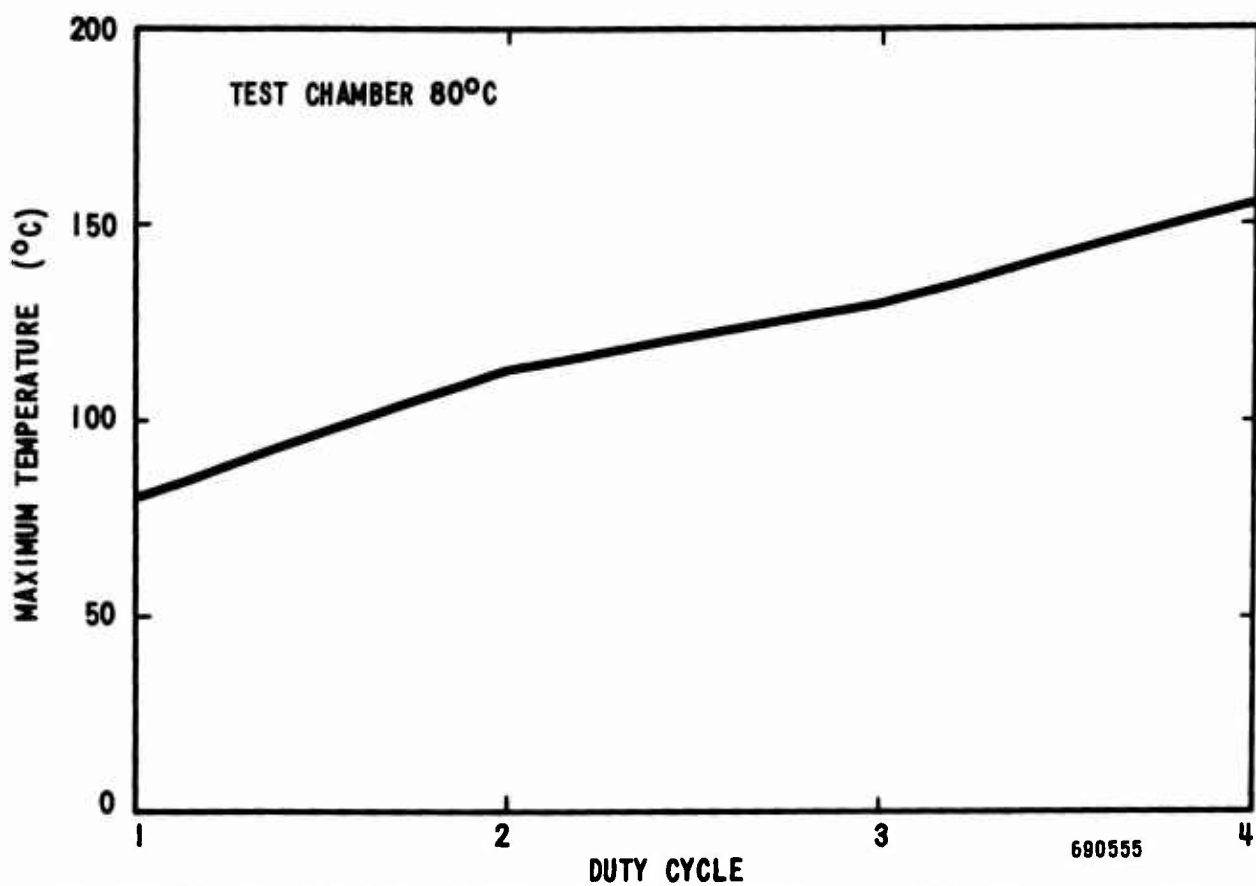


Figure 66. QR1642 No. 4 Maximum Temperature on OD of Magnets After Three Hours vs Duty Cycle

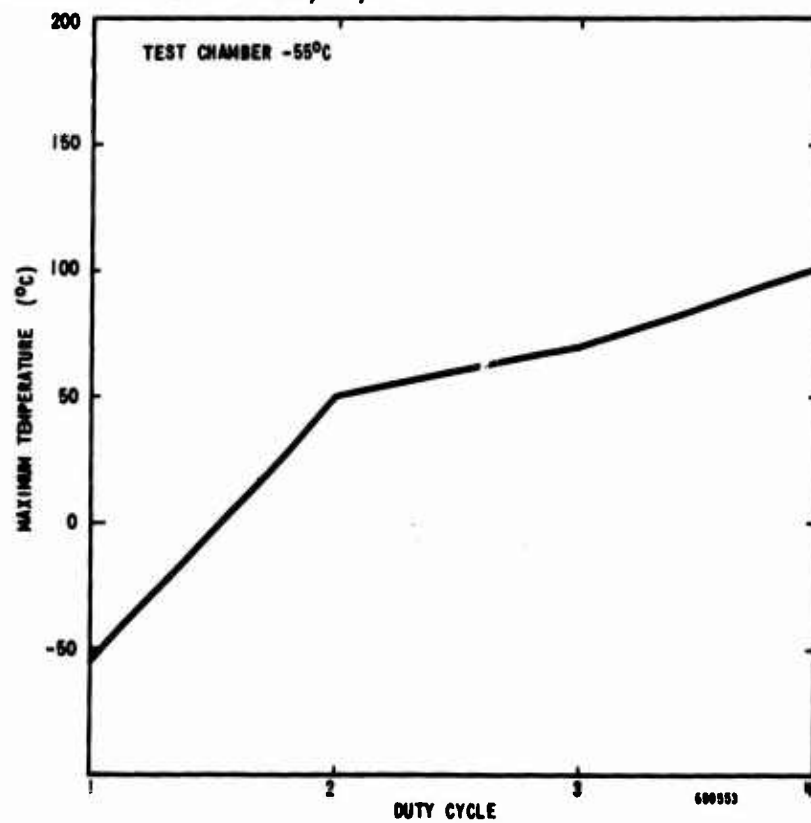


Figure 67. QR1642 No. 4 Maximum Temperature on OD of Magnets After Three Hours vs Duty Cycle

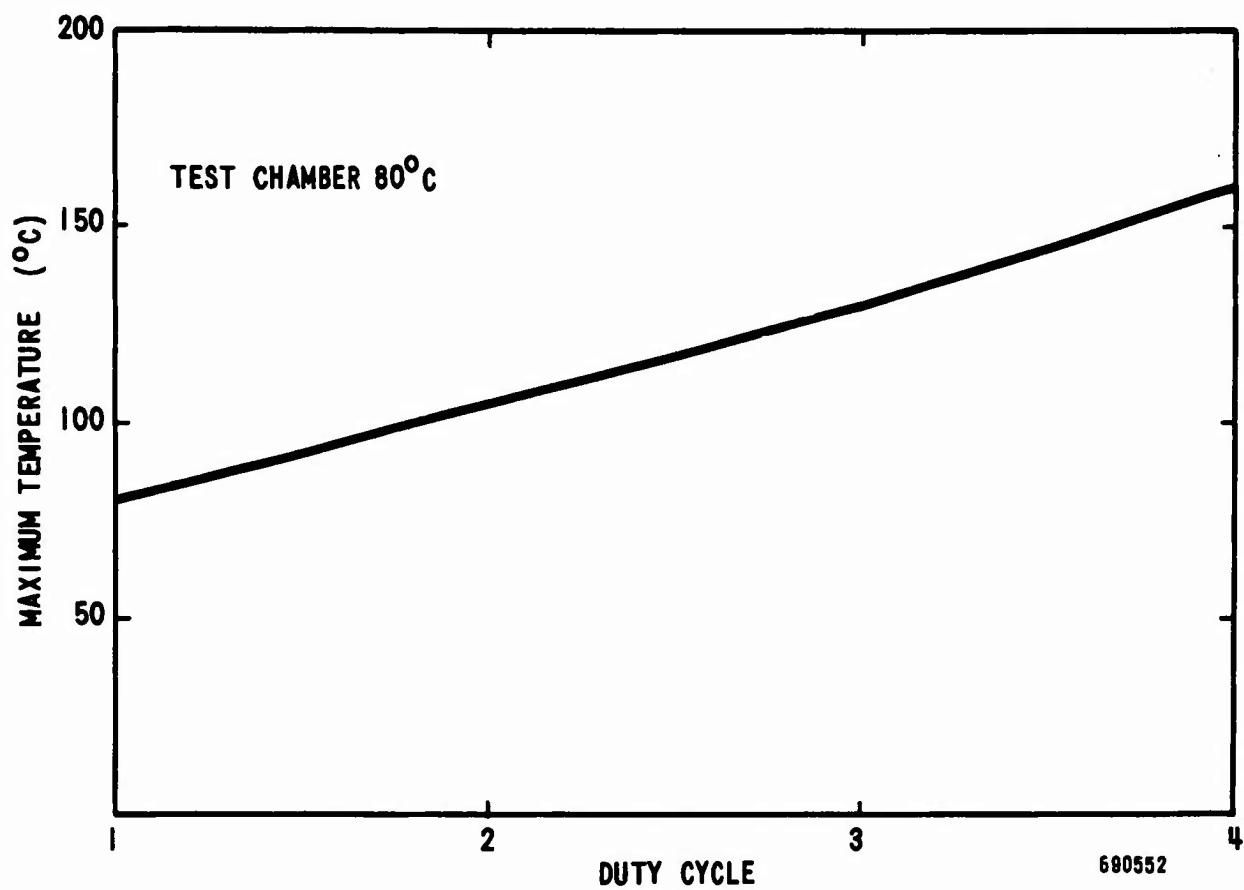


Figure 68. QR1642 No. 5 Maximum Temperature on OD of Magnet After 3 Hours vs Duty Cycle

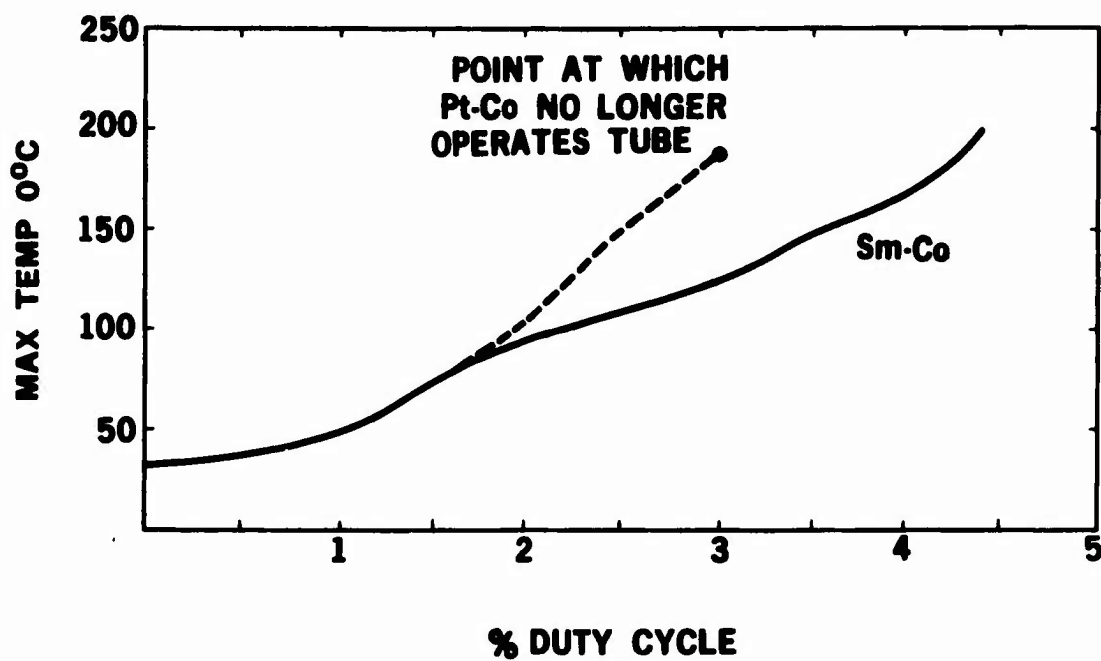


Figure 69. QR1642 Temperature vs Duty Cycle

SECTION VI

SUMMARY

Prior to the initiation of this program, limited quantities of samarium-cobalt permanent magnets were being made on a laboratory basis. Processes and techniques have been established during this program for the pilot line manufacturing of samarium-cobalt permanent magnets for use in high performance PPM focused traveling-wave tube amplifiers. The objective was to establish a capacity of 1000 magnets per month, and this rate has been substantially exceeded.

Pilot plant production of samarium-cobalt magnets is illustrated in the flow chart of Figure 70. The individual steps are summarized below. The procedures which refer specifically to the manufacture of magnets for the QR1642 traveling-wave tube are generally followed in Sm-Co magnet production.

1. Melting: Samarium and cobalt metal in the approximate ratio of 2:3 are induction melted in aluminum oxide crucibles in a purified helium atmosphere. The alloy is cast into a water-cooled copper mold.
2. Alloy Crushing and Grinding: The alloy casting is broken up by hand into small chunks and then reduced to micron size powder in a three-step process, as follows:
 - a. Jaw crushed
 - b. Pulverized in argon
 - c. Attritor-milled in toluene
3. Drying: The toluene grinding fluid is removed from the powder in a vacuum shelf drier. High production rates are achieved by slightly heating the powder slurry.
4. Storing: To protect the powder from oxidation and to minimize safety hazards, ready-to-press powder is stored in a nitrogen dry box.
5. Pressing: Powder compacts ~ 65% of theoretical density are pressed at 75,000 psi in an aligning field of about 8000 Oe. The entire cycle of die filling, field application, pressing and part ejection is done automatically in a 100-ton automatic powder press. A 600-pound electromagnet, synchronously coupled with the press, provides the aligning field.
6. Sintering: The green pressed magnets are sintered to ~ 95% of theoretical density in an atmosphere of pre-purified helium. Optimum magnetic properties result from processing at 1130°C for 1 hour.

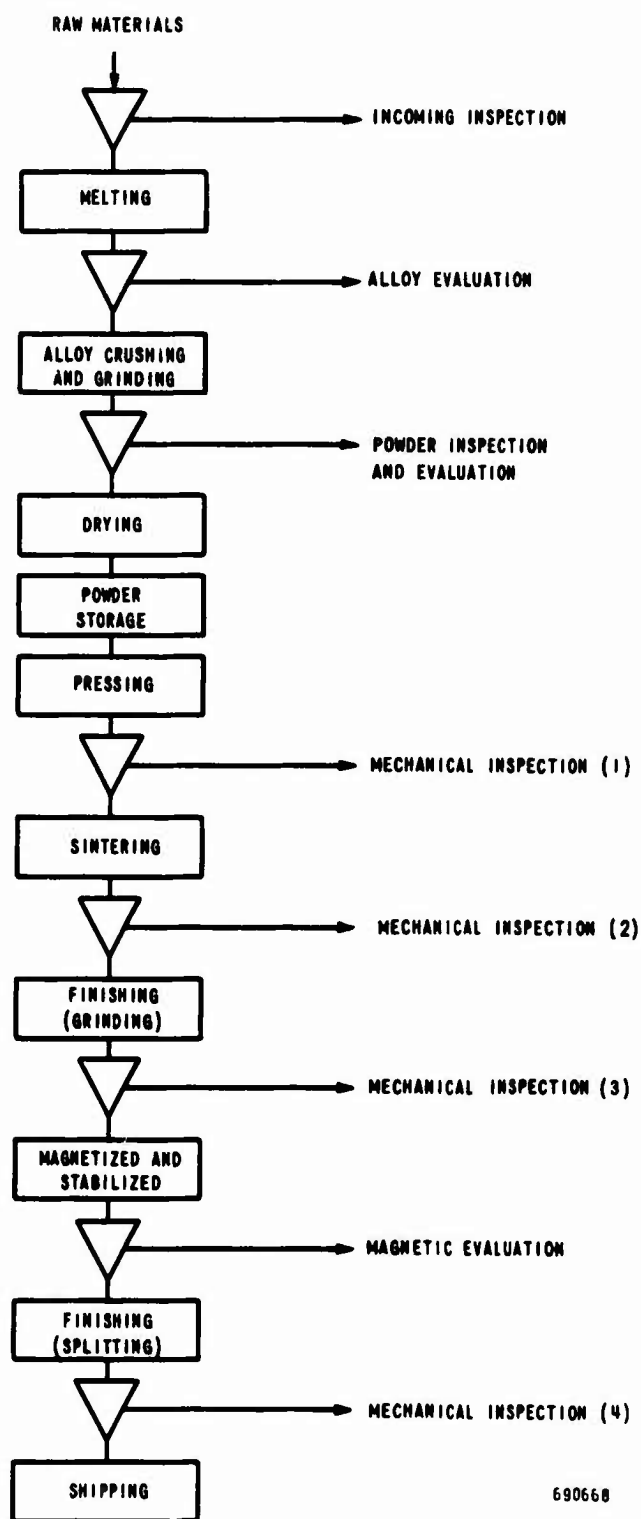


Figure 70. Flow Chart for Manufacture of Samarium-Cobalt Magnets

7. Finishing and Splitting: Final magnet thickness is maintained to within the required tolerance by surface grinding. Matched half-ring pairs are produced by scoring and pressure splitting. Input-output magnets are slotted to within the specified tolerance with a diamond wheel cutter.
8. Magnet Evaluation: A functional measurement has been found to be most convenient. Finished magnets are magnetized, stacked in the PPM configuration and the peak axial field of each magnet is measured. To stabilize magnetic properties, the stack is thermally cycled above the operating temperature and the measurements repeated.
9. Packaging and Shipping: Each matched half-ring pair is placed in a multi-cavity insert. Stacked layers of the inserts are packaged in tightly closed plexiglass containers with adequate foam insulation to prevent damage in handling. When air shipping, magnet shielding is supplied in accordance with MIL-S-4473C.

The quality controls that have been incorporated in the pilot plant are also included in Figure 70. The individual steps and methods of inspection are continually being altered and improved to meet production requirements. The current procedures are summarized below:

1. Incoming Inspection: The raw materials are sampled and spectrographically analyzed. Samarium is also metallographically examined to control the amount of impurity second phase. Crucibles are examined for cracks and irregularities in wall thickness.
2. Alloy Evaluation: The cast alloy is broken up and inspected for unmelted cobalt. Samples are taken for spectrographic analysis and metallographic examination.
3. Powder Evaluation: The pulverized product is sieved to remove oversize material. A small amount is then attritor-ground and several ring magnets are fabricated according to standard practice. A measurement of the sintered density is followed by magnetic evaluation according to the procedures for production TWT magnets (Section III-8).
4. Mechanical Inspection: Following pressing, sintering, and both finishing operations, the magnets are inspected for cracking and chipping. The inspection after sintering also includes density measurements.
5. Magnetic Evaluation: As described in Section III-8, magnetic evaluation consists of peak axial field measurements before and after temperature stabilization of magnets stacked in the PPM configuration. Magnets with final values below 3000 Oe are rejected while those above 3400 Oe are partially demagnetized into the range 3000 - 3400 Oe.

Sufficient quantities of magnets are yet to be processed to establish accurate levels of yield to be expected with the facility. To a large extent, yield will depend upon the exact magnet specifications required, particularly with regard to the maximum temperature for acceptable device operation. Substantial efforts were made to establish temperature characteristics of magnets with second quadrant properties that were representative of the variability that was encountered during this program.

Estimating costs for magnets produced by techniques developed under this program require assumptions about yield over long production runs. Magnetic yield, in turn, depends upon the temperature-demagnetizing environment of the specific application. For the QR1642, estimates have been based on a range of operating temperatures from 160°C to 225°C. Magnetic yield varies almost linearly over this interval. In large quantities (5000 parts), magnets of the size produced on this program can be delivered at present for \$10 - \$15 each, depending upon the specifics of temperature stabilization. This includes complete magnetic testing and stabilizing, as well as splitting for direct placement of magnets on TWT's. A corresponding per pound cost of finished, fully-stabilized magnets is \$1,000 to \$1,500. These figures are expected to drop significantly with larger volume and increased capacity process facilities.

A summary of properties are included in Table XXXVI. Some judgment has been exercised with a view toward establishing probable values to be expected at acceptable production yields.

In general, magnets capable of high temperature use have been produced. In spite of the high chemical reactivity of samarium, when combined with cobalt the resulting magnets are very stable in oxidizing and high humidity environments. Magnetic properties can be very stable to temperatures exceeding 200°C, and the degree of stability depends upon demagnetizing factors. Still to be determined, and extremely important, are those metallurgical factors that relate to stability. A variety of measurements were made in an attempt to at least identify the relationship of functional stability in use with intrinsic magnetic properties. For example, maintaining a high peak axial field in a PPM stack after temperature cycling was in part correlated with intrinsic coercive force and intrinsic energy product. If indeed this is correct, it still remains to precisely determine which metallurgical factors influence these two properties. It appears that such correlations are not simple and direct, but that functional performance of magnets depends in some complex way upon the details of the complete second quadrant curve and its temperature dependence.

The device evaluation portion of this program clearly established the superior performance possible with samarium-cobalt magnets. Clearly higher power and the attendant higher temperature are now possible with TWT's. This capability is achieved without sacrifice in device operating life.

Table XXXVI
Properties of Sintered Sm-Co Magnets

Property	Value	Comments	Reference
Residual Induction B_r	7800 Gauss	Probable range ± 200 Gauss	Tables III, IV, V, VIII, Figure 20
Coercive Force H_c	6800 Oe	Probable range ± 300 Oe	Tables III, IV, V, VIII, Figure 20
Intrinsic Coercive Force H_{ci}	18,000 Oe	Probable range up to 22,000 Oe	Tables III, V
Energy Product BH_{max}	14×10^6 GOe	Probable range $13\text{-}15 \times 10^6$ GOe	Tables III, IV, VIII
Intrinsic Energy Product $4\pi MH$	65×10^6 GOe	Probable range up to 80×10^6 GOe	Tables III, V
Irreversible Temperature Coefficient of:			
Flux	.04 - .07%/°C	Coefficient linearly proportional to demagnetizing field.	Tables XI, XII, XV, XVI, - Figures 26, 27, 30-33, 35, 37, 39
B_r	.02 - .03%/°C	Increases strongly with increasing temperature.	
H_c	.03 - .05%/°C		
H_{ci}	.01 - .02%/°C		
$(BH)_{max}$.05 - .10%/°C		
Peak Axial Field B_o	.035 - .045%/°C (.010 has been measured)		
Reversible Temperature Coefficient of:			
Flux	.035 - .045%/°C	Increases slightly with increasing temperature and demagnetizing field.	Tables X, XV, XVI, - Figures 32, 34, 36-38, 40, 42
B_o	.045 - .055%/°C	Values obtained after removal of irreversible loss	
Long Term Stability	Cycling during 750 hr. to 200°C caused <4% drop in B_o (PPM). No measurable change in B_o ($\pm 1\%$) during 900 hrs. at 230°C in PPM stack.		Tables XIII, XIV, - Figure 41

Table XXXVI

Properties of Sintered Sm-Co Magnets (Cont.)

Property	Value	Comments	Reference
Oxidation Rate	Negligible to 250°C		Section III-8, Figure 44
Specific Gravity	8.2 g/cc		
Percent of Theoretical Density	93%		
Percent Open Porosity	0%	Probable range up to 95%	Table II, Figure 11
Electrical Resistivity	5×10^{-5} ohm-cm	No moisture absorption. All closed, unconnected porosity.	
Thermal Expansion Coefficient (0-300°C)	10.0×10^{-6} in/in/°C		
Thermal Conductivity (100°C)	0.020 cgs		
Tensile Strength	8,000 psi	Probable range to 10,000 psi	
Compressive Strength	10,000 psi	Probable range to 12,000 psi	
Flexural Strength	12,000 psi	Probable range to 14,000 psi	
Mechanical Integrity	< 3%	No weight loss during normal handling.	
Hardness	$R_c > 55$		
Impact Strength		Capable of withstanding handling, assembly, and operation of TWT consistent with MIL-5400 Class II environmental requirements.	Appendix A - Test Data, Section V
Magnetization Field	50 kOe, 10 msec pulse	> 95% of magnetic properties achieved compared with values at 100 kOe dc.	Figures 15, 19, 20
Maximum Temperature Operation	225°C	Maximum temperature of operation in device. Test at a load line of -0.3. In lower demagnetizing fields, possible range up to 300°C.	Figure 67 Figures 35, 36, 37

BLANK PAGE

APPENDIX A

SPECIFICATION

FOR

ELECTRON TUBE, TRAVELING-WAVE AMPLIFIER TUBE

TYPE QR1642

SPECIFICATION FOR ELECTRON TUBE,
TRAVELING-WAVE AMPLIFIER TUBE, TYPE QR1642

APPROVALS	
Project Eng.	<i>A.W. Kelley</i>
Quality Assurance	<i>Ed W. Gough</i>
Dept. Manager	<i>Burt R. Smith</i>

RAYTHEON COMPANY
Microwave and Power Tube Division
Waltham, Massachusetts

Revisions		Approved
Original Issue	0	
Revision	0	
Sheet 1 of 13 sheets		

SPECIFICATION FOR ELECTRON TUBE, TRAVELING-WAVE AMPLIFIER, TYPE QR1642

The electron tube requirements described herein shall consist of this document and the latest issue of Specification MIL-E-1 .

Description: Broadband, 3 kW, 8.0 - 12.0 GHz, grid pulsed tube, 12 db gain, air-cooled,
 Periodic permanent magnet (see Note 1), transparent, 2.0 db insertion loss max.

Absolute Ratings:

Parameter Units	Ef V	tp μs	Du Ratio	pd dbm	EC V	Altitude ft.
Maximum	6.6	20	0.04	55	-100	75,000
Minimum	6.1	---	---	---	---	---

Absolute Ratings:

Parameter	Eb	Ews	iK	if	Air Cooling	Air -Cooling Temp °F	VSWR	tk	Freq.
Unit	kV	kV	a	a	lb/min			sec	GHz
Maximum	6.8	10.5	2.0	15 surge	2.55	176	2.0		12.0
Minimum		9.7	---	-----	.55	-10	---	120	8.0

Physical Characteristics

See Figure 2

Weight: 4.5 lb max.

Raytheon Company
 QR1642
 17 September 1970
 Sheet 2 of 13

Test Conditions (See Notes 1, 12, 14):

Parameter	Ef	tp	prf	Ews	Eb	pd	Load VSWR	T	Ec	Baro- metric Pres- sure	Cool- ing Air Flow	tk	i beam
Unit	v	μs		kv	kv	dbm	ratio	°C	V	psia	cfm	sec	
Test 1													
Minimum	6.3	5.0	800	9.7	6.8	52		25±5	-150	14.7	11.0	120	
Maximum			8000	10.5		54	1.15						
Note		13	13	14		13	15				16	17	14

Symbol Definitions

<u>Frequency:</u>	F1 = 8.0	GHz	Ef	Heater Voltage	pd	RF drive power
	F2 = 9.0	GHz	tp	Time of rf Pulse	Ec	Grid Bias Voltage
	F3 = 10.0	GHz	prf	Pulse Rep. rate/sec	ec	Grid Pulse Voltage (peak)
	F4 = 11.0	GHz	Ews	Helix/Shell Voltage	iws	Helix plus Shell current (peak)
	F5 = 12.0	GHz	Eb	Collector Voltage		

General:

Qualification - Required

Only the tests or requirements listed below or elsewhere in this TRS shall apply.

- 3.6

Marking: See Note 9
- 3.7

Workmanship
- 4.1

Responsibility for inspection
- 1105

Performance of marking
- Weight: 4.5 lb max
- Mechanical Dimensions: See Figure 2.

Test Method	Requirement or Test	Notes	Test Condition	Conditions	Sym	Limits		Unit
						Min	Max	
QUALITY CONFORMANCE INSPECTION, PART I								
	Small Signal Gain	11	1	pd = 40 dbm F1 to F5	SSG	11.0		db
	RF Power Output	11, 2	1	F1 to F5	po	62.0	66.0	dbm
	Insertion Loss, Input to Output	11, 20	---	F1 to F5	L		2.0	db
	VSWR	11, 15	---	F1 to F5	Ratio		2.0:1	
	Heater Current		---	6.3 VAC	If	3.0	4.0	A
	Cathode Current		1		ik		1.75	A
	Collector Current		1	pd = 0	ib		1.50	A
	Ground Current IWS	11	1		iw/s		.4	A
	Grid Current		1		ic		.33	A
	Grid Drive		1		ec	+55	+165	V

Raytheon Company
QR1642
17 September 1970
Sheet 4 of 13

Test Method	Requirement or Test	Notes	Test Conditions	Conditions	Sym	Limits Min	Max	Unit
<u>QUALITY CONFORMANCE INSPECTION, PART 2</u>								
	Barometric Pressure	4, 21	---	pd = 0 75, 000 ft. T=25°C				
	Non Operating	21	---	10 to 500 Hz See Figure 1				
	Grid Capacitance				Cg	30		pf
<u>QUALITY CONFORMANCE INSPECTION, PART 3</u>								
	Humidity	8, 21	---					
	Salt Spray	7						
	Shock	6,						
	Operating Vibration	5, 21, 22	1	Pd = 0				

Raytheon Company
QR1642
17 September 1970
Sheet 5 of 13

Test Method	Requirement or Test	Notes	Test Condition	Conditions	Sym	Limits		Unit
						Min	Max	
QUALITY CONFORMANCE INSPECTION, PART 3 (cont'd)								
	High Temperature Operating	3	1	T = 176° F				
	Low Temperature Operating	3	1	T = -65° F Cooling Air -10° F				

NOTES:

1. Beam Focus - Beam focusing shall be provided by a periodic permanent magnetic structure. Adequate shielding shall be provided as a part of the tube to allow for operation without interference with a minimum spacing of 1/2 in. between adjacent tubes, measured at the major shell diameter. The magnetic field at a distance of 8 in. from the tube shall not exceed 0.2 gauss, excluding the earth's magnetic field.
2. The tube shall meet the rf power output requirement with a maximum average dc power input, inclusive of filament power, of 530 W for all operating voltages and environmental conditions specified at 4.4% duty cycle. Depressed collector techniques are employed to obtain this.
3. The tube shall be capable of operation over the temperature range of -65° to $+176^{\circ}$ F. Unless otherwise specified, the cooling air temperature will be the same as the ambient temperature supplied during tube operation. The maximum exposed surface temperature under all operating and environmental conditions shall be 392° F. The mounting surface for the tube will be 212° F maximum under all operating and environmental conditions.
4. TWT's shall be capable of withstanding long periods of exposure to 75,000 feet altitude in a non-operating condition wherein all rated voltages except heater and grid voltages are applied.
5. The tube shall be designed to operate satisfactorily when subjected to the vibration requirements of MIL-E-5400 of amplitude and acceleration levels specified in Figure 1.
6. The TWT shall not suffer damage or subsequently fail to provide the performance specified under Quality Conformance Inspection, Part I when subjected to shock conditions described in MIL-E-5400 for equipment with the exception of the G value shall be 30 G's.
7. When tested in accordance with Method 101, Test Condition B of MIL-STD-202, there shall be no corrosion of the base material.
8. When tested in accordance with Method 103, Test Condition A of MIL-STD-202, there shall be no visible deterioration, corrosion, or degradation of performance.

Raytheon Company
QR1642
17 September 1970
Sheet 7 of 13

9. Marking - Marking shall be in accordance with MIL-STD-130 and shall consist of the following:

- a. Manufacturer's Part Number and Manufacturer's Designating Symbol
- b. Manufacturer's Serial Number
- c. Specific Voltage and Current Ratings shown in Figure 2.
- d. Date code

10. Altitude - The tube shall be capable of operation up to altitudes of 75,000 feet.

11. Measurement shall be performed at a maximum of 200 MHz increments from F1 to F5.

12. All voltages are with respect to cathode unless otherwise specified.

13. Duty Cycle - The tube shall be capable of operating continuously at 4.0% duty cycle. The rf duty cycle will be achieved with a beam duty cycle of 4.4% at a pulse width of 5.5 μ s as measured at the 50% amplitude point of the beam current pulse.

14. Testing shall be performed at the values of grid bias, helix voltage and beam current as specified on the tube label. Performance testing shall be at the maximum duty cycle.

15. The tube shall have a maximum VSWR of 2.0:1 for both input and output with a nominal input and output rf impedance of 50 ohms. The tube shall be capable of operating at the specified input levels into mismatch of 2.0:1 without damage to the tube.

16. The tube manufacturer should be consulted for cooling requirements at other than ambient conditions.

17. At an ambient temperature of 77° F and -65° F, the tube shall not be damaged or subsequently suffer degradation in performance if cathode voltage is applied two minutes after application of filament voltage. At the end of 3 minutes after initial application of filament voltage for the 77° F ambient condition and at the end of 5 minutes for the -65° F ambient condition, the tube shall provide specified performance.
18. The operating grid drive voltage shall be set to a value within the specified voltage range.
19. The total weight of the TWT shall not exceed 4.5 lb max.
20. The insertion loss to a rf drive signal of 0.20 mW shall not exceed 2.0 dB.
21. At the completion of this test the TWT shall meet the requirements of Quality Conformance Inspection, Part I.
22. The filament current and beam current shall not exhibit significant changes during vibration.

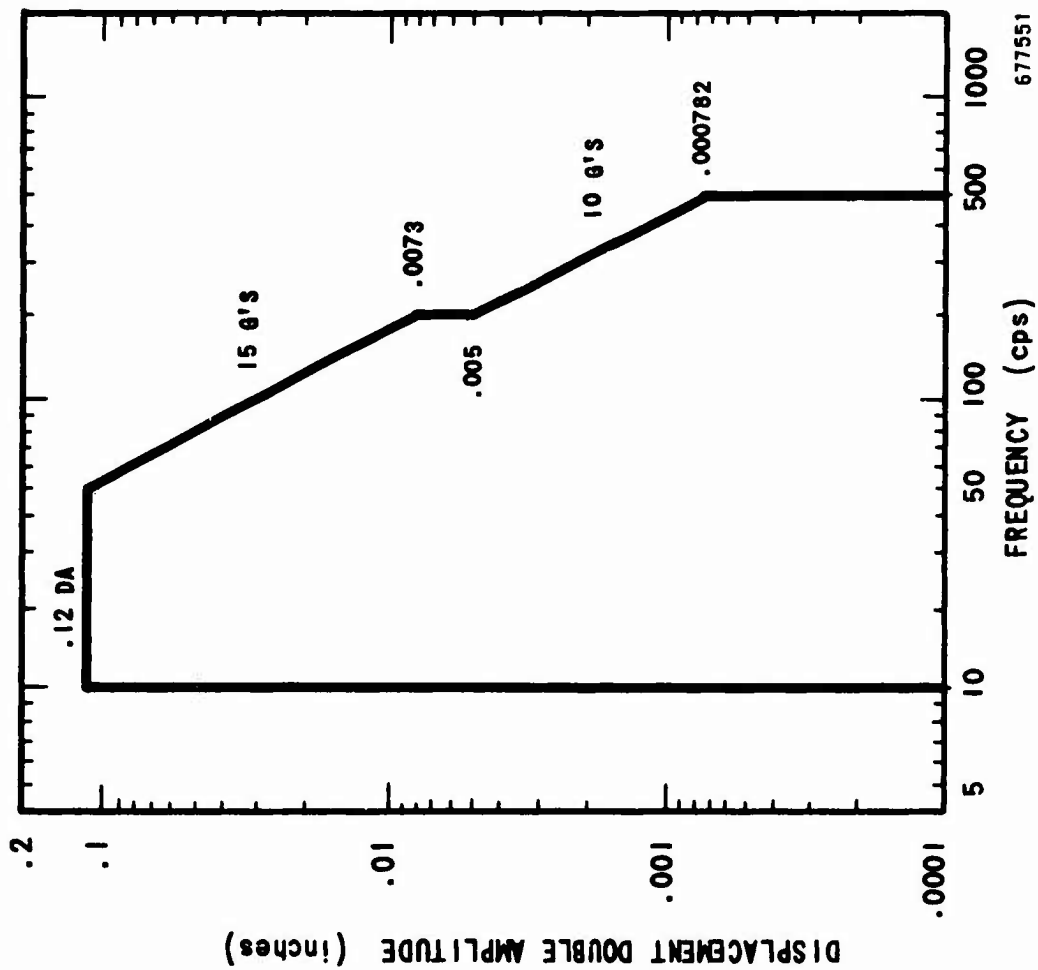
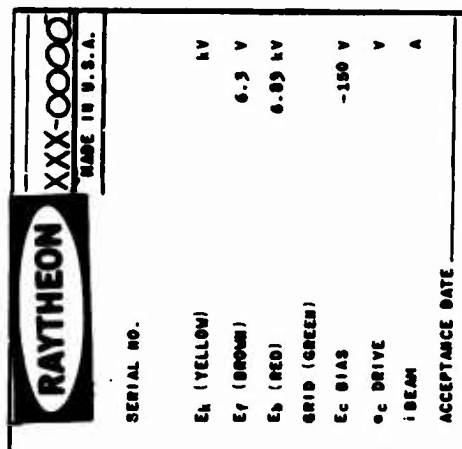
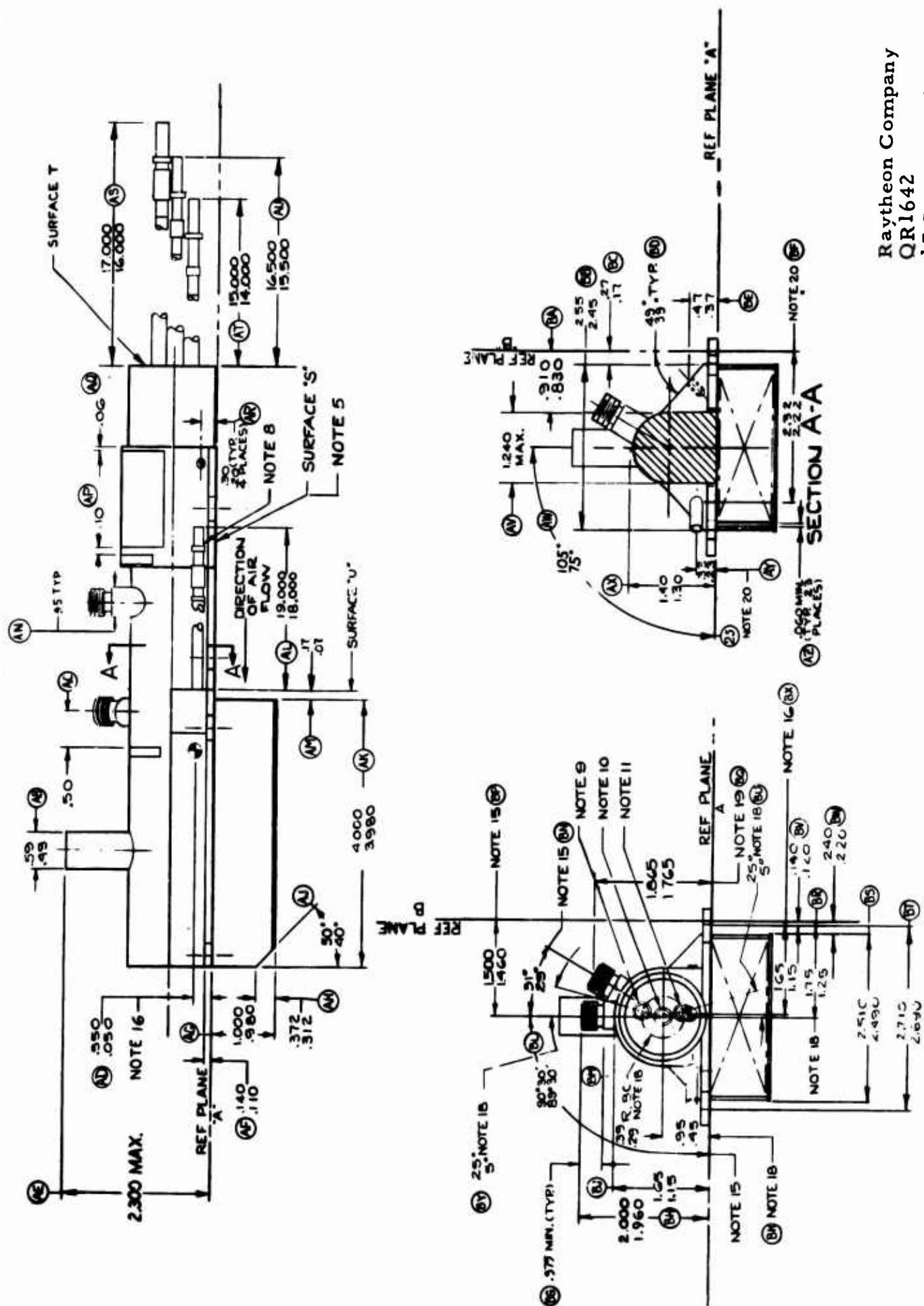


Figure 1. Vibration Curve

Raytheon Company
 QR1642
 17 September 1970
 Sheet 10 of 13



Raytheon Company
QR1642
17 September 1970
Sheet 11 of 13



Raytheon Company
 QR1642
 17 September 1970
 Sheet 12 of 13

Figure 2b. QR1642 Tube Outline Drawing

DIMENSIONS						
LETTER	INCHES		LETTER	INCHES		
	MIN	MAX.		MIN	MAX.	
QUALITY CONFORMANCE ACCEPTANCE						
D	.32	.42	AY	25	.33	
E	.310	.320	BB	245	.255	
F	.295	.345	BC	.17	.21	
K	.125	.175	BE	.37	.47	
Q	.93	1.03	BF	2.22	2.32	
X	1.29	1.39	BJ	1.15	1.65	
AB	.49	.59	BK	.45	.95	
AD	.050	.550	BR	1.25	1.75	
AG	.980	1.000	BS	2.490	2.510	
AK	3.980	4.000	BT	2.690	2.710	
AM	.07	.17	BU	5°	25°	
			BV	.120	.140	
AR	.30	.30	BW	.220	.240	
AX	1.30	1.40	BX	1.15	1.65	
			BY	5°	25°	
QUALITY CONFORMANCE ACCEPTANCE (PROD)						
G		.200	BH	1.960	2.000	
L	3.615	3.665	BP	1.460	1.500	
M	5.239	5.369	NOTE 5			
N		8.420	NOTE 6			
U		1.250	NOTE 7			
AA	.192	.198	NOTE 12			
AE		2.300	NOTE 21			
AS	16.000	17.000				
AT	14.000	15.000				
AU	15.500	16.500				
AZ	.060					
QUALITY CONFORMANCE ACCEPTANCE (DESIGN)						
A	4.445	4.455	AJ	40°	50°	
B	6.690	6.700	AL	18.000	19.000	
C	3.440	3.450	AV		1.240	
H	2.953	2.963	AW	75°	108°	
J	2.280	2.290	BA	.830	.910	
P	.670	.680	BD	39°	49°	
R	1.930	1.990	BG	.375		
S	.160	.190	BL	69°30'	80°30'	
T	.110		BM	.29°	.39°	
V	.345	.355	BN	29°	31°	
W		.300	BQ	1.765	1.865	
Y	2.405	2.415				
Z	.180					
AP	.110	.140				
AH	.312	.372				
NOMINAL DIMENSIONS						
LETTER INCHES						
AC	.75					
AP	.10					
AQ	.08					
AN	.45 TYP					

- REFERENCE PLANE "A" PASSES ALONG THE MOUNTING SURFACES OF LUGS "R"
- REFERENCE PLANE "B" IS PERPENDICULAR TO REFERENCE PLANE "A" PASSING THRU THE AXES OF HOLES "N" AND "Y" AT PLANE "A"
- REFERENCE PLANE "C" IS INITIALLY PERPENDICULAR TO PLANES "A" AND "B" PASSING THRU THE AXIS OF DIAMETER "I" AT PLANE "A"
- TUBE FINISH TO BE BLACK PAINT PER RAYTHEON SPECIFICATION 11762 AND 11269 AND MEET REQ. OF FEDERAL STANDARD 595, TEST METHOD 181
- MOUNTING SURFACES OF LUGS AND SURFACE "S" TO BE COPLANAR WITH REFERENCE PLANE "A" WITHIN .005 AND BE ELECTRICALLY CONDUCTIVE. SURFACE "S" TO HAVE A 32 MICROINCH FINISH OR BETTER
- OUTPUT J2 - SSP FEMALE PER SCALECTRO CORP. DRAWING P55-902-0089 7/16-38MS MOD. MUST ACCEPT CLASS 2 80 GAGE ONLY. MAJOR DIAMETER MUST NOT BE LESS THAN .9275
- INPUT J1 - SSP FEMALE PER SCALECTRO CORP. DRAWING P55-902-0089 7/16-38MS MOD. MUST ACCEPT CLASS 2 80 GAGE ONLY. MAJOR DIAMETER MUST NOT BE LESS THAN .9275
- COLLECTOR LEAD - RED
- GRID LEAD - GREEN
- HEATER LEAD - BROWN
- HEATER CATHODE LEAD - YELLOW
- GROUND LEAD MOUNTING HOLE P6-32NC-MOD. MUST ACCEPT CLASS 2 80 GAGE ONLY MAXIMUM MINOR DIAMETER .116. .187 MIN DEPTH. NO PAINT ON DIA SHOW
- LABEL (OPERATING PARAMETERS)
- TUBE WEIGHT 4 LBS 4 OZ ± 3 OZ
- APPLIES TO AXIS OF PITCH DIAMETER OF SSP CONNECTOR
- APPLIES TO CENTER OF GRAVITY
- LABEL (INPUT TERMINAL IDENTIFICATION)
- APPLIES TO THE AXIS OF OD OF HEATER LEAD AT SURFACE "T"
- APPLIES FROM REF PLANE "A" TO AXIS OF PITCH DIAMETER OF SSP CONNECTOR
- APPLIES TO THE AXIS OF THE OD OF COLLECTOR LEAD AT SURFACE "U"
- ALL NON-PAINTED METAL SURFACES TO BE NICKEL PLATED PER QQ-N-290 - CLASS 2 - TYPE VI
- LABEL (OUTPUT TERMINAL IDENTIFICATION)
- A MAXIMUM TORQUE OF 12 INCH POUNDS MAY BE APPLIED TO THE INPUT AND OUTPUT CONNECTORS
- APPLIES TO AXIS OF DIAMETER "AB" PROTRUSANCE

Figure 2c. QR1642 Tube Outline Drawing, Notes and Dimensions

Raytheon Company
QR1642
17 September 1970
Sheet 13 of 13

APPENDIX B

**QR1642
ENVIRONMENTAL TEST PROCEDURE**

1.0 SCOPE

This test is to demonstrate the TWT's capability of performance with temperature extremes as defined by Raytheon Company Specification, Quality Conformance Inspection, Part 3 for the QR1642.

Samarium cobalt magnet temperature will be monitored to demonstrate the superior temperature stability of samarium cobalt at the temperature extremes.

2.0 APPLICABLE DOCUMENTS

Raytheon Company Specification for Type QR1642.

3.0 EQUIPMENT

The equipment required to complete this test is indicated in Figures 1, 2, and 3.

4.0 PROCEDURE

- 4.1 Tube to be tested per data sheet A.
- 4.2 Place the tube under test (TUT) in the chamber, making such connections and instrumentation as to comply with Figures 1 and 2. When changing chamber conditions, the rate of change of temperature shall not exceed 1°C per second. Tube cooling air will be delivered to the TUT as indicated in Figure 3.
- 4.3 With the tube non-operating, apply 10.5 kV between cathode, heater, grid and shell, and 6.83 kV between collector and cathode $E_f=0$. Increase chamber temperature to $+176^{\circ}\text{F}$. Maintain this condition for 30 minutes.
- 4.4 Direct air across fin structure of TUT and discharge externally to temperature chamber. Adjust flow rate per Figure 3.
- 4.5 Turn on E_f and preheat tube at 6.3 volts for 2 minutes. Adjust voltages to label voltage of TUT. Tube shall operate within 5 minutes from time zero. Complete performance data sheet B. Tube to be operated for 15 minutes at each duty cycle level to obtain thermal stability. After completion of data sheet A, shut off all tube voltages and air.
- 4.6 Reduce chamber temperature to -65°F . With the tube non-operating, apply label voltages to TUT. $E_f=0$. Maintain this condition for 30 minutes.
- 4.7 Repeat step 4.4.
- 4.8 Repeat step 4.5.

4.9 Remove TUT from chamber and repeat step 4.1.

5.0 QUALITY ASSURANCE

Compare results of step 4.1 and 4.9 to determine if performance is in accordance with tube specification.

6.0 NOTES

Testing may be interrupted to accommodate maintenance, calibration and normal work shifts. Restarting shall be at the point of interruption and the TUT shall be restabilized before proceeding with the test.

DATA SHEET A

T AND A STEP NO. _____ SERIAL NO. _____ DATE _____ OPER. _____
 DUTY CYCLE 4.4% PULSE WIDTH 5.5 μ SEC PRF 8000


LABEL VALUES	RECORD
E _k _____	i _{ws} (no rf) _____
i _{beam} _____	
ec _____	

FREQ	pi WATTS	po kW	pi WATTS	po kW	FREQ	pi WATTS	po kW	pi WATTS	po kW
					10.0	158		250	
					10.2	158		250	
					10.4	158		250	
8.0	158		250		10.6	158		250	
8.2	158		250		10.8	158		250	
8.4	158		250		11.0	158		250	
8.6	158		250		11.2	158		250	
8.8	158		250		11.4	158		250	
9.0	158		250		11.6	158		250	
9.2	158		250		11.8	158		250	
9.4	158		250		12.0	158		250	
9.6	158		250						
9.8	158		250						

REMARKS

680788-2a

REVISIONS:

NAME	DATE	B-4	 LEXINGTON MASS. 02173
APPROVED			
		CODE 49956	SH

DATA SHEET B

T AND A STEP NO. _____ SERIAL NO. _____ DATE _____ OPER. _____


DUTY CYCLE 4.4% PULSE WIDTH 5.5 μ SEC PRF 8000 FREQ 9.8 GHz $p_i = 250$ WATTS

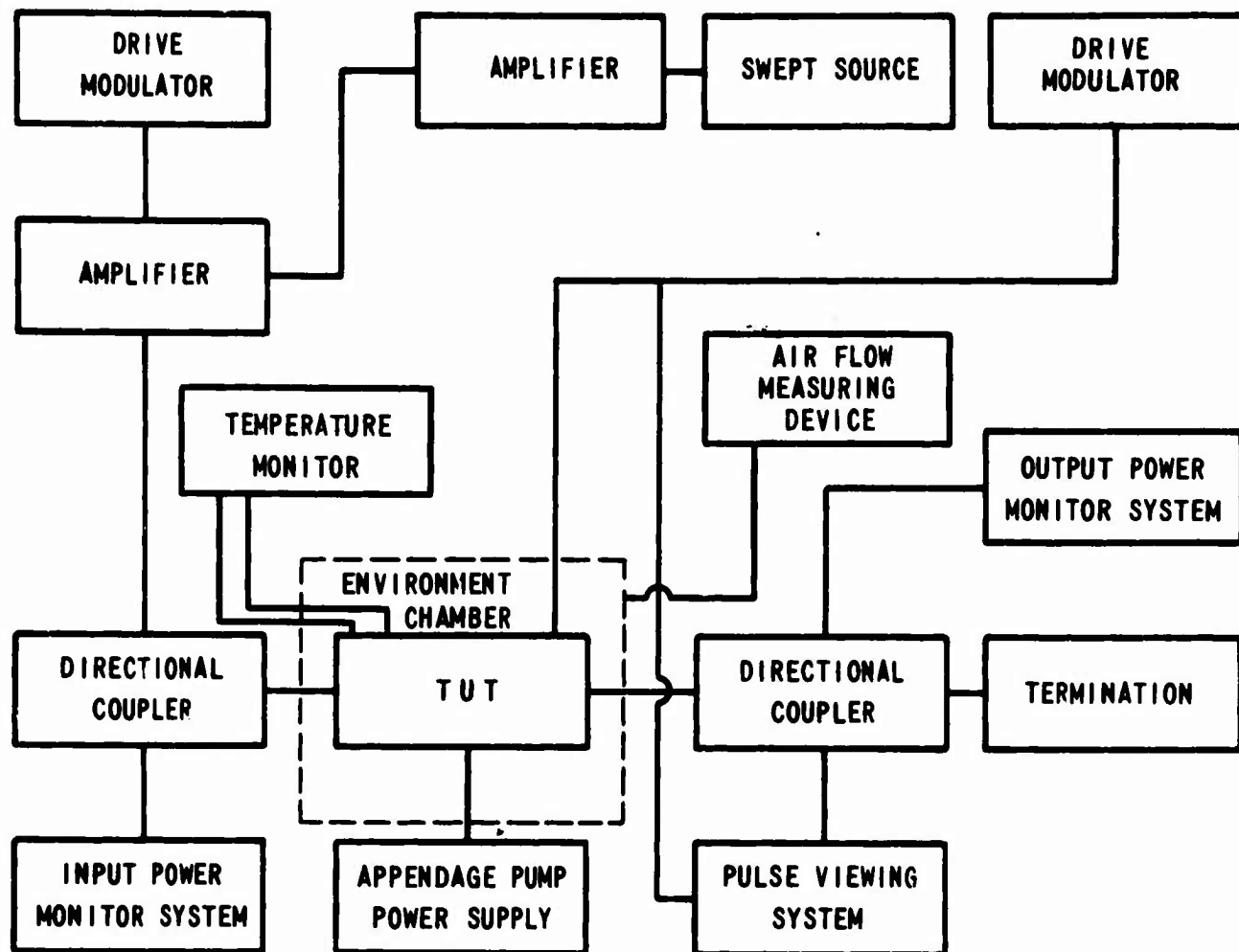
LABEL VALUES	RECORD
E_k _____	i_{ws} (no rf) _____
i_{beam} _____	$T_{chamber}$ _____
ec _____	

TIME HRS	p_o kW	i_{beam} A	i_{ws} A	T1	T2	T3	T4	T5	T6	du
0										2%
0.25										
0.50										
0.75										
1.00										
0										3%
0.25										
0.50										
0.75										
1.00										
0										4%
0.25										
0.50										
0.75										
1.00										

680788-1

REVISIONS:

NAME	DATE	B-5		LEXINGTON MASS. 02173
APPROVED			CODE 49956	SH



680786

Figure 1. Schematic Diagram for Testing QR1642

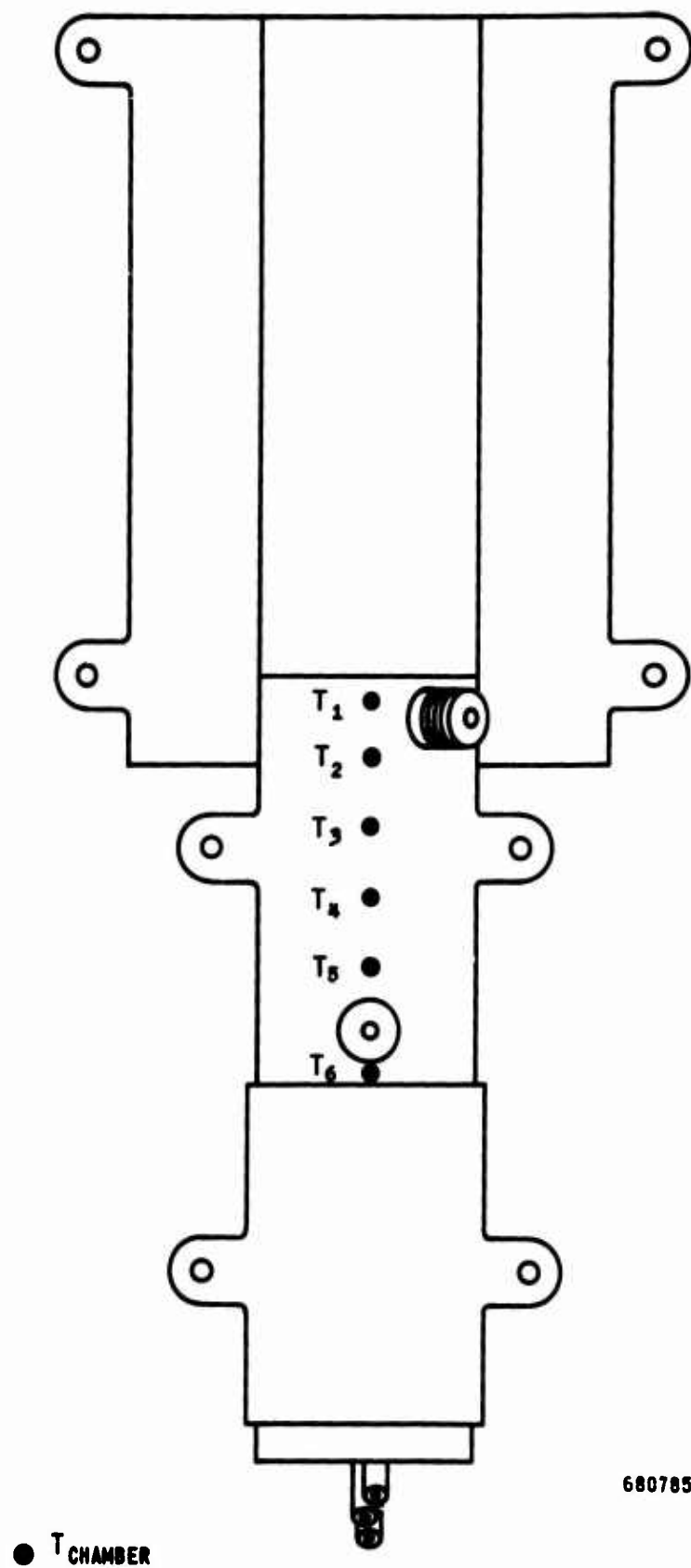


Figure 2. Thermocouple Locations for Monitoring Temperature During Testing of QR1642

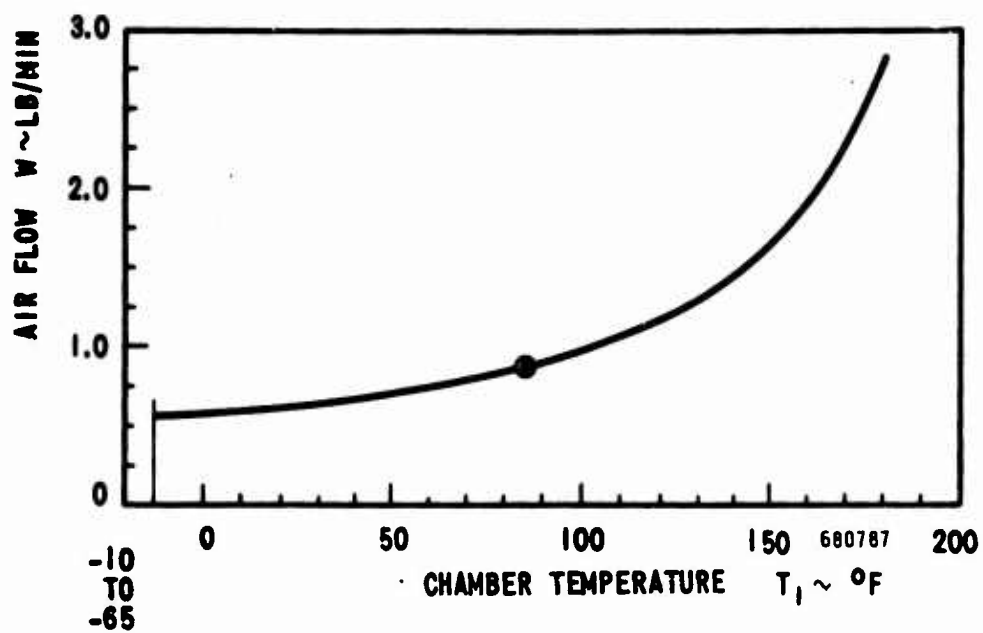
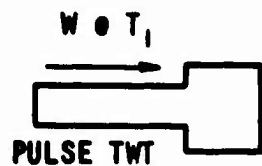


Figure 3. Air Flow Requirements